TACKLING THE INVERSE PROBLEM FOR NON-AUTONOMOUS SYSTEMS: APPLICATION TO THE LIFE SCIENCES

by
Tomislav Stankovski

THESIS SUBMITTED FOR THE DEGREE OF
DOCTOR OF PHILOSOPHY

DEPARTMENT OF PHYSICS
LANCASTER UNIVERSITY
LANCASTER, UK

February, 2012

ProQuest LLC.
789 East Eisenhower Parkway
P.O. Box 1346
Ann Arbor, MI 48106 – 1346

DECLARATION

This thesis is my original work and has not been submitted, in whole or in part, for a degree at this or any other university. Nor does it contain, to the best of my knowledge and belief, any material published or written by another person, except as acknowledged in the text.

CONTENTS

ACKNOWLEDGEMENTS

First and foremost I offer my sincerest gratitude to my supervisor, Prof. Aneta Stefanovska, who introduced me to the world of nonlinear biomedical physics. I am very grateful for her unreserved support throughout my thesis, guiding me with her knowledge, experience and enthusiasm.

I wish to sincerely thank Prof. Peter V. E. McClintock for his support, guidance and will to share his great experience and wisdom.

I especially wish to thank Dr. Andrea Duggento, with whom I have collaborated on much of the work presented. He was great tutor, colleague and friend, and it was a great pleasure to work with him.

I wish to thank Prof. Dwain Eckberg for the collaboration and for providing the data for the physiological study. I appreciate greatly the valuable discussion with Dr. Martin Rasmussen, Prof. Peter Kloeden and Dr. Martin Wechselberger regarding the study of non-autonomous systems. I wish also to thank Prof. Metodija Kamilovski for his advices on analogue simulation.

A special gratitude for both scientific assistance and kind friendship goes to many of my colleagues Dr. Alan Bernjak, Dr. Alireza Bahraminasab, Dr. Lawrence Sheppard, Dr. David Kenwright, Dr. Rodrigue Tindjong, Dr. Martin Horvat, Dr. Uchechukwu Vincent, Adam Bradbury, Dmytro Iatsenko. For valuable discussion and improving the written thesis, I also wish to thank my colleagues and friends Phil Clemson, Gemma Lancaster, Philip Stephens, Yvann Stephens, Rachel Sparks, Spase Petkoski and Dr. Yevhen Suprunenko.

I am especially grateful to my friends and family, for their encouragement and support. I thank my father for inspiring me, and my mother for giving me the mental strength to cope with the challenges throughout my studies.

Last, but by no means least, I wish to express my gratitude to my beloved wife. Her unreserved and unconditional support, understanding and encouragement helped me to get through over the last four years. I will never be grateful enough to her.

ABSTRACT

The common assumption that a dynamical system found in nature can be considered as isolated and autonomous is frequently a poor approximation. In reality, there are always external influences, and these are often too strong to ignore. In the case of an interacting oscillatory systems, they may e.g. modify their natural frequencies or coupling amplitudes. The main objective of this thesis is to study, detect and understand in greater detail the effect of external dynamical influences on interacting self-sustained oscillators.

Theoretical framework for the analysis of synchronization between non-autonomous oscillating systems is discussed. Multiple-scale analysis is applied on a phase oscillators model with slowly varying frequency. This analysis revealed the analytic form of the synchronization state with respect to slow and fast time-variations. Limit-cycle oscillators are used to study amplitude dynamics and to investigate synchronization transitions, which occur in the bifurcation points where the equilibrium solution for the phase difference and amplitudes changes their stability. Bifurcation diagrams as functions of coupling parameters are also constructed. In a case of non-autonomous interacting oscillators, the phase difference varies dynamically, the external influences can be the cause for synchronization transitions between different synchronization orders, and lag synchronization is hardly achievable. It is also demonstrated that the time-variations of the form of the coupling function alone can be the cause for synchronization transitions.

A method is introduced for analysis of interactions between time-dependent coupled oscillators, based on the signals they generate. It distinguishes unsynchronized dynamics from noise-induced phase slips, and enables the evolution of the coupling functions and other parameters to be followed. The technique is based on Bayesian

inference of the time-evolving parameters, achieved by shaping the prior densities to incorporate knowledge of previous samples. The dynamics can be inferred from phase variables, in which case a finite number of Fourier base functions are used, or from state variables exploiting the model state base functions. The latter is used for detection of generalized synchronization. The method is tested numerically and applied to reveal and quantify the time-varying nature of synchronization, directionality and coupling functions from cardiorespiratory and analogue signals. It is found that, in contrast to many systems with time-invariant coupling functions, the functional relations for the interactions of an open (biological) system can in itself be a time-varying process. The cardiorespiratory analysis demonstrated that not only the parameters, but also the functional relationships, can be time-varying, and the new technique can effectively follow their evolution.

The proposed theory and methods are applied for the analysis of biological oscillatory systems affected by external dynamical influences. The main investigation is performed on physiological measurements under conditions where the breathing frequency is varied linearly in a deterministic way, which introduces non-autonomous time-variability into the oscillating system. Methods able to track time-varying characteristics are applied to signals from the cardiovascular, and the sympathetic neural systems. The time-varying breathing process significantly affected the functioning and regulation of several physiological mechanisms, demonstrating a clear imprint of the particular form of externally induced time-variation. Specifically, the low breathing frequencies provoked more information flow, interfering the coordination and increasing the coupling strength between the oscillatory processes. Statistical analyses are performed to identify significant relationships. The proposed inferential method is applied to cardiorespiratory signals of this kind. The technique successfully identified that the cardiorespiratory coordination depends on, and is regulated to a great extent by, the respiration dynamics. The time-varying respiration acted as a cause for synchronization transitions between different orders. Additional complexity is encountered by the coupling functions which are also identified as time-varying processes.

A technique based on wavelet synchrosqueezed transform shows how the instantaneous phase can be extracted from complex mixed-mode signals with time-varying characteristics. The latter is demonstrated on several physiological signals of this kind. The dynamical characterization for the reproducibility of blood flow is shown to be more appropriate than the time-averaged analysis. This also implies that care must be taken when external perturbations are made consecutively.

Finally, the study focuses on analysis of analogue simulation of two non-autonomous van der Pol oscillators. The oscillators are unidirectionally coupled, and the frequency of the first oscillator is externally and periodically perturbed. The analogue simulation presents another model which encounters real experimental noise. The intermittent synchronization and the corresponding transitions are detected both through phase, and generalized synchronization, based on a common inferential basis.

1. INTRODUCTION

The only constant in life is change – it was Heraclitus, the famous philosopher, who laid down this sentence that has a profound and universal meaning. Many of us enjoy eating the sweet, healthy honey, produced by hard-working bees, collecting pollen from flower to flower. The flowers' seeds blown by the wind allow for the spread and the reproduction of the flowers. The wind itself depends on the sea and the position of the Moon with respect to the Earth, which in turn, rotates around the Sun. Regardless of how trivial it seems, the influence between these phenomena is essential, and very important in nature. If they were to be isolated, then some of their states, behavior or even their very existence would be questioned. External influences are what cause time evolutions to change, building up the diversity, synergy and complexity in nature – which makes life so fascinating.

The systems found in nature are thermodynamically open – they exchange mater and energy with their environment and the coexisting systems. Such systems are often found in biology and can be seen in many places, including cell populations in yeast and the processes that occur in animal vasculature. If one studies their time-evolution, they are considered to be dynamical systems [1]. Due to the time-dependent variations associated with the external influences, they can be also treated as non-autonomous dynamical systems [2]. The sources of time-dependent variations can influence the observed systems in various ways by altering their dynamical characteristics. Qualitative transitions and bifurcations can occur, which contribute to a non-equilibrium state [3]. A large group of systems exist that tend to maintain a certain degree of balance between the energy inflow and energy outflow, resulting in a time evolution that is repeatable on specific time scales. These systems form the group of nonlinear oscillators. One particular group of these are self sustained oscil-

lators, which in absence of external perturbations, have perfect balance between the dissipation and the constant energy source [4]. In nature, however, the reality is that processes are rarely found to be strictly periodic. External influences usually cause the oscillating processes to be quasi-periodic, or periodic with several characteristic frequencies.

Many biological processes are found to be oscillating. For example, it is known that six oscillatory processes exist in the human cardiovascular system [5, 6], or that the systems dynamics can be described by population and ensembles of many oscillators [7, 8]. If two or more oscillators coexist in the same environment, they can interact with each other in different directions and with different coupling strengths and coupling functions. When their rhythms adjust, due to these interactions, synchronization occurs [8–10]. Being able to understand and study the oscillating systems, their interactions and synchronization is of great importance in science and medicine. In a medical context, nonlinear oscillators and synchronization have been used extensively in relation to the non-invasive studies of anesthesia [11], ageing [6] and cardiorespiratory interactions [12], to name a few.

The cardiovascular system is one of the central systems in the human body, and is the main focus of this study. It is a complex oscillatory system [5, 6], associated with six physiological processes: cardiac, respiration, myogenic, neurogenic, endothelial metabolic and endothelial oscillatory activity. Each of the oscillators has characteristic periodic behavior, where the parameters that define the dynamics often vary with time. Fig. 1.1 (a) shows the time-variation of a human blood flow signal. The main cardiac activity is well observed as an oscillatory component around 1 Hz. From the projections, one can easily see that both the amplitude and the frequency are varying with time. When two or more oscillating processes interact, synchronization can occur. One of the most widely used methods for qualitative measurement of cardiorespiratory synchronization, the synchrogram [9] is shown on Fig. 1.1 (b). The 2π phase events of the heart relative to the 2π phase events of the breathing are plotted vertically. If (horizontal) stripes appear, synchronization is detected at certain synchronization ratio (for details see Appendix C). The synchrogram shows synchronization of the

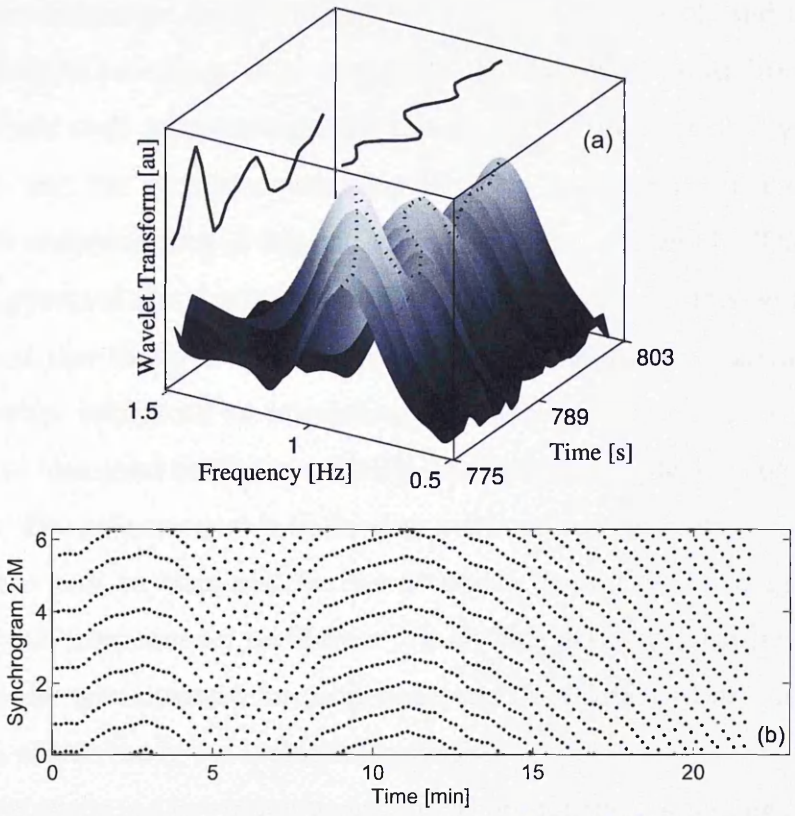

Fig. 1.1: Time-variations present in human cardiovascular oscillations. Wavelet transform of a human peripheral blood flow signal, within the cardiac frequency interval (a). Cardiorespiratory synchrogram (b).

heart with the respiration at a ratio of 2:8 (i.e.1:4) for the first 4.5 minutes, before a transition to a non-synchronized state. At 8 minutes, synchronization returns, but this time with a ratio of 2:9.

Although synchronization is obviously present in Fig. 1.1 (b), it is also apparent that the previous statement, that horizontal stripes are indicative of synchronization, does not always hold strictly true. The slightly curved nature of these horizontal lines indicates the presence of a time variability in the system. The analysis of Fig. 1.1 naturally raised several questions: why do qualitative transitions exist between synchronized and unsynchronized states, and why do transitions exist between different ratios? Could it be because the frequency and coupling of one or both of the oscillators is time varying? What can we learn about the dynamics of these time variations? The two figures demonstrate that time-variability is an inevitable part of

cardiovascular dynamics. Open biological systems can consist of, and interact with, many physiological processes. It is very likely that the time variability of these systems arises from their influence on each other. If this time variability is not taken into account, and the oscillators are considered to be isolated, an incomplete and even spurious understanding of the underlying dynamics will result. These ideas and observations provided the motivation and the problem to be addressed in this work.

The aim of this thesis is to study, detect and understand in greater detail the effect of external influences on interacting self-sustained oscillators – as motivated and applied to biological oscillators. Firstly, the underlying phenomena are analyzed theoretically. The primary goal is to develop methods and techniques that can detect the phenomena and to estimate the characteristic quantities, for a general case of interacting (non-autonomous) oscillators. Analyzing data from cardiovascular measurements, under non-autonomous conditions, can then demonstrate the benefits and the potential of this study for biological systems.

Theoretical study is a key requirement for a thorough understanding of an underlying problem and serves as functional foundation for successful and correct applications. Starting from the governing equations and studying the respective dynamics and qualitative behaviors, constitutes the direct (bottom-up) approach. Non-autonomous systems form an important group of dynamical systems [2, 13]. In this work, the attention is focused on those non-autonomous systems that are of importance for this particular study – the self-sustained oscillators. A vast number of publications exist that deal with the phenomena of synchronization [8, 14–17], but only in autonomous conditions, or they treat synchronization of non-autonomous systems [18, 19] which are not self-sustained oscillators – which is beyond the scope of our interest. Synchronization analysis of non-autonomous self-sustained oscillators was conducted, and the effect of the external force was linked with the qualitative dynamical transitions. The synchronization state itself is determined by the stability of the phase difference solution. In order to describe the underlying problem, various cases with different types of external sources and affected parameters are also investigated. This theoretical part broadens the perception and the understanding for general case of interacting

non-autonomous oscillators and lies down the necessary theoretical background for the rest of the work.

For biological and many other experimental studies, one needs to use various methods and techniques in order to infer and detect the phenomenon of interest. Using the measured signals as a starting point, and trying to understand and estimate the underlying dynamics and phenomena, is said to be an inverse (top-down) problem. Given the phases of two oscillators, the standard approaches in evaluating the presence of synchronization are based on the statistical properties of only the phase difference [20–22]. A vast number of work has been done regarding the possibility of detecting the couplings and directionality between oscillators [23–28]. However, the proposed techniques rely on a reasonable density of the observed phase-space, and they are easily challenged by the presence of time-variability and strong correlation of the two signals. On the other hand, recent work regarding the Bayesian inference of noisy inherent dynamics [29–32] opens new possibilities that have never been tested for the proposed problem. In this study, a new, self-consistent approach is proposed for detection of inherent phase dynamics from phase time-series of interacting noisy oscillators. It allows one to simultaneously estimate the synchronization, the directionality and the nature of coupling functions. The distinct characteristic of this approach is that due to the use of particular information propagation, one can trace the time-variability and the effect of the external forces on the parameters that drive the dynamics. It is also shown that useful inference can be conducted from the state space time-series. The Lyapunov asymptotic stability of the driven oscillator can then serve as an indication of the presence of synchronization. The developed methods and techniques, can be applied not only to biological signals, but to any experimental oscillatory time-series.

The proposed theory and methods are particulary suitable for the study of biological oscillating systems and their interactions. The presence of time-variability of characteristic parameters and the existence of external sources have already been identified in several publications [5, 6, 33]. In this thesis, the analyses are performed on data obtained from resting human subjects, whose breathing has been externally, and deterministically perturbed. The subjects' breathing is paced as a *ramp* i.e. the

respiration frequency is gradually decreased/increased within a certain time interval. This procedure induces time-variability in the observed oscillating processes in a controlled deterministic manner - thus presenting a case with true non-autonomous nature. The measured signals included electrocardiogram (ECG), blood pressure (BP), carbon dioxide (CO2) concentration and muscle sympathetic nerve activity (MSNA). The rare MSNA measurement has been used in the past for successful characterization of human sympathetic activity in diverse cases [34–36]. The data analyses were performed with several methods that can deal with the time-variability present in the signals: wavelet transform, wavelet phase coherence and windowed wavelet phase coherence [37, 38]. The results, together with the respective statistical analysis, identified the relationships and the coherence between the oscillatory components and the effect of the non-autonomous perturbations. In addition to this, a study has been conducted on cardiorespiratory interactions, which have played an important role in several previous studies [6, 11, 25]. Before starting the cardiorespiratory analysis, one needs to estimate the instantaneous phase from the complex ECG signal, a problem for which there is currently no known method that yields satisfactory results. Therefore, a technique is proposed for the detection of instantaneous phase from complex mix-mode signals, based on wavelet synchrosqueezed decomposition. The effect of time-varying perturbations on cardiorespiratory directionality, synchronization and their respective qualitative transitions, are identified and analyzed.

Furthermore, the study also explored the reproducibility of laser Doppler flowmetry (LDF) blood flow measurements, and how dynamical characterization is more appropriate than time-averaging approaches. Signals are analyzed from both human blood flow, and from numerical simulations of coupled oscillators that have been subjected to non-autonomous perturbations. It is shown that the variability, as well as the mean value, of the flux should be considered, and when subjecting the microvasculature to a perturbation, care should be taken to understand the role of oscillatory processes and the respective transient physiological response [39].

In order to investigate non-autonomous effects on other real oscillating systems, signals from analogue simulation are analyzed. The analogue simulation [40] is per-

formed in controlled experimental conditions, and a small amount of noise, which can be additive and/or multiplicative, is embedded in the signals, due to imperfections in the electronic equipment. The model consists of two unidirectionally coupled van der Pol oscillators, with the first one having periodic time-varying frequency. One of the main purposes of this study is to demonstrate how one should treat and detect the underlying phenomena from experiments. Comparative analysis of phase and generalized synchronization are also presented, together with their implications and limitations resulting from the presence of time-varying sources.

The thesis is organized as follows.

In Chapter 2 the main theoretical aspects of non-autonomous systems and their interactions are presented. The basic characteristics and formulations for non-autonomous systems and non-autonomous self-sustained oscillators are given, together with the generic formalism and definition of synchronization between such oscillators. Multiple-scale analysis is conducted on coupled non-autonomous phase oscillators revealing the relationship between the speed of the influence and the synchronization state. Concentrating on specific limit-cycle models, synchronization determination and dynamical characteristics for different cases of time-varying parameters are investigated. Detailed stability and bifurcation analysis are also demonstrated, followed by observation of the framework for different nature (periodic, stochastic and chaotic) of non-autonomous sources. The time-varying coupling function and its implications for synchronization transitions are discussed in detail. The content from this chapter serves as a theoretical foundation for the subsequent chapters.

Chapter 3 presents a method for the reconstruction of time-varying dynamics. The technical aspects about the implementation of Bayesian inference (which is the core of the method) are demonstrated. The use of inferred parameters for the detection of synchronization, coupling nature and directionality is presented in detail, and applied to several types of oscillatory systems. The detection of interacting time-varying dynamics in state space is also discussed, together with its implications for the detection of generalized synchronization.

The application of the proposed theory and methods on biological oscillatory processes is demonstrated in Chapter 4. The first part investigates the effect of time-varying breathing on the cardiovascular system and sympathetic nerve activity. Wavelet transform of time-varying frequency content is obtained and cardiorespiratory interactions are studied. A particular technique for phase detection from complex mix-mode signals is also presented. The second part of chapter 4 focuses on the reproducibility of LDF blood flow, which compares the dynamical approach with the time-averaged measures, and provides evidence that care is needed when the oscillators are subject to consecutive external perturbations.

Chapter 5 outlines analogue simulation of interacting non-autonomous van der Pol oscillators and demonstrates how synchronization can be treated in experiments. Under a common inference framework, both phase and generalized synchronization are treated. The last Chapter 6 provides a summary of work and outlines the future perspectives.

2. THEORETICAL BACKGROUND: NON-AUTONOMOUS SYSTEMS AND SYNCHRONIZATION

Physicists usually try to study isolated systems, free from external influences, that can be described precisely by well-defined equations. In practice, of course, this ideal is seldom completely realised and it is normally necessary to take account of a variety of external perturbations. Where the latter are parametric, i.e. tending to alter the parameters of the modelling equations, a wide range of often counter-intuitive effects can arise, e.g. the occurrence of noise-induced phase transitions [41] or spontaneous shifts in synchronization ratio in cardiovascular interactions [11], and particular care is needed in analysing the underlying physics. Such phenomena are especially important in relation to oscillatory systems, whose frequency or amplitude may be modified by external fields. One approach to the problem involves focusing on the idealised model system but, at the same time, accepting that it is *non-autonomous*, i.e. that one or more of its parameters may be subject to external modulation. Without some knowledge of the form of modulation, little more can be said other than admitting to the corresponding inherent uncertainty in the analysis. It often happens, however, that the external field responsible for the non-autonomicity may itself be deterministic, e.g. periodic. At the other extreme, it might be either chaotic or stochastic. In each of these cases, it is possible to perform a potentially useful analysis.

Oscillatory systems are widespread in nature and they are mostly, to a greater or lesser extent, non-autonomous. Analysis of their signals can often be used to infer information about them, even where very little is known *a priori*. Where two or more oscillatory systems mutually interact, synchronization may occur, in which there is a mutual adjustment of their respective frequencies [9]. It is a widespread phenomenon that arises in e.g. engineering [42], biology [11, 12, 43], communications [16], ecology

[44], meteorology [45], and deterministic chaos [15, 46, 47]. It is often useful to investigate synchronization phenomena because of the information such studies provide about the oscillators and, in particular, about their interactions. The situation considered is one where the non-autonomicity induces its own dynamics, superimposed on top of the dynamics of the synchronizing oscillatory systems. The possibility of understanding this higher dynamics is potentially important because it promises to allow the time series analyst to determine details of the non-autonomicity – e.g. its frequency and amplitude, and which term(s) of the model equation is/are affected – from measured signals. Thus the following discussion serves as a theoretical base for the study of the synchronization phenomenon under non-autonomous conditions.

2.1 Non-autonomous systems

Non-autonomous (Greek: *auto*-'self' + *nomos*-'law') systems are those whose law of behaviour is influenced by external forces. From a dynamical point of view, a set of differential equations are non-autonomous if they include an explicit time-dependance. The external influence can have different nature, for instance, it could be a periodic force, a quasi-periodic function or a noisy process, and it could affect the systems in a various ways i.e. it might be additive, could enter in the definition of a parameter, or might modulate the functional relationships that define the interactions between systems. When we focus our attention on only one or few components of a high dimensional autonomous dynamical system, we will actually be dealing with non-autonomous differential equations because of the time-variability embedded within their interactions with the rest of the system.

Often in the literature, and especially in inverse problems, the non-autonomous dynamics have been associated or referred to as non-stationary. The stationarity is a statistical property of the output signal, and as such is characterized by the application of tools for statistical mechanics [48]. In seeking to justify and motivate a different approach to the problem, first the connection between non-stationary and non-autonomous dynamics is outlined. The solution of an autonomous dynamical

systems $\mathbf{x}(t) = f(\mathbf{x})$ depends only on the time difference $(t - t_0)$ between the current state $\mathbf{x}(t)$ and the initial condition $\mathbf{x}(t_0)$. It therefore follows that the statistical behaviour of a bounded-space solution, if far enough from the initial condition, must be time-independent. In contrast, when a process is bounded and non-stationary, then it is clearly impossible to represent the driving dynamics with autonomous equations. For this reason, non-autonomous dynamics $\mathbf{x}(t) = f(\mathbf{x}, t)$ must constitute the core mechanism underlying a non-stationary output signal. On the other hand, for an appropriate time-dependence of the external dynamical field, it is possible that a non-autonomous dynamics may be perfectly stationary in the statistical sense. Hence non-autonomous dynamics can act as a functional "generator" for both stationary and non-stationary dynamics.

Non-autonomous dynamical systems have attracted considerable attention from mathematicians, much effort being expended on the development of a solid formalism [2, 13]. This included mainly the process and the skew product flow formalism. For the two-parameter semi group or process formalism, instead of only the time difference $t-t_0$, both the current time t and the starting time t_0 are important and play role. The skew product formalism includes an autonomous dynamical system as a driving mechanism which is responsible for the temporal and qualitative change of the vector field of the non-autonomous system. It has been discussed that, even though the process formalism is intuitive and the skew product formalism abstract, the latter contains more information about how the system evolves in time. The treatment of pullback attractors, with fixed target set and progressively earlier starting time $t_0 \to -\infty$ (as opposite from forward attractors with moving target and fixed t_0) gives additional insight for the analysis of non-autonomous attractors. The proposed theory has been found useful in number of applications, including switching and control systems [49] and complete (dissipative) synchronization [18, 19]. Being recently established and still evolving, this mathematical theory promises many application in more complex non-autonomous systems.

In the physics community, on the other hand, there seems to have been a degree of reluctance to address the problem as it really is and, in general, the issue has

been sidestepped by reducing the non-autonomous equation to an autonomous one by addition of an extra variable to play the role of time-dependence in $\mathbf{f}(\mathbf{x}, t)$. It has been argued that this approach is not mathematically justified because the new dimension is not bounded in time (as $t \to \infty$), and that attractors can not be defined easily. Certain transformation can be employed to bound the extra dimension, but this approach does not work in general case. Beside this, the procedure of reduction to autonomous form has been safely employed in many situation - especially in studies closely related with experiments, where the dynamical behaviour is observed for finite length of time. There are two cases, in particular, that recur in the literature: (i) where the dynamical field is a periodic function of t (i.e. $\mathbf{x} = \mathbf{f}(\mathbf{x}, \sin(t))$, often referred as an "oscillating external perturbation"); and (ii) when the dynamical field is stochastic (the noise being the time-dependent part). The first case is obviously one where an extra variable is often substituted, and the latter case involves the application of the mathematical instruments of stochastic dynamics. These can be seen as the two limiting-cases of an external perturbation that comes from a system with either one degree of freedom, or with an infinite number of degrees of freedom. In between these two extremes there is a continuum of cases when the time dependence is neither precisely periodic, nor purely stochastic. An example of an intermediate case of this kind would be a dynamical system $\mathbf{x} = \mathbf{f}(\mathbf{x}, g(t))$ where $g(t)$ is the n-th component of a chaotic (low dimensional) dynamical system.

The equations of the non-autonomous systems involve terms containing the independent variable on the right hand side. Hence, obtaining the exact solution can be difficult and not a trivial task, often unavoidable ending up as unsolvable. Moreover, there is no general mathematical technique for evaluation of solutions, but (similarly to nonlinear systems) each non-autonomous equation has its own type, or belongs to a group of solutions. Popular techniques for treatment (or sidestepping) include perturbation methods, non-homogenous differential equation, Floquet theory or instantaneous solutions.

The non-autonomous systems constitute a vast and very general class of systems. For the purpose of this thesis, and as motivated by the biological systems to be an-

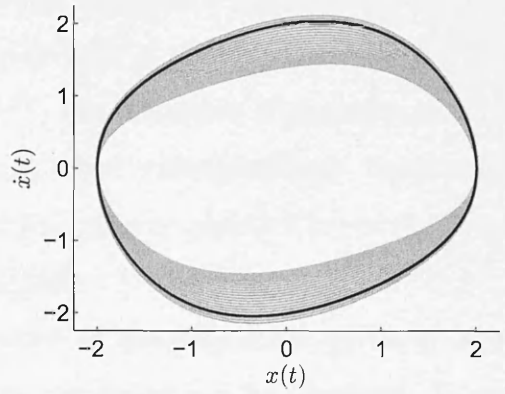

Fig. 2.1: Phase portrait of non-autonomous van der Pol oscillator with time-varying frequency. The black line is for autonomous ($\tilde{A} = 0$) and grey line for non-autonomous ($\tilde{A} = 0.3$) portrait. The system is given as: $\ddot{x} - \mu(1 - x)\dot{x} + [\omega + \tilde{A}\sin(\tilde{\omega}t)]^2 x = 0$, where $\omega = 1$, $\tilde{\omega} = 0.01$ and $\mu = 0.2$.

alyzed, the discussion is concentrated on non-autonomous self-sustained oscillatory systems. Anishchenko *et al* have enumerated [50] all of the common cases of non-autonomicity in oscillating dynamical systems, including those in which limit cycles are induced by external non-autonomous fields. In what follows, however, the discussion is restricted to self-sustained oscillators, which are taken to be those that exhibit stable limit cycles in the absence of the non-autonomous contribution. Thus, even though the characteristics of the oscillator (its frequency, shape of limit cycle, etc...) are varying, it can still be considered as self-sustained at all times.

2.1.1 Single non-autonomous self-sustained oscillator

Before discussing the interactions and the respective states and phenomenons (like synchronization, directionality or stability), an outline of the general characteristics of a single self-sustained oscillator subject to external non-autonomous source will be given. Consider an oscillator $d\mathbf{x}/dt = \mathbf{f}(\mathbf{x}(t))$ with a stable periodic solution $\mathbf{x}(t) = \mathbf{x}(t + T)$ in an absence of external influence, characterized by a period T. The field $\mathbf{f}(\mathbf{x}(t), t)$ can be set to be an explicit function of the time. This will be the case, for instance, if one or more of the parameters that characterize $\mathbf{f}$ are bounded (periodic or non-periodic) functions of time. The periodic solution $\mathbf{x}(t)$ is, in general,

lost; and the definition of the period T becomes somewhat "blurred". An example of such non-autonomous oscillator is presented on Fig. 2.1. In the absence of a periodic solution $\mathbf{x}(t) = \mathbf{x}(t+T)$, the definition of period could be replaced by the concept of "instantaneous period" (and correspondingly "instantaneous frequency"): at any instant of time τ the instantaneous period $T(\tau)$ of the dynamics is the period of the limit cycle solution of $\mathbf{f}(\mathbf{x}(t), \tau)$, with τ fixed.

Following the definition of phase-function, given by Kuramoto [10], a generalization for non-autonomous oscillators can be discussed. In an autonomous system, the phase over the limit cycle is defined as quantity which increases by 2π during each cycle of the dynamics. A non-autonomous version of the phase-function $\phi(\mathbf{x}, t)$ could then be defined as:

$$\frac{d\phi(\mathbf{x},t)}{dt} = \omega(t) + \frac{\partial\phi(\mathbf{x},t)}{\partial t}, \tag{2.1}$$

where $\omega(t) \equiv 2\pi/T(t)$ is the instantaneous frequency, i.e. the characteristic frequency of the limit cycle of the dynamics defined at a given time:

$$\omega(\tau) = 1/T(\tau) \int_0^{T(\tau)} \bigtriangledown_x \phi(\mathbf{x}(t), \tau) \cdot \mathbf{f}(\mathbf{x}(t), \tau) dt,$$

a natural generalization of the phase for an autonomous oscillator where $d\phi(\mathbf{x})/dt \equiv 2\pi/T = \bigtriangledown_x \phi\, \mathbf{f}(\mathbf{x})$. The second term in (2.1) can be present for example due to the non-isochronoucity of the oscillator i.e. due to the effect that the perturbed amplitudes have on the phase dynamics.

2.2 Synchronization of non-autonomous self-sustained oscillators

Synchronization between coupled oscillator is a universal physical phenomenon that arises in many areas of science. It is defined as: mutual adjustment of rhythms due to weak interactions between oscillatory systems [9]. When the oscillators are weakly nonlinear and the couplings are weak as well, the synchronization phenomenon can be described qualitatively and sufficiently well by the corresponding phase dynamics.

The latter is often referred to as phase synchronization [9, 15]. To set up a general description of synchronization between non-autonomous systems, two non-autonomous oscillators are set to interact through coupling function g_1, g_2 parameterized by the coupling constants ϵ_1, ϵ_2[1]:

$$\begin{aligned}\dot{\mathbf{x}}_1 &= \mathbf{f}_1(\mathbf{x}, t) + \epsilon_1\, \mathbf{g}_1(\mathbf{x}_1, \mathbf{x}_2) \\ \dot{\mathbf{x}}_2 &= \mathbf{f}_2(\mathbf{x}, t) + \epsilon_2\, \mathbf{g}_2(\mathbf{x}_1, \mathbf{x}_2)\,.\end{aligned}$$

When the frequency mismatch is relatively small, one can observe for which parameter values the system is synchronized and does not exhibit phase-slips [9], i.e. when $|\psi(\phi_1, \phi_2, t)| < \text{constant}$, where the phase difference is defined as[2]: $\psi(\phi_1, \phi_2, t) \equiv \phi_2(\mathbf{x}_2(t), t) - \phi_1(\mathbf{x}_1(t), t)$. Using Equ. (2.1) the time derivative of the phase difference $d\psi/dt$ can be expressed explicitly as:

$$\begin{aligned}\frac{d\psi(\phi_1, \phi_2, t)}{dt} &= (\bigtriangledown_x \phi_2)\ (\mathbf{f}_2(\mathbf{x}_2, t) + \epsilon_2\, \mathbf{g}_2(\mathbf{x}_1, \mathbf{x}_2)) + \\ &\quad -(\bigtriangledown_x \phi_1)\ (\mathbf{f}_1(\mathbf{x}_1, t) + \epsilon_1\, \mathbf{g}_1(\mathbf{x}_1, \mathbf{x}_2)) + \\ &\quad + \frac{\partial \phi(\mathbf{x}_2, t)}{\partial t} - \frac{\partial \phi(\mathbf{x}_1, t)}{\partial t} \\ &= \epsilon_2\, \bigtriangledown_x\, \phi_2 \cdot \mathbf{g}_2(\mathbf{x}_1, \mathbf{x}_2) - \epsilon_1\, \bigtriangledown_x\, \phi_1 \cdot \mathbf{g}_1(\mathbf{x}_1, \mathbf{x}_2) \\ &\quad + \frac{\partial \phi(\mathbf{x}_2, t)}{\partial t} - \frac{\partial \phi(\mathbf{x}_1, t)}{\partial t} + \frac{2\pi}{T_2(t)} - \frac{2\pi}{T_1(t)}.\end{aligned}$$

The synchronization condition $|\psi(\phi_1, \phi_2, t)| < \text{constant}$ will be satisfied if there exists a stable solution for the dynamics $d\psi(\phi_1, \phi_2, t)/dt$. Because the velocity field is a function of time explicitly dependant on the terms $\frac{\partial \phi(\mathbf{x}_i, t)}{\partial t}$, the existence of a stable equilibrium $\psi_{\text{eq}}(t)$ satisfying $d\psi(\phi_1, \phi_2, t)/dt = 0$ does not mean that the relative phase remain constant. Not even the existence of a time-dependent stable root can guarantee an absence of phase-slips: as $\psi_{\text{eq}}(t)$ changes, the instantaneous phase difference $\psi(t)$ may fall outside the basin of attraction, in which case a phase-slip occurs, perhaps to

[1] In general, the coupling parameters and functions can also be time-dependent (as discussed later), but for simplicity and clarity they are considered autonomous in this notation.

[2] The last statement holds also for higher frequency ratios in the form $\psi = n\phi_2 - m\phi_1$ where n and m are integer numbers.

another equilibrium point. But if $\psi_{\mathrm{eq}}(t)$ changes in time slowly enough for the solution $\psi(t)$ to remain continuously within its attracting basin, then the phase difference will vary with time (as imposed by the non-autonomous source) while the system remains within the state of synchronization.

2.3 Phase oscillators model

When limit-cycle oscillators are coupled weakly, their interactions can be studied by means of phase oscillators [10] – which, by neglecting the amplitude dynamics, represent approximative notation of the oscillators' full dynamics. The justification of the latter arises because the amplitudes are robustly stable, unlike the phase dynamics which correspond to the direction of the limit-cycle and are border-line stable. In terms of Lyapunov exponents this means that the amplitude dynamics are described by negative, while the phase with zero Lyapunov exponents. This sensitive stability of the phase dynamics can be easily affected even by weak perturbations in terms of coupling interactions or other external sources. Therefore, the phase oscillators serve as functional models that can describe qualitatively the interactions, the synchronization phenomenon and the corresponding transitions.

A simple model of two coupled phase oscillators is used for the study of synchronization phenomenon under the influence of external non-autonomous sources. This elementary model does not capture the whole dynamics (mostly because it omits the amplitude dynamics), but serves as a good starting example where the synchronization phenomenon and the respective qualitative nature can be observed in easy and transparent way. The following also presents one of the most used procedures for treating non-autonomous problems – which includes reductions to autonomous form and multiple time scale analysis [51, 52].

The model consists of two phase oscillators, where the frequency of the first oscil-

lator is periodically perturbed:

$$\begin{aligned}\frac{d\phi_1}{dt} &= \omega_1 + \tilde{A}\sin(\tilde{\omega}t) + \epsilon_1 \sin(\phi_2 - \phi_1) \\ \frac{d\phi_2}{dt} &= \omega_2 + \epsilon_2 \sin(\phi_1 - \phi_2).\end{aligned} \tag{2.2}$$

The two oscillators are synchronized if their phase difference is bounded $|\phi_2(t) - \phi_1(t)| = |\psi(t)| < \text{const}$ [9], and if the equilibrium solution remains in its attraction basin. Hence, for synchronization purposes the dynamics of Eqs. (2.2) can be studied through the phase difference $\psi(t)$ dynamics.

The non-autonomous source (for different frequency and amplitude) can affect the dynamical behavior of the phase difference and the synchronization state itself. Instead of being constant, like in autonomous case, now the phase difference can vary with time, as imposed by the non-autonomous source. If the amplitude of the non-autonomous source is relatively large, for certain time intervals the oscillators can go in and out of synchrony – which due to the periodicity of the perturbation can result in intermittent synchronization. The effect of the non-autonomous sources on the dynamical behaviour of the interacting oscillators including amplitude dynamics, will be discussed in more detail in Sec. 2.4.

The equations in system (2.2) are nonlinear non-autonomous equations that can not be solved exactly. In such situation the most common approach for analytical treatment of non-autonomous equations is introducing an additional dimension for the independent variable. Even though mathematically not fully justified (for reasons discussed above in Sec. 2.1), this procedure often allows useful analysis to be conducted. If the oscillating frequency mismatch ($\omega = \omega_2 - \omega_1$) is significantly larger compared to the frequency $\tilde{\omega}$ of the non-autonomous source ($\tilde{\omega}/\omega \ll 1$), one can try to analyze the dynamics on two separate and independent time scales (slow and fast). When the frequency $\tilde{\omega}$ is smaller than the order of the other parameters – singular perturbation theory can be applied.

Grouping the phases into the phase difference variable $\psi(t) = \phi_2(t) - \phi_1(t)$ and

transforming the equations to autonomous form, system (2.2) becomes:

$$\begin{aligned} \frac{d\psi}{dt} &= \omega - \tilde{A}\sin(z) - \epsilon\sin(\psi) \\ \frac{dz}{dt} &= \varepsilon\nu, \end{aligned} \tag{2.3}$$

where $\tilde{\omega} = \varepsilon\nu$, with ε being the small parameter and $\nu = \text{const}$; and the frequency mismatch is $\omega = \omega_2 - \omega_1$ with group coupling $\epsilon = \epsilon_1 + \epsilon_2$. The variable $\psi(t)$ is fast, while $z(t)$ is slow variable.

First, system (2.3) is analyzed for *slow time-scale* by introducing $\tau = \varepsilon t$ and rescaling accordingly to:

$$\begin{aligned} \varepsilon\frac{d\psi}{d\tau} &= \omega - \tilde{A}\sin(z) - \epsilon\sin(\psi) \\ \frac{dz}{d\tau} &= \nu. \end{aligned} \tag{2.4}$$

As $\varepsilon \to 0$ the trajectories of system (2.3) converge during slow epochs to solutions of the slow subsystem (2.4) - often called the critical manifold or quasi-steady state. Substituting τ back for the z variable ($z = \tau\nu = \tilde{\omega}t$), the solution of the slow subsystem is expressed as:

$$\psi(t) = \arcsin\left(\frac{\omega - \tilde{A}\sin(\tilde{\omega}t)}{\epsilon}\right). \tag{2.5}$$

The results, for particular parameters are presented on Fig. 2.2. The synchronized case on Fig. 2.2 (a) shows the phase difference variations with period $T = \tilde{\omega}/2\pi$, while the intermittent synchronization and the transitions to in and out of synchrony are presented on Fig. 2.2 (b). Both examples demonstrate that for slow non-autonomous source, solution (2.5) resembles the dynamics in good agreement with the numerical simulation (compare red and grey lines).

The stability of the phase difference $\psi(t)$, and thus the synchronization state, can be determined by linearization about the quasi-steady equilibrium. Linearization for

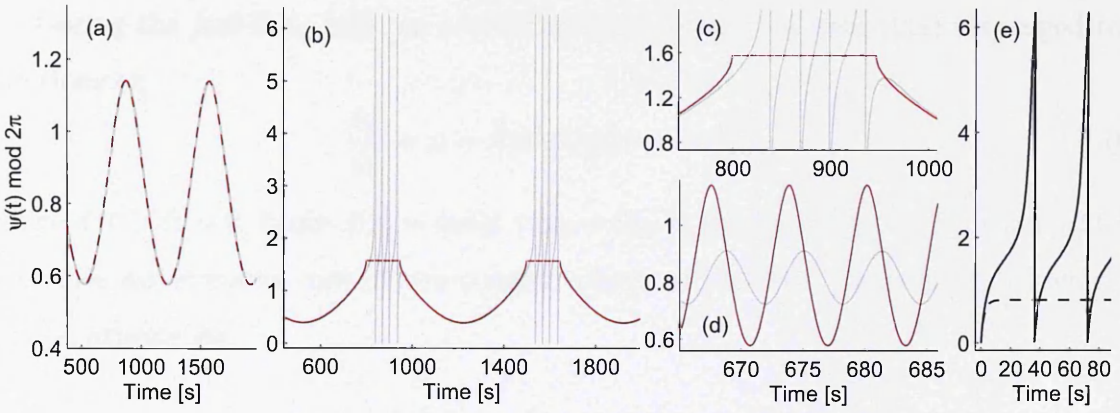

Fig. 2.2: (a)-(d) Comparison of slow time scale analytic solution (2.5)-red line and numerical simulation of the full system (2.2)-grey line, with $\tilde{A} = 0.1$, $\tilde{\omega} = 0.009$, $\omega = 0.4$ and $\epsilon = 0.55$: (a) synchronization case, (b) intermittent case $\tilde{A} = 0.19$ - horizontal red line indicates where solution (2.5) is not defined; (c) enlarged transitions segment from (b); (d) synchronous case for fast external force $\tilde{\omega} = 1$. (e) The fast time scale analytic solution (2.7) with black: dashed line for synchronization case, and with full line unsynchronized case for $\epsilon = 0.36$ exhibiting phase slips.

the solution (2.5) yields:

$$\frac{d\psi(t)}{dt} = -\epsilon\sqrt{1 - \frac{[\omega - \tilde{A}\sin(\tilde{\omega}t)]^2}{\epsilon^2}}.$$

The stability requirement $(d\psi(t)/dt < 0)$ gives the synchronization condition: $[\omega - \tilde{A}sin(\tilde{\omega}t)]/\epsilon < 1$. The latter allows the critical couplings for transitions between synchronization, intermittent synchronization and non-synchronization to be determined:

$$\begin{cases} \epsilon > \omega + \tilde{A} & : \text{synchronization} \\ \omega - \tilde{A} < \epsilon < \omega + \tilde{A} & : \text{intermittent synchronization} \\ \omega - \tilde{A} > \epsilon & : \text{non} - \text{synchronization} \end{cases}$$

Even though the solution for the slow time scale (2.5) qualitatively captures the dynamics (as shown on Fig. 2.2 (a) and (b)) it fails to describe the fast transitions, as pointed out on the enlarged segment on Fig. 2.2 (c). Also the dynamics perturbed by faster non-autonomous sources can not be described by the same solution - Fig. 2.2 (d). This is where the fast epochs of the original system play an important role.

During the *fast time-scale*, as $\varepsilon \to 0$ the trajectories of system (2.3) converged to solutions of:

$$\frac{d\psi}{dt} = \omega - \tilde{A}\sin(\tilde{\omega}t_0) - \epsilon\sin(\psi), \tag{2.6}$$

where $dz(t)/dt = 0$, hence $z(t) = \text{const} = z_0 = \tilde{\omega}t_0$ in the limit $\varepsilon \to 0$. Equation (2.6) describes *autonomous case* of two coupled phase oscillators - the solution of which can be express as:

$$\psi(t) = \arctan\left(\frac{1}{\omega_a}\left[\tan(\frac{1}{2}t\sqrt{\omega_a^2 - \epsilon^2})\sqrt{\omega_a^2 - \epsilon^2} + \epsilon\right]\right), \tag{2.7}$$

where $\omega_a = \omega - \tilde{A}\sin(\tilde{\omega}t_0)$ for simpler notation. The latter solution Eq. (2.7) is responsible for the dynamics of the fast synchronization transitions. The phase slips appearing where the slow-time scale solution is not defined (horizontal lines Fig. 2.2 (b) and (c)) - are govern by dynamics described by this solution (2.7) - Fig. 2.2 (e). The fast initial transient dynamics are also described by Eq. (2.7). The physical interpretation implies that the effect from the fast external sources on averaged is reduced within one cycle of oscillation, and the variations of $\psi(t)$ are hinder, converging to the autonomous case.

The multiple time-scale approach allowed the dynamics of the full system (2.2) to be described and understand by analyzing the fast and slow time-scale subsystems (2.3) and (2.4), respectively. The solution (2.5) of the slow subsystem described the time-varying dynamics and the intermittent synchronization transitions. The fast time-scale solution (2.7) converged to solution of autonomous synchronization case. The latter solution described the fast transitions and the phase slips dynamics during the unsynchronized states.

2.4 Limit-cycle oscillators model

In this section the synchronization phenomenon is presented on a model of interacting limit-cycle oscillators. The effect of the non-autonomous sources on the interactions is studied both on phase and amplitude dynamics. Dynamical characterization is

also shown for different types of non-autonomous sources, acting on several important properties of the oscillators' interaction. The systems also serve as model for determination of the stability and synchronization state.

2.4.1 The model

The Poincaré oscillator was chosen as an example of a non-autonomous limit-cycle system whose dynamical field can be made explicitly time-dependent. In polar coordinates (r, ϕ), it rotates at a constant-frequency, attracted with exponential velocity towards the radius, $\dot{r} = \alpha r(a - r)$; $\dot{\phi} = \omega$. Here ϕ represents both the angle variable and the phase of the oscillator, making it isochronous oscillator. Another advantageous property of the Poincaré oscillator is that the signal is purely sinusoidal, without any high frequency harmonics, which allows better traceability of any frequency variations over time.

A model of two weakly interacting Poincaré oscillators in terms of Euclidean coordinates, takes the form:

$$\begin{aligned} \dot{x}_1 &= -q_1 x_1 - \omega_1(t) y_1 + \epsilon_1(t) g_{11}(x_1, x_2) \\ \dot{y}_1 &= -q_1 y_1 + \omega_1(t) x_1 + \epsilon_1(t) g_{12}(y_1, y_2) \end{aligned} \tag{2.8}$$

$$\begin{aligned} \dot{x}_2 &= -q_2 x_2 - \omega_2(t) y_2 + \epsilon_2(t) g_{21}(x_1, x_2) \\ \dot{y}_2 &= -q_2 y_2 + \omega_2(t) x_2 + \epsilon_2(t) g_{22}(y_1, y_2) \end{aligned} \tag{2.9}$$

$$q_i = \alpha_i \left(\sqrt{x_i^2 + y_i^2} - a_i \right).$$

The dynamics of each subsystem is described by states (x_i, y_i), where $i = 1, 2$ denotes the oscillator. Parameters α_i and a_i are constants (a_i being the amplitude parameter), ω_i are angular frequencies, ϵ_i are the coupling amplitudes and $g_{i1}(x_1, x_2)$, $g_{i2}(y_1, y_2)$ are the coupling functions. The frequency and coupling parameters each consist of a leading constant part and a small non-autonomous term: $\omega_1(t) = \omega_1 + \tilde{A}_{11} \sin(\tilde{\omega}_{11} t)$, $\omega_2(t) = \omega_2 + \tilde{A}_{21} \sin(\tilde{\omega}_{21} t)$, $\epsilon_1(t) = \epsilon_1 + \tilde{A}_{12} \sin(\tilde{\omega}_{12} t)$ and $\epsilon_2(t) = \epsilon_2 + \tilde{A}_{22} \sin(\tilde{\omega}_{22} t)$, where $\tilde{A}_{i1}$ and $\tilde{\omega}_{i1}$ are small compared to ω_i, while $\tilde{A}_{i2}$ and $\tilde{\omega}_{i2}$ are small compared

to ϵ_i. Note that, in the absence of the non-autonomous terms ($\tilde{A}_{11} = \tilde{A}_{12} = \tilde{A}_{21} = \tilde{A}_{22} = 0$), the oscillators generate self-sustained oscillations [4, 50]. This implies that the non-autonomicity here should be seen, not as a source of oscillations, but more as an external perturbation/influence on the autonomous form of the oscillators, which of course have their own inherent oscillatory dynamics. In this case, the non-autonomous terms present in the system (2.8), (2.9) obviously come from periodic external modulations – some forms of non-periodic non-autonomous terms, and their implications for synchronization, are discussed in Sec. 2.4.6.

2.4.2 Analytic calculations

As already indicated, the phases of the oscillators in Eqs.(2.8) are given by the angular coordinate ϕ:

$$\dot{\phi}_i = \frac{d}{dt} \arctan \frac{y_i}{x_i},$$

where the *arctan* is defined as four-quadrant operation. Developing the right-hand term for the derivative of the phase difference $\dot{\psi} \equiv \dot{\phi}_2 - \dot{\phi}_1$, one obtains:

$$\begin{aligned} \dot{\psi} = &- \omega_2(t) + \omega_1(t) + \frac{\cos\phi_2}{r_2}\epsilon_2(t)g_{22}(x_1, x_2) - \frac{\sin\phi_2}{r_2}\epsilon_2(t)g_{21}(x_1, x_2) + \\ &- \frac{\cos\phi_1}{r_1}\epsilon_1(t)g_{12}(x_1, x_2) + \frac{\sin\phi_1}{r_1}\epsilon_1(t)g_{11}(x_1, x_2). \end{aligned} \tag{2.10}$$

The case where the coupling functions are linear and of the form: $g_1(x_1, x_2) = x_2 - x_1, g_2(y_1, y_2) = y_2 - y_1, g_3(x_1, x_2) = x_1 - x_2, g_4(y_1, y_2) = y_1 - y_2$ was considered. After some trivial algebra, the analytic expression for $\dot{\psi}$ is obtained (details given in Appendix B).

Next, a change of variables was performed by substitution of $\phi_2 = \psi + \phi_1$. Because ϕ_1 changes much faster that ψ, one can average $\dot{\psi}$ by integrating over ϕ_1:

$$\langle\dot{\psi}\rangle = \frac{1}{2\pi}\int_0^{2\pi} \dot{\psi}\, d\phi_1 = -\omega_2(t) + \omega_1(t) - \left(\epsilon_2(t)\frac{r_1}{r_2} + \epsilon_1(t)\frac{r_2}{r_1}\right)\sin\psi.$$

Similarly, after the integration of the fast variable, one can write the mean velocity

of the amplitudes r_1 and r_2 as:

$$\langle \dot{r}_1 \rangle = \frac{1}{2\pi} \int_0^{2\pi} \dot{r}_1 \, d\phi_1 = a_1 r_1 \alpha_1 - {r_1}^2 \alpha_1 - \epsilon_1(t)(r_1 - r_2 \cos\psi)$$

$$\langle \dot{r}_2 \rangle = \frac{1}{2\pi} \int_0^{2\pi} \dot{r}_2 \, d\phi_2 = a_2 r_2 \alpha_2 - {r_2}^2 \alpha_2 - \epsilon_2(t)(r_2 - r_1 \cos\psi).$$

To obtain an equilibrium solution for the synchronization regime requires that one solves

$$\begin{cases} \dot{\psi} = \omega_1(t) - \omega_2(t) + \left(-\frac{r_2 \epsilon_1(t)}{r_1} - \frac{r_1 \epsilon_2(t)}{r_2} \right) \sin\psi = 0 \\ \dot{r}_1 = a_1 r_1 \alpha_1 - {r_1}^2 \alpha_1 - r_1 \epsilon_1(t) + r_2 \epsilon_1(t) \cos\psi = 0 \\ \dot{r}_2 = a_2 r_2 \alpha_2 - {r_2}^2 \alpha_2 - r_2 \epsilon_2(t) + r_1 \epsilon_2(t) \cos\psi = 0 \end{cases} \tag{2.11}$$

and analyze the equilibrium of the system in respect of the three variables ψ, r_1, r_2. To find the solution for the system in Eq.(2.11) a numerical multidimensional minimizer [53] was employed, which returns a solution $\{\psi_{\text{eq}}, r_{1\text{eq}}, r_{2\text{eq}}\}$. The equilibrium is stable when the eigenvalues of the Jacobian matrix of the functions $\{\dot{\psi}, \dot{r}_1, \dot{r}_2\}$, in respect of the three variables $\{\psi, r_1, r_2\}$, have negative real parts.

It is important to note that this approach of stability analysis through the eigenvalues for the parameters at each time i.e. through instantaneous eigenvalues, is not valid in general when the systems are time-varying. There are number of practical examples, however, where this approach has been safely used for determination of synchronization [54, 55], but also some counter examples were pointed out as well [56]. For the model under investigation and the types of non-autonomous sources considered, this approach was able to determine correctly the stability of system (2.11) and the synchronization state. The last was consistent with other methods for synchronization detection, Lyapunov exponents evaluation and numerical bifurcation analysis.

2.4.3 Dynamical behaviour and synchronization analysis

There are many natural oscillatory systems that have characteristic frequencies which vary in time, examples being the cardiovascular system [5, 6, 26] and brain [33]. In order to understand them, one needs to consider the origins of this variability and to establish how it affects the nature of the oscillations and the mutual interactions between the oscillators. As a first step, synchronization between a pair of limit-cycle oscillators is studied, where one of the oscillators has an explicitly time dependent frequency. It is unidirectionally coupled to the other oscillator, which is autonomous. The two Poincaré oscillators (2.8) and (2.9) are set up with the following parameters: $\alpha_i = a_i = 1$, $\epsilon_1 = 0$, $\epsilon_2 = 0.38$, $f_1 = 1\,\mathrm{Hz}$, $f_2 = 0.95\,\mathrm{Hz}$ (where $\omega_i = 2\pi f_i$; $i = 1, 2$) and the coupling functions are specified as linear $g_{21}(x_1, x_2) = x_1 - x_2$ and $g_{22}(y_1, y_2) = y_1 - y_2$. The oscillating frequency of the first oscillator is time-varying due to the presence of the non-autonomous term – in respect of parameters this mean that $\tilde{A}_{11} = 0.23$ and $\tilde{f}_{11} = 0.003\,\mathrm{Hz}$, and the other parameters are $\tilde{A}_{12} = \tilde{A}_{21} = \tilde{A}_{22} = \tilde{f}_{12} = \tilde{f}_{21} = \tilde{f}_{22} = 0$.

The model was simulated numerically by fourth-order Runge-Kutta integration; the same method was also used for the other simulations described below. The time

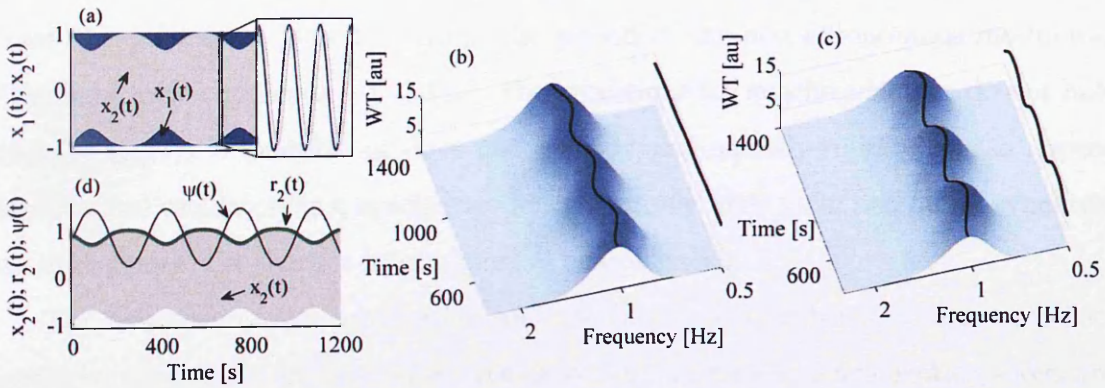

Fig. 2.3: Dynamical behaviour of the unidirectionally-coupled ($1 \to 2$) Poincaré oscillators (2.8), (2.9), with slow periodic variations in the frequency of oscillator-1. The parameter values used are given in the text. (a) Signals $x_1(t)$ and $x_2(t)$ are shown by the full and dashed lines respectively. Parts (b) and (c) show time-frequency analyses of $x_1(t)$ and $x_2(t)$ respectively using the wavelet transform. The variations in frequency and amplitude can be seen from the lines of peak values, and their projections on the amplitude-time planes, respectively. (d) Comparison of analytically evaluated ($r_2(t)$, $\psi(t)$) and numerical ($x_2(t)$) analyses. The values for $\psi(t)$ are given in $\{-\pi, \pi\}$ radians.

evolution of the signals is shown on Fig. 2.3 (a). The corresponding time-frequency wavelet representation of the first oscillator is shown in Fig. 2.3 (b); (details about wavelet analysis are given in chapter 4). The time-frequency variations of the peak value line are clearly evident. For the chosen parameters, the oscillators can synchronize, even though the frequency of the first oscillator is time-varying. The second oscillator oscillates with a correspondingly time-varying frequency Fig. 2.3 (c), due to the effect of synchronization. The oscillator has turned from one whose frequency is constant into one whose frequency is time-varying, and in order to retain the phase locking its amplitude also starts to vary with time (shown in Fig. 2.3 (a) and on the projection in Fig. 2.3 (c)). The variations of r_2 and ψ are presented in Fig. 2.3 (d). It is immediately evident that the phase difference is not constant (as in classical autonomous synchronization) but varies with time, as imposed by the non-autonomous term. The evaluation of the stability condition of $(r_{1\mathrm{eq}}(t), r_{2\mathrm{eq}}(t), \psi_{\mathrm{eq}}(t))$ for system (2.11) showed that the two oscillators are synchronized.

Next, it was investigated what happens when the two oscillators lose synchrony. The coupling was set to $\epsilon_2 = 0.26$ and the amplitude of the non-autonomous term was increased to $\tilde{A}_{11} = 0.25$; (all the other parameters were same as in Fig. 2.3). It was found that for some intervals within the period of the non-autonomous modulation (the light gray regions in Fig. 2.4 (a)) the conditions for synchronization do not hold: $(r_{2\mathrm{eq}}(t), \psi_{\mathrm{eq}}(t))$ is unstable or does not exist, a continuously-running phase appears and the two oscillators lose synchrony. More precisely, they go in and out of synchrony as time passes, i.e. there is intermittent synchronization.

The existence of synchronization and the corresponding transitions were investigated by application of method for the detection of phase synchronization - synchrogram [9] Fig. 2.4 (b) and (c). (Details of the implementation are given in Appendix C.) The synchrogram provides a qualitative measure where (for autonomous systems) the appearance of horizontal lines is normally taken to correspond to the synchronous state. The method clearly detect synchronization consistently with our analysis. The synchrograms show, however, that now synchronization is characterized by a smooth curve rather than a horizontal line, owing to the continuously changing phase shift

induced by the non-autonomous modulation.

The non-autonomous source can also induce transitions between different frequency synchronization ratios. This situation is often encountered in high order interactions of open oscillatory systems - obvious example being the cardiorespiratory system (to be discuss in later chapters). Numerical example of this kind is presented on Fig. 2.4 (c) – the Poincaré oscillators (2.8), (2.9) now had quadratic coupling function $g_{21}(x_1, x_2) = (x_1 - x_2)^2$ and $g_{22}(y_1, y_2) = (y_1 - y_2)^2$, with other parameters $\tilde{A}_{11} = 0.4$, $\tilde{\omega}_{11} = 0.008\,\mathrm{Hz}$, $\omega_1 = 2$, $\omega_2 = 3.013$ and $\epsilon_2 = 0.8$. The synchrogram shows consecutive transitions from 2:2 (or 1:1) to 2:3 frequency locking, with short non-synchronized epoches in between. The external influence caused not only the system to loose and gain synchrony, but also induced qualitative transitions between different synchronization states.

Another important property that defines the states of an interaction is the coupling

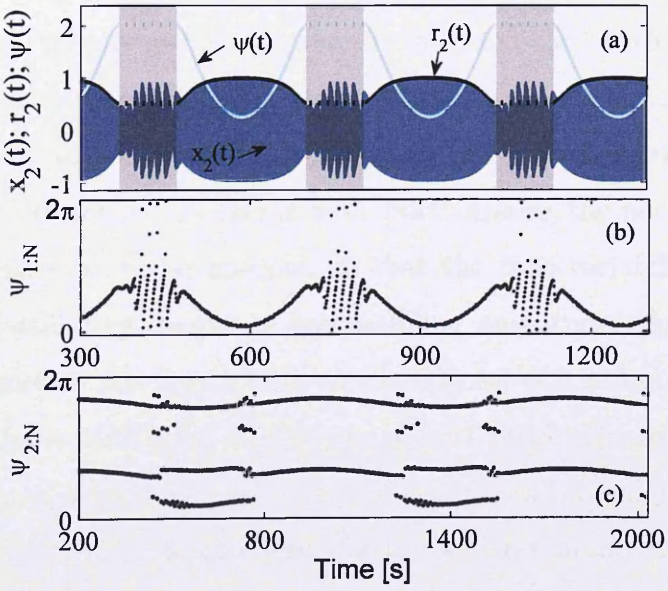

Fig. 2.4: Intermittent synchronization transitions for unidirectionally coupled ($1 \rightarrow 2$) Poincaré oscillators (2.8), (2.9). (a) $r_2(t)$, $\psi(t)$ are obtained from analytic calculations and $x_2(t)$ (only its envelope is resolved) from numerical simulation. The light gray regions indicate the non-synchronous state. The dashed lines of $\psi(t)$, $r_2(t)$ within this state indicate existence of phase-slips or that an analytic solution does not exist. (b) 1:N synchrogram for the case under (a). (c) 2:N synchrogram showing synchronization transitions from 2:2 to 2:3 ratio.

strength. Similarly, to the previously discussed case of time-varying frequency, the coupling parameter can also be affected by non-autonomous force, turning the synchronization state time-varying. The corresponding phase difference and amplitudes will turn time-varying, while the oscillating frequencies will not vary substantially. There can be synchronization transitions depending on the nature of the external force.

The definition states that the synchronization phenomenon is a result of the interplay between the frequency missmach and weak interaction between the oscillators. Hence, the interaction of oscillators found in nature often encounter the case where a non-autonomous external modulation is acting on both the frequency and the interaction strength at the same time. Moreover, the time-varying interactions can be bidirectional, affecting both of the oscillators and the underlying synchronization state. Such circumstances are relatively complex, but they reflect more closely the time-variability present in the open complex oscillatory systems found in nature [5]. Therefore, the two Poincaré oscillators were investigated each with non-autonomous time-varying frequency, interacting bidirectionally, with the coupling amplitude time-varying as well. This represents the full model (2.8), (2.9) i.e. where all the components are active and none of the parameters is zero. Furthermore, the non-autonomous parameters were considered to be unequal, so that the time-variability introduced is different in each oscillating frequency and coupling amplitude. In respect of non-autonomous parameters this meant that: $\tilde{A}_{11} = 0.3, \tilde{A}_{21} = 0.225, \tilde{A}_{12} = 0.155, \tilde{A}_{22} = 0.13, \tilde{f}_{11} = 0.005, \tilde{f}_{21} = 0.0075, \tilde{f}_{12} = 0.004$ and $\tilde{f}_{22} = 0.0045$. The rest of the parameters were set to be: $\alpha_i = a_i = 1$, $\epsilon_1 = 0.32$, $\epsilon_2 = 0.4$, $f_1 = 1\,\text{Hz}$ and $f_2 = 0.95\,\text{Hz}$. The results presented on Fig. 2.5 indicate that due to the external forces, both of the amplitudes and the frequencies are varying with time, while the oscillators are in a state of synchronization. The form of the variations is rather complex, even though the non-autonomous sources are simple periodic signals. It is important to note that this complex figure will cause potential difficulty to a data analyst when trying to identify the nature of the dynamics and the effect on synchronization. Therefore, proper tools are needed for inference and analyses of the underlaying dynamical characteristics.

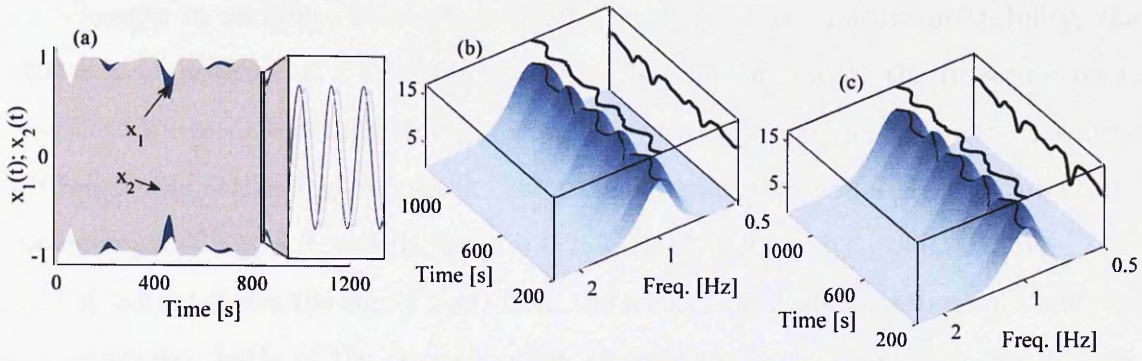

Fig. 2.5: Numerical simulations of bidirectionally coupled Poincaré oscillators (2.8), (2.9), with variations in the oscillator frequencies and the strengths of the inter-oscillator couplings, but such that the oscillators remain in synchrony. (a) Signals $x_1(t)$ and $x_2(t)$ are indicated by full blue and grey dashed line respectively. Time-frequency wavelet analysis is applied (b) to $x_1(t)$ and (c) to $x_2(t)$.

The external source can affect different properties of the systems, here only the cases that are of interest for this study were outlined. For example, the unidirectionally coupling can be reverse, where the autonomous can drive the non-autonomous oscillator. In this case the time-variability can be reduced or totally suppressed. The non-autonomous source can affect not only the parameters, but also the functional relationship existing among the oscillators. Very important example of this kind is the time-variability of the coupling function - for which special attention will be given in the next chapter.

2.4.4 Stability and bifurcation analysis

This section presents the analysis needed to determine the stability of synchronization state of non-autonomous oscillators. Note that the investigating is not focused on the stability of the oscillators themselves, but on the stability of the composite system (2.11), through which one can determine whether or not the two oscillators are synchronized [9, 57]. One can do this by evaluation of the three eigenvalues obtained from the Jacobian matrix of the linearized system (2.11), $\lambda_1, \lambda_2, \lambda_3$, for given parameters at every instant of time. Because the oscillating systems (2.8), (2.9) have a relatively large number of parameters, especially those coming from the four non-autonomous terms, there are rich possibilities for dynamical changes in stability and bifurcations:

e.g. changes in stability, bifurcation points, changes in the nature of stability, the existence or absence of a solution, etc. For the sake of clarity, the presentation is restricted to the case of unidirectional coupling with only one non-autonomous source applied to the oscillating frequency. The parameters of the model are the same as in the example of Fig. 2.3, except for $\epsilon_2 = 0.255$, $\tilde{A}_{11} = 0.23$ and $\tilde{f}_{11} = 0.0015\,\text{Hz}$.

Fig. 2.6 (a) shows the signal $x_2(t)$ from the second oscillator together with the real and imaginary parts of the corresponding eigenvalues, from which one can observe the stability of system (2.11) over a long time span. The actual stability analysis for the transition from synchronization to non-synchronization (and *vice versa*) will be discussed in relation to the short time segment shown in Fig. 2.6 (b). The stability will be investigated through observation of the eigenvalues in four characteristic regions. In region I, the real parts of the eigenvalues are all negative and there are no imaginary parts (they are all equal to zero). This means that the equilibrium solution of (2.11) is a stable node and that the two oscillators are synchronized. On crossing into region II, two complex conjugate eigenvalues appear. The real parts are still negative, however, and so the equilibrium is still stable, but it has now turned into a stable spiral. When crossing from region II into region III.1, the real parts of the complex eigenvalues become positive, and a Hopf bifurcation occurs. This point is denoted by the small circle in Fig. 2.6 (b). The equilibrium has become unstable and, because the imaginary parts still exist, it is an unstable spiral. Starting from entry to region III.1 the oscillators oscillate in synchrony, even though the equilibrium of (2.11) is unstable. This discrepancy can be seen as a transitional region where the synchrony is "fading away". The phase difference $\psi(t)$ grows rapidly (spiraling out) until phase slips appear overtly in region III.2. Here the oscillators are not in synchronization.

Similarly, one can observe a stability/synchronization analysis of the case when the oscillators make a transition from the non-synchronous to the synchronous state. The phase slips then disappear and the phase difference $\psi(t)$ decreases, spiraling inwards. Note that the bifurcation point in Fig. 2.6 (b) is presented in terms of time, and not in respect of parameters as normally. One may do so, because the parameters are explicitly time-dependent and are thus fully determined at every instant of time

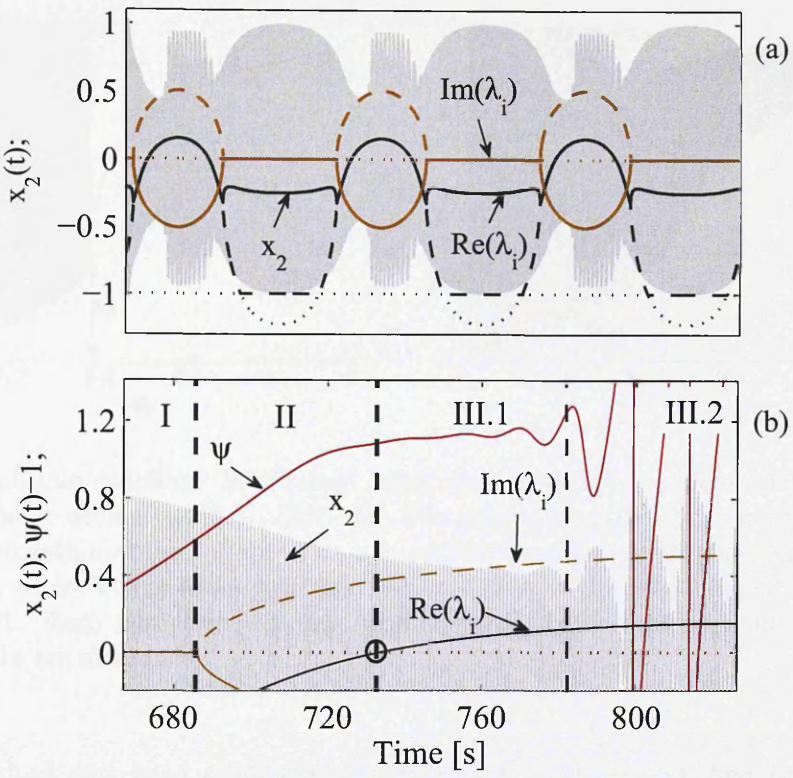

Fig. 2.6: Stability analysis of the synchronization state for unidirectionally-coupled (1 → 2) Poincaré oscillators (2.8), (2.9). (a) Three black lines for the real parts of the eigenvalues of system (2.11) (with solid, dashed and dotted lines) and three brown lines for the imaginary part of the eigenvalues of system (2.11), together with signal $x_2(t)$. Note that the lines overlap occasionally. Two different colors exist for the qualitatively distinct (real and imaginary) groups of lines. (b) Loss of synchronization and stability through a Hopf bifurcation together with other stability/synchronization characteristic regions: I–III.2 (separated by black vertical dashed lines). This panel provides enlarged time segment for one transition from (a); cf. the time scale on (a) compared with (b).

– which is advantageous for this kind of non-autonomous analysis, because one can observe the qualitative changes through bifurcation together with the other dynamical properties (e.g. signals, instantaneous phase, synchronization state) throughout all time.

For completeness, however, an alternative representation of the bifurcation phenomena, in terms of parameters is presented. The bifurcation diagram (often referred as an orbit diagram, since it does not present the unstable objects [58]) is constructed directly from the time-series of the numerical simulation of the oscillators. This

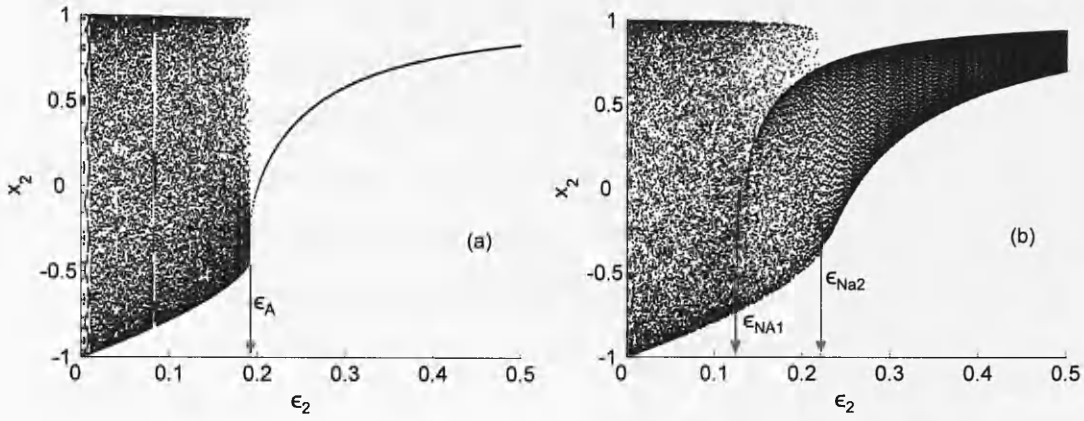

Fig. 2.7: Amplitude-coupling bifurcation diagram describing synchronization of the Poincaré oscillators (2.8), (2.9). (a) The autonomous case, illustrating stable synchronization above ϵ_A. (b) The non-autonomous case with time-varying frequencies, where intermittent synchronization occurs within the range $0.124 < \epsilon_{NA2} < 0.221$. Each numerical run has random initial conditions and the first transient 1000 s are discarded.

classical method was used extensively in the past to study synchronization and/or chaotic behavior [59–61]. First, the method is presented for the classical case of two autonomous oscillators. The results are used later for comparison with the non-autonomous case. For autonomous oscillators, there are no time-variations $\tilde{A}_{11} = 0$, the two oscillators are unidirectionally coupled, the frequencies are $f_1 = 0.15\,\text{Hz}$, $f_2 = 0.11\,\text{Hz}$ and all the other parameters are the same as in Fig. 2.3. One can observe the time series in respect of the coupling amplitude, following a long interval for transient effects to die away. For fixed values of the coupling amplitude, one plots the points from the phase space of the second oscillator each time when the first oscillator passes through a perpendicular phase plane. The latter can be interpreted also as: points equally separated in time by the period ($T_1 = 1/f_1$) of the first oscillator. In practical terms, the model (2.8),(2.9) was simulated for specified coupling amplitudes (e.g. $\epsilon_2 = 0.15$), and then the maxima (or zero-crossing, or other) events from the first oscillator were marked. From the times of these points, one then plots vertically (for $\epsilon_2 = 0.15$) the points of the second oscillator. The corresponding bifurcation diagram is shown in Fig. 2.7 (a). One may note that, for small coupling amplitudes, the points

of the second oscillator are spread widely and the two oscillators are not synchronized. The bifurcation point appears for the critical coupling amplitude $\epsilon_A \approx 0.192$, above which the two oscillators are synchronized; this state is characterized by all points for a given coupling value coinciding in a single point, and therefore forming a smooth curve as the coupling amplitude is varied. This result was in good agreement with the outcome of the analytic investigation, for which the equilibrium solution of the system (2.11) passed from unstable to stable synchronization at the critical coupling $\epsilon_A \approx 0.192$.

Next, a bifurcation diagram in much the same way was considered, but for the non-autonomous case. The time-varying frequency case of the two unidirectionally coupled oscillators was observed with $\tilde{A}_{11} = 0.1$, $\tilde{f}_{11} = 0.0025$ Hz and the other parameters as in Fig. 2.7 (a). In constructing the bifurcation diagram one cannot assume that the points from the first oscillator are equally separated in time, because the oscillating period is now varying due to the non-autonomous source. Instead, detection of the points as the maxima of each cycle of the first oscillator was performed. This makes the method adaptive, in a sense, because one can trace the variations in order to detect the different oscillating period in each cycle. From these time events, the points of the second oscillator are plotted in respect of the coupling amplitude ϵ_2. The corresponding bifurcation diagram is shown in Fig. 2.7 (b). For small coupling amplitude ($\epsilon_2 \lesssim \epsilon_{NA1} = 0.124$) the points of the second oscillator are spread widely, corresponding to the two oscillators not being synchronized. For increased values of the coupling (up to $\epsilon_2 \lesssim \epsilon_{NA2} = 0.221$) the oscillators are intermittently synchronized. The transitions in and out of synchrony are due to the periodicity of the non-autonomous term, while the total time in which the oscillators are in synchrony rises as the coupling amplitude increase. For a sufficient coupling amplitude, above some critical value $\epsilon_{NA2} \approx 0.221$, the two oscillators undergo continuous synchronization: they remain phase-locked even though their oscillatory frequencies vary with time. From Fig. 2.7 (b) one can notice that the synchronization state is not now characterized by a very dense line, but by a bounded dense region. This results from the existence of a small and bounded phase shift.

2.4.5 Non-autonomous phase shift and lag synchronization

When two oscillators are synchronized in the classical autonomous way, the phase shift is constant. In synchronization of non-autonomous self-sustained oscillators, the phase shift is varying, because the conditions (e.g. oscillating frequencies, couplings, ...) for synchronization are varying in time. In other words, the interacting state is continuously changing through different synchronization states in time, with a time-varying phase shift and amplitudes – but staying synchronized all the time, with a continuously stable solution for the phase difference (system (2.11)). The time-varying phase shift implies immediately that, under these conditions, lag synchronization [62, 63] is not possible. This was verified by the use of a similarity function S, which quantifies the time-averaged difference between the two state variable x_1, x_2 taken with the time shift τ, [62]:

$$S^2(\tau) = \frac{\langle [x_2(t+\tau) - x_1(t)]^2 \rangle}{[\langle x_1^2(t) \rangle \langle x_2^2(t) \rangle]^{1/2}}.$$

By analyzing the minimum $\sigma = \min_\tau(S(\tau))$, one can determine whether the two oscillators undergo lag synchronization. It was found that in synchronization of non-autonomous oscillators, the minimum σ cannot be sharp and nearly equal to zero (and that the minimum σ is always larger than that from autonomous synchronization under the same conditions). This is because neither the time lag nor the amplitude is constant over the whole time of observation. For very large couplings the variations of the phase difference and the amplitudes can be suppressed. The two states then became identical, $x_1(t) = x_2(t)$, and the oscillators are in complete synchronization.

2.4.6 Sources of non-autonomous dynamics

The external modulations acting as sources of non-autonomicity can be of widely differing natures, forms, intensities and speeds. In the above discussion, for the sake of clarity and simplicity, the non-autonomous external source was taken to be periodic with a simple sinusoidal form. In general, of course, the external source may be of a more complex form and nature, e.g. quasi-periodic, non-periodic, chaotic, or

stochastic.

Conditions

The non-autonomous term itself should fulfil two conditions in order to affect the underlying onset of synchronization (or at least to do so in the manner considered in this study):

1. The amplitude of the external source should be relatively bounded with intensity smaller then the property affected. For example the $\tilde{A}_{11}$ in Section 2.4.3 on Fig. 2.3 should be small compared to ω_1. For very large intensity the oscillatory dynamics may become qualitatively different (for example, exhibiting chaotic behavior or unstable oscillations), which would be beyond the scope of our interest – which is synchronization between weakly-coupled limit-cycle oscillators.

2. More important, the variations should be slow compared to the oscillatory dynamics of the affected oscillator. In other words, if the frequency of the non-autonomous term is equal to, or larger than, the frequency of the oscillators, the variations do not affect qualitatively the onset of synchronization. This was the consequence of the fast-time scale solution from the coupled phase oscillators model in Sec. 2.3. The point is that, if the non-autonomous external source introduces variations that are faster than the period of oscillation, they can be averaged within one period of the oscillations, not affecting the synchronization state.

Stochastic external source

Interactions between oscillators in the presence of random stochastic processes have been studied extensively in the past [9, 64, 65] and it has been shown that noise can either induce the synchronization between the oscillators or attenuate it [65–67]. Recently stochastic phase reduction for limit-cycle oscillators has been achieved for

noises of different kinds [68, 69]. Such studies are typically based on a statistical approach (e.g. Fokker-Planck analysis): it is necessary to have a long time of observation ($t \to \infty$) and the measures are statistically averaged over time. In practice, however, the time of observation is often restricted to shorter intervals, or there is a need to identify certain states in real time, and at every point of time, e.g. in biomedical measurements or communications.

The main features of the earlier discussion of synchronization of non-autonomous oscillators are reconsidered briefly, but for the case when the non-autonomous external sources are stochastic rather than periodic. The Ornstein-Uhlenbeck stochastic process was used as the non-autonomous source of modulation in the model (2.8), (2.9):

$$\dot{\eta}(t) = -\frac{1}{\tau}\eta(t) + \frac{\sqrt{2D}}{\tau}\xi(t)$$

where τ and D are the correlation time and noise strength respectively, and $\xi(t)$ is Gaussian white noise. The statistical properties of the colored noise are then: $\langle\dot{\eta}(t)\rangle = 0$ and $\langle\dot{\eta}(t)\eta(s)\rangle = \frac{D}{\tau}e^{-|t-s|/\tau}$. One can consider the unidirectionally coupled case of time-varying frequency from Sec. 2.4.3 presented on Fig. 2.3 (the same effect can be observed for time-varying couplings). The noisy source was added to the natural frequency of the first oscillator: $\omega_1(t) = \omega_1 + \eta(t)$, but all the other parameters and conditions were kept the same. The correlation time and the strength of the colored noise were $\tau = 50$ and $D = 25$. The resultant numerical signal is presented in Fig. 2.8 (a).

From Figs. 2.8 (b) and (c), it is clear that the amplitude and frequency of the second oscillator now vary too, due to the effect of the synchronization. One can noticed that, in accord with the above discussion of the frequency of variation of the non-autonomous source, only the lower-frequency components of the Ornstein-Uhlenbeck process affect the variations, whereas the higher frequencies did not, because they were faster than a period of the first oscillator. Using the observations made in Sec. 2.4.2 one can find that all the eigenvalues have negative real parts, demonstrating that the two oscillators remained synchronized while their frequencies are varying,

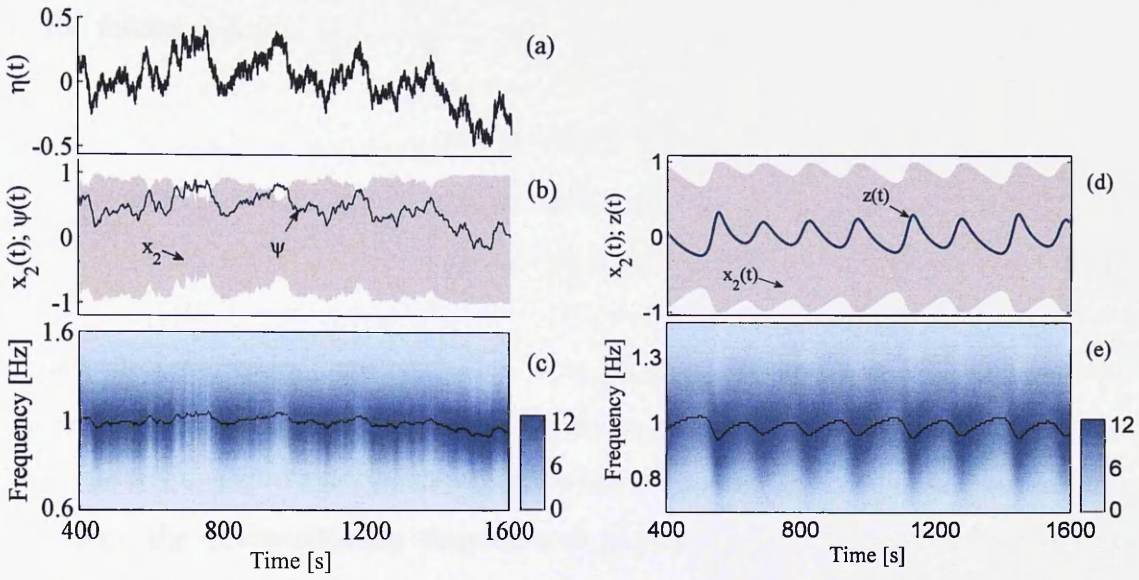

Fig. 2.8: Synchronization of unidirectionally-coupled ($1 \rightarrow 2$) Poincaré oscillators (2.8), (2.9), under conditions where there are stochastic (a)-(c) and quasi-periodic variations (d)-(e) in the frequency of oscillator-1. (a) Time evolution of the colored noise signal $\eta(t)$. (b) The signal $x_2(t)$ and the numerically evaluated phase difference $\psi(t)$. (c) Contour plot of wavelet analysis of the signal $x_2(t)$ from the second oscillator. (d) Time evolution of the chaotic signal $z(t)$ and the signal $x_2(t)$ from the second oscillator (seen as its envelope). (e) Wavelet analysis of $x_2(t)$ from the second oscillator. The frequency variations are indicated by the black line plotting the locus of the peak values.

following the dynamics of the stochastic source.

Chaotic external source

The next case to be consider was when the source of non-autonomicity is a quasi-periodic signal generated by a chaotic deterministic system. Its worth noting *en passant* that chaotic systems have played an important role in synchronization theory, both in studying the interactions among chaotic systems and defining new synchronization concepts [15, 16, 46]. Synchronization of chaotic systems and periodic non-autonomous sources has been studied in [70, 71]. Here, the interest is more in using the non-periodic forms of signals generated by chaotic systems, rather than in the chaotic properties of the systems. The well-known Lorenz system [72] was used,

in the following form:

$$\begin{aligned} \gamma\dot{x} &= \sigma(y-x) \\ \gamma\dot{y} &= x(\rho-z)-y \\ \gamma\dot{z} &= xy-\beta z \end{aligned} \tag{2.12}$$

where the parameters were set to be: $\sigma = 10$, $\beta = 8/3$ and $\rho = 28$. The constant parameter $\gamma = 0.005$ was introduced in order to reduce the velocity in the system, so that the frequency of the signals would be low compared to those of the oscillators.

Again the unidirectionally coupled case of synchronization was considered, with the frequency of the first oscillator being time-varying (Sec. 2.4.3, Fig. 2.3). The non-autonomous source now is taken to be $z(t)$ from (2.12), presented in Fig. 2.8 (d). The time-varying frequency is defined as: $\omega_1(t) = \omega_1 + \tilde{A}(z(t) - \tilde{c})$, where $\tilde{A} = 1/60$, $\tilde{c} = 23$ and the other parameters are all as discussed before. Under these conditions, the two oscillators can synchronize. In order for the second oscillator to be synchronized and to stay in frequency entrainment, its amplitude and oscillating frequency start to vary, as imposed by the quasi-periodic non-autonomous source as shown in Fig. 2.8 (d) and (e).

2.4.7 Generalization of the model

It is reasonable to wonder to what extent the above results are general, rather than confined to the particular model (2.8),(2.9) of two Poincaré oscillators. The Poincaré oscillator as a unit, in its uncoupled form, is a radial isochronal oscillator. All trajectories starting at one point of ϕ go to the same asymptotic phase and, as mentioned above, the variable ϕ represents both the phase and the angle variable ($\dot{\phi} = \omega$). There is, however, a vast group of limit-cycle oscillators where the local oscillatory frequency depends on the local amplitude. The terms introducing this nonisochronicity are related to the *shear* of the phase flow near the limit cycle. Synchronization of oscillators with shear terms has been studied along with the oscillation death (Bar-Eli) effect [57, 73]. It was reported [74, 75] that nonisochronicity can be a cause of anomalous

phase synchronization in a population of non-identical oscillators.

The phenomenon of synchronization between non-autonomous oscillators was observed in a variety of limit-cycle oscillators, including van der Pol and Stuart-Landau oscillators, as well as the Poincaré oscillators with shear terms. It was found that the qualitative characteristic of the synchronization under such non-autonomous conditions was valid for the other types of limit-cycle oscillators. The results of analogue experiments exploring synchronization between non-autonomous van der Pol oscillators will be presented in chapter 5.

2.5 Non-autonomous coupling function

So far the discussion was focused on non-autonomous parameters and how they affect the interactions. Another important property that characterizes the interactions among oscillators is the *coupling function*. Opposite to closed autonomous oscillators, the coupling function in open oscillatory systems can vary in time, both in intensity and form. In fact, a functional relationships that characterize the cardiorespiratory interactions are time-varying (as will be demonstrated in the following chapter).

But, why is coupling function important and how does it affect the interactions? It defines the functional law about the interactions and the law by which the interaction undergo transitions to synchronization i.e. transitions to equilibrium stability. (Qualitative description about the role of coupling function in oscillatory interaction is discussed in more details in chapter 3 section 3.3.2).

In order to investigate how the coupling function can affect the interacting systems and cause transitions to synchronization, a special case was considered where: the time-variability of the form of the coupling function alone is the cause for synchronization transitions. This was accomplished by maintaining the parameters (frequencies ω_i and coupling strengths ϵ_i) constant, while the form of the coupling function is varying by some predefined non-autonomous source.

A coupling function represented in the reduced phase model: $\dot{\phi}_i = \omega_i + \epsilon_i q(\phi_i, \phi_j)$, should be a 2π-periodic function. In his phase models Kuramoto [10] used a simple sine

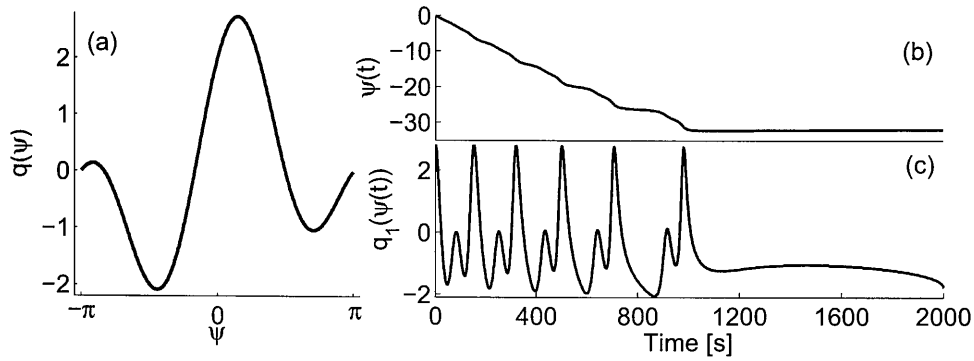

Fig. 2.9: Coupling function and synchronization transition as a result of its time-variability. (a) Form of the coupling function Eq. (2.13) with constant $a(t) = 1$ and $b(t) = 1$. Phase difference (b) and coupling function $q_1(\psi(t))$ (c) for system (2.14) indicating the synchronization transition due to the variability of the function of interactions. The parameters for the coupling function are varied linearly in time: $a(t) = 0 \rightarrow 1.4$ and $b(t) = 1.4 \rightarrow 0$; rest of parameters are constant: $\epsilon_1 = 0.013$, $\epsilon_2 = 0.01$, $\omega_1 = 0.11$ and $\omega_2 = 0.07$.

form function of the phase difference $q(\phi_1, \phi_2) = \sin(\phi_2 - \phi_1)$, Winfree [7] used function that is defined by both phases rather than just the phase difference $q(\phi_1, \phi_2) = [1 + \cos(\phi_2)]\sin(\phi_1)$, while Daido and Crawford [76–78] used more general form where the function can be expanded in Fourier series. Here the discussion is concentrated on numerical simulation of two coupled phase oscillators (similar to those presented with Eq. 2.2), but the coupling function for the phase difference consists of four Fourier components up to the second order:

$$q(\phi) = a(t)\sin(\phi) + b(t)\cos(\phi) + a(t)\sin(2\phi) + b(t)\cos(2\phi), \tag{2.13}$$

where the $a(t)$ and $b(t)$ parameters are considered to be time dependent terms. The form of the coupling function is presented on Fig. 2.9 (a). The simple model for investigation will then have the following form:

$$\begin{aligned} \dot{\phi_1} &= \omega_1 + \epsilon_1 q_1(\phi_2 - \phi_1) \\ \dot{\phi_2} &= \omega_2 + \epsilon_2 q_2(\phi_1 - \phi_2). \end{aligned} \tag{2.14}$$

By changing the parameters a and b in time one can vary the form of the coupling

function. For the case under study, the goal was to maintain the coupling strength constant while only the form of the function to vary. The latter means that besides the coupling parameters ϵ_i, also the norm of the coupling function should be constant throughout the time. Therefore the function parameters a and b were non-autonomous sources varying linearly (and then square rooted) in time, while the norm of the function was constant in every instant of the time.

Fig. 2.9 (b) shows the phase difference $\psi(t) = \phi_2(t) - \phi_1(t)$ which serves as indicator for synchronization of systems (2.14), i.e. if the phase difference is bounded ($\psi < const$) or not. Fig. 2.9 (c) shows the dynamical time-evolution of the coupling function (of second to first oscillator) as a function of phase difference. The two figures demonstrate that: at the beginning the oscillators are not synchronized and as the form of the coupling function is varied, the oscillators get more coherent and around time = 1000s there is transition to full synchronization. The latter means that the coupling function changed qualitatively the dynamical behaviour, equilibrium solution appeared and synchronized stable state is reached.

The non-autonomous coupling functional relation is important because it resembles the dynamics of many real oscillatory systems found in nature. One of the main systems of interest for this study, the cardiorespiratory system has coupling function which is evidently time-varying. The latter was discovered by the use of the method presented in the following chapter.

3. INFERENCE OF TIME-EVOLVING COUPLED DYNAMICAL SYSTEMS IN THE PRESENCE OF NOISE

Open systems are often oscillatory in nature because their dynamics are determined by a balance between energy inflow, outflow and usage which, in general, do not match. Their lack of isolation means that such systems often interact with each other. The strength, direction and the functional relationships can define the nature of interactions, which can cause qualitative states to appear, such as synchronization between the oscillators. The time-variability of the dynamical behaviour that characterizes the oscillators and their interactions cause transitions between the qualitative states.

In order to investigate and study interactions, one usually obtains observable measurements of the oscillating dynamics in a form of time-series. Through analysis of these readout signals one can detect and quantify the interacting phenomenons. In such an inverse approach, often the source of a time-variability can not be uniquely determined. Additionally, the observable time-series can involve part of a stochastic indeterministic dynamics, arising due to (for example) influence of the environment on the dynamics, or due to measurement noise.

For this reasons there is a need for technique that can infer parameters, functional relationships and transitions between states of the interactions, starting from time-series observations. Due to the nature of dynamics, the inference should be able to trace the time-variability of the intrinsic parameters, and at the same time to be able to deduce the effect of the noise. Offering such a complete and comprehensive description of the dynamics within a single formalism, the technique can be of wide applicability.

3.1 Phase dynamics decomposition

This section outlines the basic theoretical background for the implementation of the inferential framework. At the core of the technique lies the Bayesian inferential framework for stochastic dynamics, utilized to infer a time-evolution of the intrinsic parameters.

3.1.1 Main concept

The methodological approach proposed in this study exploits the Bayesian inferential technique for inference of noisy time-varying phase dynamics. The parameters, reconstructed from the base functions, allow the interactions and the respective states between the oscillators to be determined. The method can be summarized as:

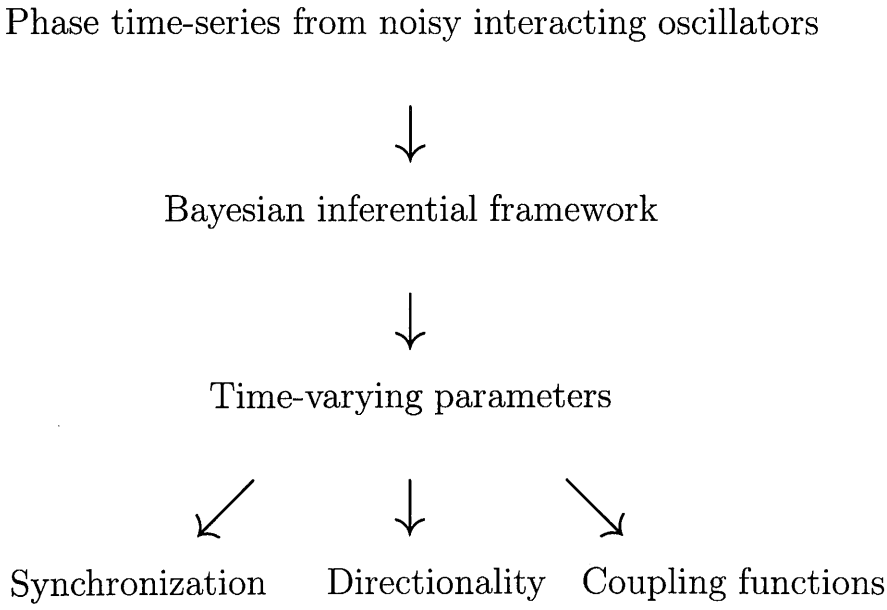

The starting point i.e. the inputs for the inference are multivariate phase time-series that encapsulate the dynamics of an interacting oscillators. The actual observable time-series represent instantaneous phases from the measured state signals, pre-estimated using appropriate phase detection methods (e.g. using Hilbert transform, angle variable or wavelet synchrosquueze transform).

Decomposition of the phase dynamics embedded within the Bayesian framework is accomplished through the use of periodic base functions – represented in a form of

finite Fourier series. The use of probabilistic apparatus from Bayesian theory enables the parameters' distribution to be inferred. Furthermore, the Bayesian probability lying at the core of the method is itself time-dependent via the prior probability as a time-dependent informational process. The outcome of the inference i.e. the time-varying parameters are then employed to estimate, quantify and describe the underlying oscillatory interactions. By reconstructing the dynamics in terms of a set of base functions, we evaluate the probability that they are driven by a set of equations which are intrinsically synchronized, thus distinguishing phase-slips of dynamical origin from those attributable to noise.

Estimation of the coupling is directly linked to the parametrization of the base functions: for oscillators which are similar enough to share the same base functions, confrontation between the parameters is sufficient for evaluation of which oscillator drives which. The examination of the interacting base function as a group, can reveal the functional relationship that describes the interactions among the oscillators.

3.1.2 Base functions

When two noisy, N-dimensional, self-sustained oscillators interact weakly [9], their motion can be described by their phase dynamics:

$$\dot{\phi}_i = \omega_i + f_i(\phi_i) + g_i(\phi_i, \phi_j) + \xi_i(t), \tag{3.1}$$

leaving all other coordinates expressed as functions of the phase: $\mathbf{r_i} \equiv \mathbf{r_i}(\phi_i)$ [10]. The constant terms ω_i represent the oscillating angular frequencies, the $f_i(\phi_i)$ functions describe the inner-oscillating dynamics, while $g_i(\phi_i, \phi_j)$ functions characterize the dynamics for the interactions between the oscillators. (The later functions $g_i(\phi_i, \phi_j)$ are often referred to as *coupling functions*). ξ is a two-dimensional spatially correlated noise, usually assumed to be Gaussian and white: $\langle \xi_i(t)\xi_j(\tau)\rangle = \delta(t-\tau)E_{ij}$. Reliable evaluation of the interaction phenomena must rely on precise inference of f_i and g_i and of the noise matrix E_{ij}. The periodic nature of the systems suggest periodic

base-functions, hence the use of Fourier terms for the decomposition:

$$\begin{aligned} f_i(\phi_i) &= \sum_{k=-\infty}^{\infty} \tilde{c}_{i,k} \sin(k\phi_i) + \tilde{c}_{i,2k+1} \cos(k\phi_i) \\ g_i(\phi_i, \phi_j) &= \sum_{s=-\infty}^{\infty} \sum_{r=-\infty}^{\infty} \tilde{c}_{i;r,s}\, e^{i2\pi r\phi_i} e^{i2\pi s\phi_j}. \end{aligned} \tag{3.2}$$

The inference of an underlying phase model through use of Fourier series has formed the functional basis for several techniques to infer the nature of phase-resetting curves and interactions viz. the structure of networks or proposed synchronization prediction [27, 79–83]. However, these techniques inferred neither the noise dynamics nor the parameters characterising the noise.

It might seem natural at this point to consider the phase difference of the two oscillators, as in the case of synchronization determination. But, due to the need to extract as much information as possible from the whole dynamical space, the two dynamical fields ϕ_1 and ϕ_2 are modeled separately.

Assuming that the dynamics are adequately described by a finite number K of Fourier terms, one can rewrite the phase dynamics of (3.1) as a finite sum of base functions:

$$\dot{\phi}_l = \sum_{k=-K}^{K} c_k^{(l)}\, \Phi_{l,k}(\phi_1, \phi_2) + \xi_l(t), \tag{3.3}$$

where $l = 1, 2$, where $\Phi_{1,0} = \Phi_{2,0} = 1$, $c_0^{(l)} = \omega_l$, and other $\Phi_{l,k}$ and $c_k^{(l)}$ are the K most important Fourier components.

It is important to note that a use of Fourier series for the phase dynamics is a general and model-independent decomposition. The latter results from the fact that the inputs used are monotonically increasing with time, regarding of the dimensions and the complexity of the signals. The phase $\phi_i(t)$ possess the sufficient information for the measures required to be inferred: synchronization, directionality and time-varying phase dynamics. If one were about to decompose the oscillatory interactions in state space, then the dynamics must be inferred using specific non-general and

model-dependent (e.g. polynomial) base function. The use of state base functions is discussed in detail toward the end of this chapter in section 3.6.

3.1.3 Bayesian inference

The following outlines a general inferential framework for stochastic dynamical processes. An M-dimensional time-series of observational data $\mathcal{Y} = \{\mathbf{y}_n \equiv \mathbf{y}(t_n)\}$, defined over the time-grid $t_n = nh$, is provided. It is assumed that a driving dynamic exists, described by an L-dimensional ($L \geq M$) stochastic process $\boldsymbol{\phi}(t)$. The underlying dynamics can be described by a set of L-dimensional stochastic differential equations in the form:

$$\dot{\boldsymbol{\phi}}(t) = \mathbf{f}(\boldsymbol{\phi}|\mathbf{c}) + \mathbf{z}(t), \tag{3.4}$$

where $\mathbf{c}$ is a set of parameters that are embedded in the dynamical field $\mathbf{f}$, and $\mathbf{z}(t)$ is considered to be an L-dimensional white Gaussian noise processes. It is assumed that the measurement noise is negligible and that a unique relationship exists: $y(t) = \phi(t)\,\forall t$, i.e. the readout data is also the dynamical variable. A Bayesian inference technique that includes inference of measurement noise and detailed derivations of similar inferential framework is discussed in [30–32, 84].

The fundamental question for the inference is: "given the readout data $\mathcal{X}$, what information can one obtain about the functions $\mathbf{f}$, about their parameters $\mathbf{c}$ and about the noisy processes $\mathbf{z}$?".

Due to the stochastic nature of the dynamics, the process of information extraction involves the building of theoretical models that cannot be verified directly but can be exploited by estimation of their probability. For these reasons, one can employ Bayesian probability - an approach in statistical inference where the probability is intended as a subjective measure of belief in an event or in the state of a variable [85–87]. In particular, the Bayes' theorem states:

$$P_{\text{post}}(\mathcal{M}|\mathcal{X}) = \frac{P(\mathcal{X}|\mathcal{M})\, P_{\text{prior}}(\mathcal{M})}{\int P(\mathcal{X}|\mathcal{M})\, P_{\text{prior}}(\mathcal{M}) d\mathcal{M}}, \tag{3.5}$$

where $\mathcal{M}$ is a set of parameters on which the probabilities are assigned; $\mathcal{X}$ represents the observational data. $P_{\text{prior}}(\mathcal{M})$ is the *prior* probability of $\mathcal{M}$: the measure of belief on the particular values of $\mathcal{M}$ before the data $\mathcal{X}$ was observed. $P(\mathcal{X}|\mathcal{M})$ (also called the likelihood) is the conditional probability of observing $\mathcal{X}$ given $\mathcal{M}$. The desired result $P_{\text{post}}(\mathcal{M}|\mathcal{X})$ is the posterior probability: the probability that the hypothesis (or parameters) are true, given the data and the previous state of belief about the hypothesis. Such a framework is ideal for applications with sequential data - the current posterior probability can act as a prior for the next sequence of data.

Thus within the Bayesian framework, the problem is reduced to the calculation of the likelihood function and the optimization of the posterior distribution with respect to $\mathcal{M} = \{\mathbf{c}, \mathbf{E}\}$.

In order to construct the expression for the likelihood function, an additional assumption is made that the sampling scheme $\{t_n = nh\}$ is sufficiently dense in respect of the dynamics that the time interval h is small enough for the Euler mid-point approximation to be valid. If this is the case, Eqs. (3.4) can be approximated by:

$$\boldsymbol{\phi}_{n+1} = \boldsymbol{\phi}_n + h\,\mathbf{f}(\boldsymbol{\phi}_n^*|\mathbf{c}) + \mathbf{z}_n, \tag{3.6}$$

where $\boldsymbol{\phi}_n^*$ is the average between two consecutive states of the dynamical variable $\boldsymbol{\phi}$:

$$\boldsymbol{\phi}_n^* = \frac{(\boldsymbol{\phi}_{n+1} + \boldsymbol{\phi}_n)}{2}.$$

In Eq. (3.6) the term $\mathbf{z}_n$ is the stochastic integral:

$$\mathbf{z}_n \equiv \int_{t_n}^{t_{n+1}} \mathbf{z}(t)\,dt = \sqrt{h}\,\mathbf{H}\,\boldsymbol{\xi}_n. \tag{3.7}$$

$\mathbf{H}$ is the matrix that satisfies $\mathbf{H}\mathbf{H}^{\mathrm{T}} = \mathbf{E}$, and $\boldsymbol{\xi}_n$ is a zero-average $\langle\boldsymbol{\xi}_n\rangle = 0$ and unitary-variance normal variable $\langle\boldsymbol{\xi}_n\,\boldsymbol{\xi}_m\rangle = \mathbb{I}\,\delta_{n\,m}$.

The main idea is to calculate the probability of $\boldsymbol{\phi}_{n+1} - \boldsymbol{\phi}_n - h\,\mathbf{f}(\boldsymbol{\phi}_n^*|\mathbf{c})$ for each single n as a function of the probability of the realization of the whole process $\{\mathbf{z}_n\}$.

The probability of a single $\mathbf{z}_n$ is:

$$P(\mathbf{z}_n) = \frac{d\mathbf{z}_n}{\sqrt{(2\pi)^L h^L \det(E)}} \exp\left\{-\frac{\mathbf{z}_n^T \mathbf{E}^{-1} \mathbf{z}_n}{2h}\right\}.$$

Thanks to the assumption that the noise under consideration is white $\mathbf{z}_n$ and statistically independent of $\mathbf{z}_m$ for $n \neq m$, one can write the joint probability of the process $\{\mathbf{z}_n\}$ as a product of the probabilities of each single $\mathbf{z}_n$:

$$P(\{\mathbf{z}_n\}) = \prod_{i=0}^{N-1} P(\mathbf{z}_i) = \prod_{i=0}^{N-1} \frac{d\mathbf{z}_i}{\sqrt{(2\pi)^L h^L \det(E)}} \exp\left\{-\frac{\mathbf{z}_i^T \mathbf{E}^{-1} \mathbf{z}_i}{2h}\right\}. \tag{3.8}$$

The likelihood probability $P(\mathcal{X}|\mathcal{M})$ over a time grid can be expressed as the probability density of a particular realization of the dynamical system $P(\mathcal{X}|\mathcal{M}) = P(\{\boldsymbol{\phi}_n\}) = \rho_0(\boldsymbol{\phi}_0) \prod_{i=0}^{N} \rho(\boldsymbol{\phi}_i)$. The expression of $P(\mathcal{X}|\mathcal{M})$ was decomposed in this way because of the need for $\prod_{i=0}^{N} \rho(\boldsymbol{\phi}_i)$ to be expressed directly in terms of $\{\mathbf{z}_n\}$.

Thanks to the change of variable from $\mathbf{z}_n$ to $\boldsymbol{\phi}_{n+1}(\mathbf{z}_n)$, and the introduction of its subsequent Jacobian term $[\mathbf{J}]_{ij} = \delta_{ij} - \frac{h}{2} \frac{\partial[\mathbf{f}(\boldsymbol{\phi}_n^*|\mathbf{c})]_i}{\partial[\boldsymbol{\phi}_n^*]_j}$, one obtains the probability of realization of the whole process $\{\boldsymbol{\phi}_n\}$:

$$\begin{aligned} &P(\{\boldsymbol{\phi}_{n+1}\}) = \\ &= \frac{d\boldsymbol{\phi}_{n+1} \det(\mathbf{J})}{\sqrt{(2\pi h)^L \det(\mathbf{E})}} \exp\left\{-\frac{h}{2}\left(\dot{\boldsymbol{\phi}}_n - \mathbf{f}(\boldsymbol{\phi}_n^*|\mathbf{c})\right)^T \mathbf{E}^{-1} \left(\dot{\boldsymbol{\phi}}_n - \mathbf{f}(\boldsymbol{\phi}_n^*|\mathbf{c})\right)\right\}, \end{aligned} \tag{3.9}$$

where the following definition was used : $\dot{\boldsymbol{\phi}}_n \equiv \frac{\boldsymbol{\phi}_{n+1} - \boldsymbol{\phi}_n}{h}$. The determinant of the Jacobian can be further approximated, since the Jacobian matrix consists of all quasi-zero elements, except in the diagonal. Obtaining the probability density function leads to the complete expression for the likelihood function given (for convenience in

logarithmic form) as:

$$-\frac{2}{N}\ln\left(P(\mathcal{X}|\mathcal{M})\right) = +\ln\left(\det(E)\right)+ \\ +\frac{h}{N}\sum_{n=0}^{N-1}\left[\left(-\frac{h}{2}\frac{\partial\mathbf{f}\left(\boldsymbol{\phi}_n^*|\mathbf{c}\right)}{\partial\boldsymbol{\phi}_n^*}\right)+\left(\left(\dot{\boldsymbol{\phi}}_n-\mathbf{f}\left(\boldsymbol{\phi}_n^*|\mathbf{c}\right)\right)^T\mathbf{E}^{-1}\left(\dot{\boldsymbol{\phi}}_n-\mathbf{f}\left(\boldsymbol{\phi}_n^*|\mathbf{c}\right)\right)\right)\right]. \tag{3.10}$$

The next task is to maximize the posterior probability i.e. to fit the likelihood Eq. (3.10) to Bayesian theorem, in order to find the optimal probability of the parameter set $\mathcal{M}$ given the data $\mathcal{X}$.

The prior probability $P_{\text{prior}}(\mathcal{M})$ was chosen to be a multivariate normal distribution in respect of the parameters $\mathbf{c}$; if $\mathbf{c}$ is an M-dimensional vector, its prior probability is written as:

$$P_{\text{prior}}(\mathbf{c}) = \frac{1}{\sqrt{(2\pi)^M\det(\boldsymbol{\Sigma}_{\text{pr}})}}\exp\left[-\frac{1}{2}(\mathbf{c}-\mathbf{c}_{\text{pr}})^T\boldsymbol{\Sigma}_{\text{pr}}^{-1}(\mathbf{c}-\mathbf{c}_{\text{pr}})\right], \tag{3.11}$$

where $\mathbf{c}_{\text{pr}}$ is a vector of *a priori* coefficients and $\boldsymbol{\Sigma}_{\text{pr}}$ is its covariance matrix. The latter two expressions Eq. (3.10) and (3.11) gave the required probabilities, from which (using the Bayesian theorem) the posterior probability can be estimated.

Before moving forward, explicit dependence of $\mathbf{f}$ in respect of parameters vector $\mathbf{c}$ needs to be defined, and the following parametrization is introduced:

$$\mathbf{f}(\boldsymbol{\phi}|\mathbf{c}) = \boldsymbol{\Phi}(\boldsymbol{\phi})\,\mathbf{c}, \tag{3.12}$$

where $\boldsymbol{\Phi}(\boldsymbol{\phi})$ is a $L \times M$ matrix of Fourier base functions, as described in previous section (3.1.2). With this linear parametrization of $\mathbf{f}$, one obtains a quadratic log-likelihood function in respect of parameters vector $\mathbf{c}$. Hence, using a multivariate normal distribution for the prior probability immediately leads to a multivariate normal distribution for the posterior. This is highly desirable because the Gaussian posterior (described only by its mean and covariance) is computationally convenient and can be easily used again as a prior for the next sequential block.

Finally, taking the discussed expressions into account, the stationary point of the log-likelihood (and thus the posterior) can be calculated recursively with the following equations:

$$\mathbf{E} = \frac{h}{N}\sum_{n=0}^{N-1}\left[\dot{\phi}_n - \mathbf{\Phi}_n\mathbf{c}\right]\left[\dot{\phi}_n - \mathbf{\Phi}_n\mathbf{c}\right]^{\mathrm{T}}, \tag{3.13}$$

$$\mathbf{w}_{\mathcal{X}}(\mathbf{E}) = \mathbf{\Sigma}_{\mathrm{pr}}^{-1}\,\mathbf{c}_{\mathrm{pr}} + h\sum_{n=0}^{N-1}\left[\mathbf{\Phi}_n^{\mathrm{T}}\,\mathbf{E}^{-1}\,\dot{\phi}_n - \frac{1}{2}\frac{\partial\mathbf{\Phi}\left(\phi_n^*\right)}{\partial\phi_n^*}\right], \tag{3.14}$$

$$\mathbf{\Xi}_{\mathcal{X}}(\mathbf{E}) = \mathbf{\Sigma}_{\mathrm{pr}}^{-1} + h\sum_{n=0}^{N-1}\mathbf{\Phi}_n^{\mathrm{T}}\,\mathbf{E}^{-1}\,\mathbf{\Phi}_n, \tag{3.15}$$

$$\mathbf{c} = \mathbf{\Xi}_{\mathcal{X}}^{-1}(\mathbf{E})\mathbf{w}_{\mathcal{X}}(\mathbf{E}), \tag{3.16}$$

where $\mathbf{\Xi}$ is the inverse of the covariance matrix $\mathbf{\Xi} = \mathbf{\Sigma}^{-1}$ (often called concentration or precision matrix).

In terms of the optimal algorithm for computational calculations, this make sense: starting from initial prior $\mathbf{\Sigma}_{\mathrm{pr}}^{-1}$ and $\mathbf{c}_{\mathrm{pr}}$, the noise matrix $\mathbf{E}$ can be calculated Eq. (3.13), then given this $\mathbf{E}$, using Eq. (3.14-3.16), the parameter vector $\mathbf{c}$ can be evaluated. The same procedure should be repeated recursively until $\mathbf{c}$ and $\mathbf{E}$ converge to stability. In absence of any prior knowledge about the system, a non-informative initial prior can be used: $\mathbf{\Sigma}_{\mathrm{pr}}^{-1} = 0$ and $\mathbf{c}_{\mathrm{pr}} = 0$.

The proposed Bayesian inferential framework can be summarized as follows. Thanks to the choice of the linear parametrization of the vector field $\mathbf{f}(\phi|\mathbf{c}) = \mathbf{\Phi}(\phi)\mathbf{c}$, a log-likelihood quadratic function in respect of parameters has been obtained. The choice of a multivariate normal distribution for the prior $P_{\mathrm{prior}}(\mathbf{c})$ leads to a posterior which is still a multivariate normal distribution. Therefore, given a realization of $\mathcal{X}$, with two input quantities, $\mathbf{c}_{\mathrm{pr}}$ and $\mathbf{\Sigma}_{\mathrm{pr}}$, respectively the mean and the covariance of the prior $P_{\mathrm{pr}}(\mathbf{c})$, the set of parameters that best describe the system, and their correlations, are described by only two other quantities: $\mathbf{c}_{\mathrm{post}}$ and $\mathbf{\Sigma}_{\mathrm{post}}$, respectively the mean and the covariance of the posterior $P_{\mathrm{post}}(\mathbf{c})$. The posterior probability density

is thus:

$$P_{\text{post}}(\{c\}) = \frac{1}{(2\pi)^{L/2}|\Xi_{\text{post}}|^{-1/2}} \exp\left[-\frac{1}{2}(\mathbf{c}-\mathbf{c}_{\text{post}})^{\mathrm{T}}\Xi_{\text{post}}(\mathbf{c}-\mathbf{c}_{\text{post}})\right]. \tag{3.17}$$

If then a new sequential data-block $\mathcal{X}$ (generated from the same dynamics) is given, we can use the posterior information from the first data-block as the prior for the second one. The latter procedure constitutes the information propagation process, the utilization of which for time-varying dynamics will be discussed in the following section.

3.1.4 Time-varying information propagation

The multivariate probability Eq. (3.17) described by $\mathcal{N}_{\mathcal{X}}(c,\Sigma)$ for the given time series $\mathcal{X} = \{\phi_n \equiv \phi(t_n)\}$ explicitly defines the probability density of each parameter set of the dynamical system. When the sequential data comes from a stream of measurements providing multiple blocks of information, one applies (3.13-3.16) to each block. Within the Bayesian theorem, the evaluation of the current distribution relies on the evaluation of the previous block of data i.e. the current prior depends on the previous posterior. Thus the inference defined in this way is not a simple windowing, but each stationary posterior depends on the history of the evaluations from previous blocks of data.

In classical Bayesian inference, if the system is known to be non-time-varying, then the posterior density of each block is taken as the prior of the next one: $\Sigma^{n+1}_{\text{prior}} = \Sigma^{n}_{\text{post}}$. This full propagation of the covariance matrix will allow good separation of the noise and the uncertainties in the parameters steadily decrease with time as more data are included. But if time-variability exists, this propagation will act as a strong constraint on the inference and will fail to follow the time-variability of the parameters. This situation is illustrated in Fig. 3.1 (a) [1].

On the other hand, if the noisy dynamical system has time-variability, one can

[1] Note that Fig. 3.1 shows inference of two coupled noisy Poincaré oscillators with time-varying frequency of one oscillator – for clarity and compactness of presentation the details are not shown here, but the reader can refer to the model and other details in Sec 3.4

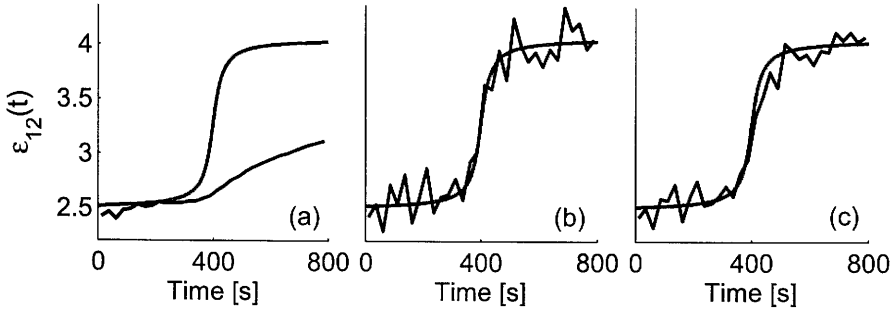

Fig. 3.1: Inference of steep time-varying frequency parameter from coupled noisy oscillators 3.22. The gray line represents the intrinsic (as in the numerical simulation) parameter, while the black line is for the inferred time-varying parameter, for: (a) full propagation: $\Sigma^{n+1}_{\text{prior}} = \Sigma^{n}_{\text{post}}$, (b) no propagation: $\Sigma^{n+1}_{\text{prior}} = 0$ and (c) propagation for time-varying processes: $\Sigma^{n+1}_{\text{prior}} = \Sigma^{n}_{\text{post}} + \Sigma^{n}_{\text{diff}}$.

consider the processes between each block of data to be independent (i.e. to consider them as Markovian processes). Then there can be no propagation between the blocks of data and each inference starts from a flat distribution: $\Sigma^{n+1}_{\text{prior}} = 0$. Now the inference will follow more closely the time-variability of parameters, but the effect from the noise and the uncertainty of the inference will be larger Fig. 3.1 (b).

If the system has time dependence, however, the method of propagating knowledge about the state of parameters obviously has to be improved and refined. Our framework prescribes the prior to be multinormal, so we synthesize our knowledge into a squared symmetric positive definite matrix. We assume that the probability of each parameter diffuses normally with a known diffusion matrix Σ_{diff}. Thus, the probability density of the parameters is the convolution of two normal multivariate distributions, Σ_{post} and Σ_{diff}:

$$\Sigma^{n+1}_{\text{prior}} = \Sigma^{n}_{\text{post}} + \Sigma^{n}_{\text{diff}}.$$

The particular form of Σ_{diff} describes which part of the dynamical fields defining the oscillators can change, and the size of the change. In general $(\Sigma_{\text{diff}})_{i,j} = \rho_{ij}\sigma_i\sigma_j$, where σ_i is the standard deviation of the diffusion of c_i in the time window t_w, and ρ_{ij} is the

correlation between the change in the parameters c_i and c_j:

$$\Sigma^n_{\text{diff(i,j)}} = \begin{bmatrix} \ddots & \cdots & \rho_{ij}\sigma_i\sigma_j \\ \vdots & \rho_{ii}\sigma_i\sigma_i & \vdots \\ \cdots & \cdots & \ddots \end{bmatrix} \tag{3.18}$$

A particular example of Σ_{diff} will be considered: it is assumed that there is no change of correlation between parameters ($\rho_{ij} = \delta_{ij}$) and that each standard deviation σ_i from the main diagonal is a known fraction of the relevant parameter, $\sigma_i = p_w c_i$, where p_w indicates that the parameter p refers to a window of length t_w. It is important to note that this particular example is rather general because it assumes that all of the parameters (from the Σ^n_{post} diagonal) can have a time-varying nature – which resembles inference of real (experimental) systems with *a priori* unknown time-variability. The resulting inference on Fig. 3.1 (c) demonstrates that the time-variability is captured correctly and that the uncertainty is reduced with time as more data are included.

If one knows beforehand that only one parameter is varying (or at most, a small number of parameters), then Σ_{diff} can be customized to allow tracking of time-variability specifically on that parameter. This selective propagation can be achieved if, for example, not all but only the selected correlation ρ_{ii} from the diagonal has non-zero value. In the remaining presentation of the thesis, however, the general (with all correlations from the diagonal) propagation for time-varying processes will be used.

3.2 Synchronization detection

After performing the inference, one can use the reconstructed parameters, given in a form of multivariate normal distribution $\mathcal{N}_{\mathcal{X}}(c, \Sigma)$, to study the interactions between the oscillators under study. One of the major points of interest is to detect whether the dynamics described by the inferred parameters undergo synchronization and if transitions exist between the qualitative states. The particular information propagation for tracing time-varying parameters can allow the synchronization state and its transitions to be observed in time.

It is important to notice that a non-zero noise can induce phase slips in a system that would be synchronized in the noiseless limit. However, the currently proposed methods for synchronization detection are based on the presence and statistics of phase-slips, rather than on the nature of the phase-slip itself [20–22]. The novelty embedded in this study is that it proposes evaluation of the probability that the equations that drive the dynamics are intrinsically synchronized and if the possibly observed phase-slips are dynamics-related or noise-induced.

Every parameter set can be distinguished depending on whether it belongs to the Arnold tongue region i.e. whether it belongs to the synchronization parameter space. For the inferred parameters one needs to find a criterium for determining if the dynamics governed by the base phase function are in a synchronized state. This binary property was called $s(c_k^{(l)}) = \{1, 0\}$. Thus the posterior probability of the system to be synchronized or not is obtained by evaluating the probability of s:

$$p_{\text{sync}} \equiv p_{\mathcal{X}}(s = 1) = \int s(c)\, \mathcal{N}_{\mathcal{X}}(c|\bar{c}, \Xi)\, \mathrm{d}c\,. \tag{3.19}$$

In general, the border of the Arnold tongue might not have an analytic form, and, even if it had, the integral has no analytic solution and must be evaluated numerically. A practical way to proceed is to estimate numerically p_{sync} by sampling many realizations from the parameters space $\{c_k^{(l)}\}_m$, where m labels each testing parameter vector, and for every set of c_m synchronization to be computed $s(c_m)$. The probability sampling is discussed in more detail in section (3.4.4).

But, how can one detect the binary property $s(c) = \{1, 0\}$ describing if a single set of parameters makes the phase dynamics synchronized or not? For the simple form of the base function $\Phi_{l,k}$ (e.g. the phase model Eq. (3.1) described in section 3.5.1) there might exist an analytic solution - then $s(c)$ is explicitly defined. But in order to keep the generality of the method, there is a need for a technique that can detect synchronization of phase dynamics described by any number and general form of the base function $\Phi_{l,k}$ defined.

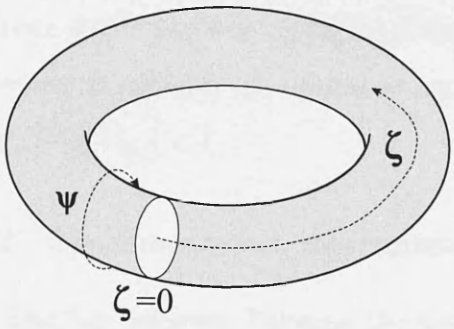

Fig. 3.2: Torus representation of the phase dynamics, given with toroidal coordinate $\zeta(\phi_1(t), \phi_2(t))$ and polar coordinate $\psi(\phi_1(t), \phi_2(t))$. The white circle denotes the Poincaré cross section.

3.2.1 Torus dynamics and map representation

In this section a simple technique to recognize whether a phase oscillatory system is synchronized or not is presented. The technique itself is a simple check through numerical integration of an ordinary differential equation system (defined by Eq.(3.1) without the inferred noise) through one cycle of the dynamics, and testing whether the synchronization condition $|\psi(t)| = |\phi_1(t) - \phi_2(t)| < K$ is always verified.

Let us assume we are observing the motion on the torus $\mathbb{T}^2$ defined by the the toroidal coordinate $\zeta(\phi_1(t), \phi_2(t)) = (\phi_1(t) + \phi_2(t))/2$, and the polar coordinate $\psi(t)$. For determination of synchronization the phase difference $\psi(t)$ will be defined as $\psi(\phi_1(t), \phi_2(t)) = \phi_1(t) - \phi_2(t)$. Schematic representation of the phase dynamics on torus is shown on Fig. 3.2. Let's consider a Poincaré section defined by $\zeta = 0$ and assume that $d\zeta(t)/dt|_{\zeta=0} > 0$ for any ψ. This means that the direction of motion along the toroidal coordinate is the same for every point of the section. Ideally one would follow the time-evolution of every point in the section and check if there is a periodic orbit; if a periodic orbit exists and if its winding number is zero, then the system is synchronized. If such a periodic orbit exist, then there is at least another periodic orbit with one of them being stable and the other unstable.

The solution of the dynamical system over the torus induces a map $M : [0, 2\pi] \to [0, 2\pi]$ that defines, for each ψ_n on the Poincaré section, the next phase ψ_{n+1} after one round of the toroidal coordinate: $\psi_{n+1} = M(\psi_n)$. The map M is continuous, periodic,

and has two fixed points (one stable and one unstable) if and only if there is a pair of periodic orbits for the dynamical system, i.e. synchronization is verified if ψ_e exists such that $\psi_e = M(\psi_e)$ and $\left|\frac{dM(\psi)}{d\psi}|_{\psi_e}\right| < 1$.

3.2.2 Synchronization discrimination

The procedure of synchronization detection between the two oscillators that generate the phase time-series reduces to investigation of synchronization of the synthetic phase model model using the parameters returned from the Bayesian machine. To calculate $s(c)$ for any of the sampled parameter sets, one can proceed as follows:

i) from an arbitrary fixed ζ, and for an arbitrary ψ_0 integrate numerically (with the standard fourth order Runge-Kutta algorithm) the dynamical system prescribed by the phase base function (Eq.(3.3) without the noise) for one cycle of the toroidal coordinate, obtaining the mapped point $M(\psi_0)$.

ii) the same integration is repeated for multiple ψ_i coordinates next to the initial one, obtaining the map $M(\psi_i)$

iii) by finite difference evaluation of $dM/d\psi$ a modified version of the Newton's root finding method is employed in respect of the function $M(\psi) - \psi$. The method is modified by calculating M at the next point ψ_{n+1} such that

$$\psi_{n+1} = \psi_n + 0.8 * |(M(\psi_n) - \psi_n)/(M'(\psi_n) - 1))|.$$

Note that in this version, Newton's method can only test the function by moving forward; in fact a) the existence of the root is not guaranteed; b) we are not interested in the root itself but only in its existence.

iv) If there is a root, $s(c) = 1$ is returned. If the root is not found, $s(c) = 0$ is returned.

3.3 Interactions description

On of the main goals of this study is to infer and describe the interactions between oscillators in a dynamical environment subject to external deterministic and stochastic influences. The interactions characterize the inner relationships between several or large population of oscillators, and represent a base that defines phenomenological states (such as synchronization) and the flow of information i.e. structure of the connectivity.

The nature of an interaction mainly depends on the physical properties of the oscillating systems, their functionality and how they react to perturbations. The central idea is to use the inferred parameters from $\mathcal{N}_{\mathcal{X}}(c, \Sigma)$ to describe the interacting properties. Because the dynamics are reconstructed separately as described by Eq. (3.1), usage can be made only of those inferred parameters from the base functions $g_i(\phi_i, \phi_j)$ which are linked to the influences between the oscillators.

One can seek to determine the properties that characterize the interaction in terms of a strength of coupling, predominant direction of coupling or even by inference of a coupling function. As to the use of information propagation allows inference of time-varying dynamics, the interactions' properties can be traced in time as well. This is especially important for inference of open interacting oscillatory processes, which are often found in nature, where the time-variability interactions can lead to transitions between qualitative states, such as synchronization or oscillating death.

3.3.1 Directionality estimation

The interaction strength or the coupling amplitude quantifies the net information flow between the oscillators. It has been found useful in many investigations, including determination of causality relationships [6, 88] or reconstruction of structure of networks [80, 83]. Several approaches have been proposed for quantification of the couplings, including mutual theoretic information [23, 25], phase dynamics decomposition [24, 28], wavelet bispectrum [26] and perturbation techniques [79, 83, 89]. However, these techniques inferred neither the noise dynamics nor the parameters characterizing the

noise, and not all of them were able to cope with the time-variability of the intrinsic parameters.

The coupling amplitude quantifies the total influence between the oscillators in some direction: for example how much the dynamics of the first oscillator affect the dynamical behavior of the second oscillator ($1 \rightarrow 2$). If the coupling is in only one or in both directions, we speak of unidirectional or bidirectional coupling, respectively. In the proposed inferential framework, the coupling amplitudes are evaluated as normalized measures from the interacting parameters inferred from the coupling base functions $q_i(\phi_i, \phi_j)$. The quantification is calculated as a Euclidian norm:

$$\begin{aligned} \epsilon_{21} &= \|q_1(\phi_1, \phi_2)\| \equiv \sqrt{c_1^2 + c_3^2 + \ldots} \\ \epsilon_{12} &= \|q_2(\phi_1, \phi_2)\| \equiv \sqrt{c_2^2 + c_4^2 + \ldots}, \end{aligned} \tag{3.20}$$

where e.g. in the proposed implementation the odd inferred parameters were assigned to base functions $q_1(\phi_1, \phi_2)$ for the coupling that the second oscillator imposed on the first ($\epsilon_{21} : 2 \rightarrow 1$), the even for the first on second oscillator ($\epsilon_{12} : 1 \rightarrow 2$).

The direction of coupling often gives useful information about the interactions, and is defined as normalization about the predominant coupling amplitude:

$$\mathrm{D} = \frac{\epsilon_{12} - \epsilon_{21}}{\epsilon_{12} + \epsilon_{21}}. \tag{3.21}$$

If $\mathrm{D} \in (0, 1]$ the first oscillator drives the second ($1 \rightarrow 2$), or if $\mathrm{D} \in [-1, 0)$ the second ($2 \rightarrow 1$) drives the first. The quantified values of the coupling strengths ϵ_i or the directionality D represent measures of combined relationships between the oscillators. Thus, a non-zero value can be inferred even when there is no interactions. The latter discrepancy can be overcome by careful surrogate testing [90, 91] – by rejecting values below an acceptance surrogate threshold, which can be determined as the mean plus two standard deviations of many realization of the measures.

3.3.2 Coupling function reconstruction

Beside the coupling strength and the directionality, one can also infer the function that characterize the interactions. This coupling function defines the law that describes the functional relationships between the oscillators, and its characteristic form results from the nature of the oscillators and how their dynamics react under perturbations. The inference of an underlying phase model has formed the basis for techniques to infer the coupling functions [28, 80–82]. However, these techniques did not inferred the noise dynamics nor the parameters characterising it, and they did not inferred or treated time-varying dynamics.

The coupling function is defined as the law through which the interactions undergo transitions to synchronization i.e. transitions to equilibrium stability. This physical meaning is illustrated schematically on Fig. 3.3 (a) for the case of simple phase oscillators with sine coupling function (following Kuramoto [10]). The black lines represent situations where the oscillators are not synchronized and there are no stable solutions for the phase difference. For certain parameters (frequency mismatch and coupling amplitudes) the coupling function intersect the equilibrium axis ($\dot{\psi} = 0$), and two solutions appear, one stable and one unstable, and the oscillators are synchronized.

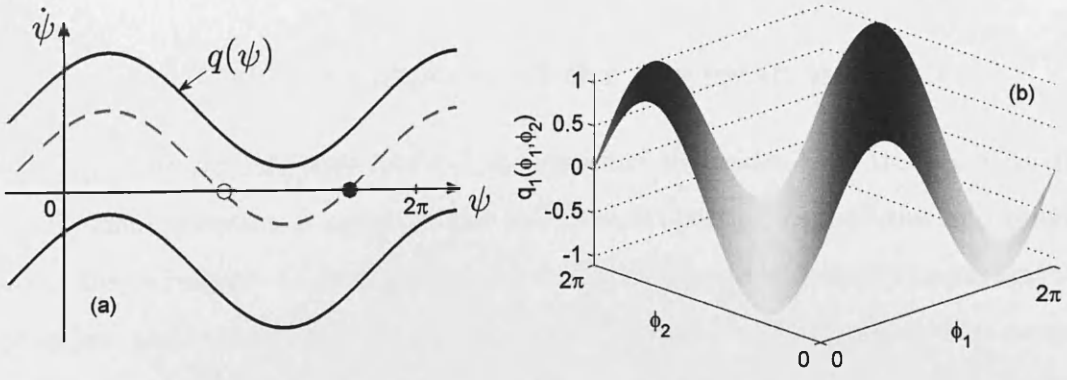

Fig. 3.3: Schematic representation of coupling function. The coupling as a function of the phase difference $\psi = \phi_2 - \phi_1$ and its implications for synchronization transitions (a). The full line is for unsynchronized while the dashed for the synchronized case – the white circle corresponds to stable and black to unstable equilibrium solutions. (b) The coupling as a function of both phase variables.

To determine synchronization, it is sufficient to analyze the coupling function through the phase difference alone. In general, however, one can study the function with respect to both the phases Fig. 3.3 (b). Winfree [7] used a function that is defined by both phases, rather than just the phase difference, while Daido and Crawford [76–78] used more a general form where the function was expanded in its Fourier series.

The coupling function should be 2π-periodic. In the inferential framework under study, the coupling functions was decomposed into finite number of Fourier components. The function describing the interactions between the two oscillators was decomposed by the odd parameters $q_1(\phi_1, \phi_2) \in \{c_1, c_3, \ldots\}$ and the corresponding base functions $\Phi_n[q_1(\phi_1, \phi_2)] \in \{\sin(\phi_1, \phi_2), \cos(\phi_1, \phi_2)\}$ up to order n of the decomposition. The reverse function $q_2(\phi_1, \phi_2) \in \{c_2, c_4, \ldots\}$ was similarly decomposed.

The time-variability propagation allows the coupling function to be inferred in time. This constitutes one of the novelties of the approach, because now one can trace the time-evolution of this functional relationships. From chapter 2 section 3.5.4 it is clear that the latter is very important, and can act as a reason for transitions to synchronization. The importance for studying time-varying coupling functions is even greater given that it is a property observed in real life oscillatory systems - such as the cardiorespiratory system.

3.4 Technical aspects of the Bayesian inference

Before applying the inference method, as presented theoretically in the previous discussion, some attention is spent on the technical properties, capabilities and limitations of the technique. Understanding the technical aspects is crucially important for appropriate and correct applications, especially because the final framework is a combination of several concepts and their functioning together must be set up correctly.

There are number of technical aspects characterizing the technique, which include inference of stochastic dynamics and parameters with time-varying nature, where the resulting measures are probabilistic distributions. For this reasons, we considered the following: how the different number of base functions affects the inference, how does

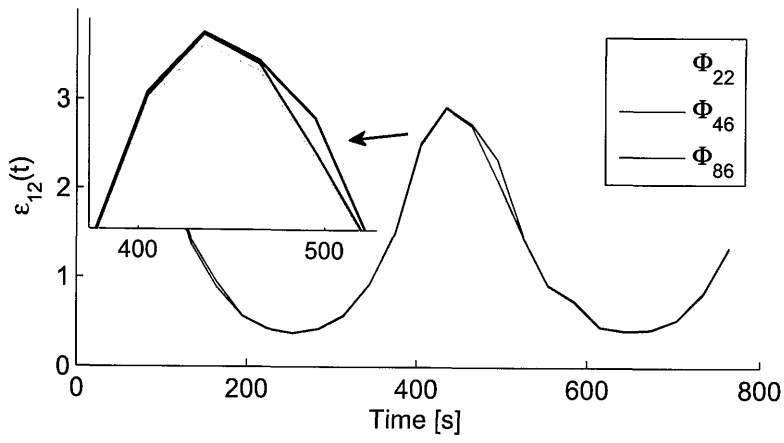

Fig. 3.4: Inference of time-varying coupling amplitude with different number of base functions, applied on signal from numerical simulation of model (3.22); parameters are given in the text. The particular number of base functions is shown on the legend. The difference of precision is mostly observe around the local maxima – also enlarge on the inset.

the inference behave under different strengths of noise, what time-resolutions of the time-varying parameters can be traced and how to sample the combined measures of the resulting probability distributions. There exist many other technical aspects, but the ones presented here are considered to be sufficient for proper understanding of the particular (and similar) implementation of inferential technique.

3.4.1 Number of base functions

In this section, the discussion is focussed on the question of what is the optimal number of base functions to be used. The problem is basically an interplay between achieving the desired precision and computational speed. To infer the dynamics more precisely, we need to use larger number of base functions. This is even more pronounced when one tries to infer properties (like time-varying frequencies, coupling functions, ...) that have 'non-sine' steep form. Then, in order to trace the higher harmonics, the inference needs to include expansion of the Fourier components up to higher orders. On the other hand, having large number of base functions for inference reduces the computational speed of the algorithm, and the functions that are not part of the actual dynamics can infer (pick up) some components from the noise. The base functions

within the inferential framework are presented as multivariate Gaussian distribution in matrix form. Thus a large number of base functions increases the parameter space vastly and the iterative calculations (especially the evaluation of inverse of a matrix) slow down the speed of processing exponentially. It is worth noting that, even though the Bayesian inference is popular for its real-time applications, the proposed inference framework for general phase dynamics does not allow (in computational speed sense) real-time applications.

In order to demonstrate the inference precision of time-varying parameters the technique was applied on a numerically simulated signal. The simulation was performed on a model of two coupled Poincaré oscillators subject to white noise:

$$\begin{aligned}
\dot{x}_1 &= -\Big(\sqrt{x_1^2+y_1^2}-1\Big)x_1 - \omega_1(t)y_1 + \varepsilon_{21}(t)(x_2-x_1) + \xi_1(t) \\
\dot{y}_1 &= -\Big(\sqrt{x_1^2+y_1^2}-1\Big)y_1 + \omega_1(t)x_1 + \varepsilon_{21}(t)(y_2-y_1) + \xi_1(t) \\
\dot{x}_2 &= -\Big(\sqrt{x_2^2+y_2^2}-1\Big)x_2 - \omega_2(t)y_2 + \varepsilon_{12}(t)(x_1-x_2) + \xi_2(t) \\
\dot{y}_2 &= -\Big(\sqrt{x_2^2+y_2^2}-1\Big)y_2 + \omega_2(t)x_2 + \varepsilon_{12}(t)(y_1-y_2) + \xi_2(t),
\end{aligned} \tag{3.22}$$

where the frequency $\omega_i(t)$ and the coupling amplitudes $\varepsilon_{ij}(t)$ were allowed to be time-varying in some situations. The same model will be used for the remaining discussion of this section. The coupling function is a linear state difference $(x_j - x_i,\, y_j - y_i)$ and at this point is considered to have constant (non time-varying) form.

A particular case was considered, where the coupling amplitude from the first oscillator was periodically time-varying: $\varepsilon_{12}(t) = \varepsilon_{12} + \tilde{A}\sin(\tilde{\omega}t)$. The parameters were: $\omega_1(t) \equiv \omega 1 = 2\pi 1.1$, $\omega_2(t) \equiv \omega 2 = 2\pi 2.77$, $\varepsilon_{21} = 0$, $\varepsilon_{12} = 1.7$, $\tilde{\omega} = 2\pi 0.0025$, $\tilde{A} = 1.3$ and noise strength $E_1 = E_2 = 0.5$. Evaluation of the coupling amplitude is done through calculation of the norm (Eq. 3.20) from the inferred coupling parameters. Results of the $\varepsilon_{12}(t)$ inference from the same signal for three cases with different number of base functions are presented on Fig. 3.4. From the parameter estimations around the local maxima (also enlarged on the inset), one can notice that the inference is not following the sine form promptly. This can be due to particular

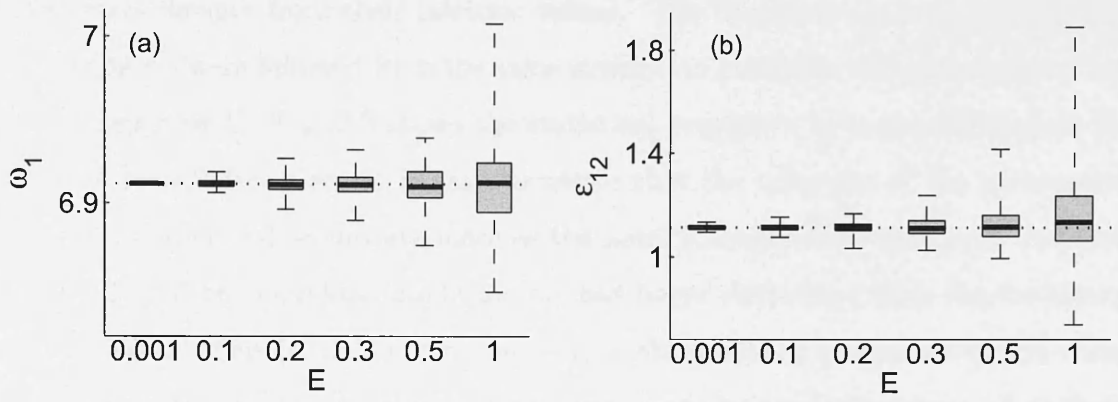

Fig. 3.5: Statistical properties for inference of parameters for different noise intensity E. The dotted line shows the intrinsic values of the parameters presented with boxplots. The boxplots indicate: median with black tick line, the lower and the upper quartile are shown within the gray box, while the range (minima, maxima) is denoted with the vertical dashed line. Outliers are ignored.

effect of the noise, or if the two oscillators have become more coherent around these parameter values. The figure demonstrates that the three cases were different, and that the inference with larger numbers of base functions was getting closer to the intrinsic parameter values.

3.4.2 Effect of noise intensity

The proposed technique tries to infer dynamics of coupled oscillators subject to noise. One of the main functions are to decompose what is considered to be intrinsic dynamics from the effect of the noise. The question posed here is: how well can we infer the parameters when the dynamics are subject to noise of different strengths. The answer implicitly depends on how is the propagation of information is achieved. The results will be best for full propagation and constant parameters, but because the objective is inference of time-varying dynamics, the following investigation is done for propagation that can trace time-varying parameters.

The same numerical example (3.22) is considered, but for constant parameters and different noise strengths. The parameters were: $\omega_1 = 2\pi 1.1$, $\omega_2 = 2\pi 1.77$, $\varepsilon_{21} = 0.05$, $\varepsilon_{12} = 1.17$ and $E_1 = E_2 = E$. The main idea is to investigate how much will the

parameters deviate from their intrinsic values. The frequency ω_1 and the coupling amplitude ε_{12} were followed from the same simulation performed for each value of the noise intensities E_i. Fig. 3.5 shows the statistical properties in terms of boxplots for different noise intensities. It is easy to notice that the inference of the parameters is worse i.e. their values deviate more as the noise intensity E is increased. Another feature is that the coupling amplitude ε_{12} has larger deviations than the frequency ω_1 parameter. This is probably because ε_{12} is the result of evaluation of the norm as a combination of several inferred parameters, and the noise effect from all of them contributes to the final deviation. Finally, it is worth pointing that in experiments (cardiorespiratory and analogue interactions), the noise strength inferred was not usually very high ($0.01 \leq E \leq 0.2$).

3.4.3 Time resolution

The main objective of this study is to infer time-varying dynamics. The issue addressed here is: how fast/slow dynamics can be traced by the proposed technique and what precision is achieved. The problem is related to the size of the sequential windows i.e. the amount of information included within one block of data. The issue is also implicitly dependent on a time-resolution (i.e. frequencies) of dynamics of the interacting oscillators.

Using the numerical model (3.22), the time-resolution was investigated for case where the frequency $\omega_1(t) = \omega_1 + \tilde{A}_1 \sin(\tilde{\omega}t)$ and coupling amplitude $\varepsilon_{12}(t) = \varepsilon_{12} + \tilde{A}_1 \sin(\tilde{\omega}t)$ were varying periodically at the same time. The parameters were: $\omega_1 = 2\pi 1.1$, $\omega_2 = 2\pi 2.77$, $\varepsilon_{21} = 0$, $\varepsilon_{12} = 1$, $\tilde{\omega} = 2\pi 0.002$, $\tilde{A}_1 = 0.1$ $\tilde{A}_2 = 0.5$ and noise strengths $E_1 = E_2 = 0.15$. The parameters were reconstructed using four different lengths of the inference windows. The results presented on Fig. 3.6 demonstrate that for small windows (0.5s) the parameters are sparse and sporadic, while for very large windows (100s) the time-variability is faster than the size of the window and there is cut-off on the form of the variability. A better suited window size will be in between this two. Another interesting feature is that for the smallest window (0.5s), the coupling amplitude is improved with information propagation as time progresses,

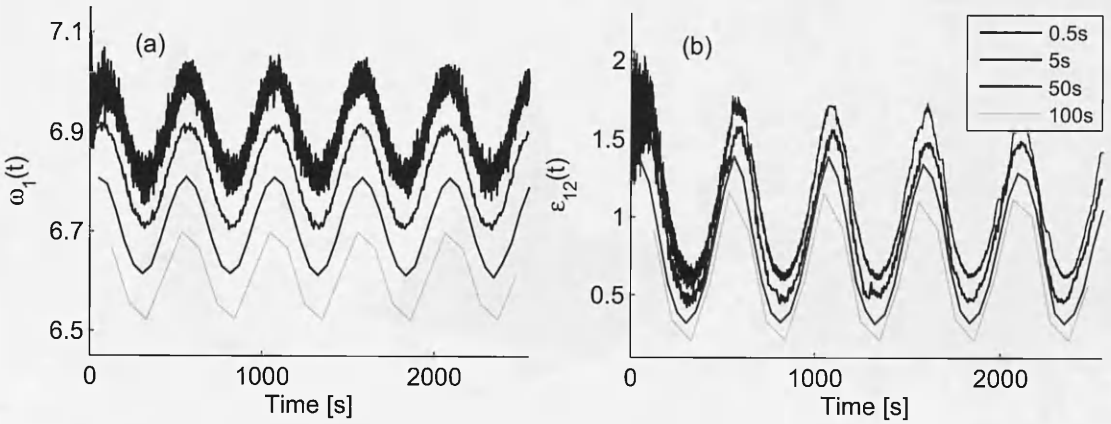

Fig. 3.6: Inference of a time-varying frequency (a) and coupling parameter (b) from model (3.22) for four different lengths of the inference windows. The size of the windows is shown on the legend.

while the frequency inferred (as a constant component without base function) is sparse throughout the whole time interval.

3.4.4 Probability sampling

The final result of the inference is given with the set $\mathcal{N}_{\mathcal{X}}(c|\bar{c}, \Sigma)$. Every inferred parameter has the nature of a Gaussian distribution, and it is a part of a multivariate Gaussian distribution for the whole parameter space given by the mean vector $\bar{c}$ and the covariance matrix Σ. If one needs to infer a measure that is evaluated from the combination of the inferred parameters then, in theory, one needs to evaluate the probability of the measure from the multivariate Gaussian distribution $\mathcal{N}_{\mathcal{X}}(c|\bar{c}, \Sigma)$. Assume that a binary property of the measure $m(c) = \{1, 0\}$ is given. For example, $m(c)$ can be the synchronization index $s(c) = \{1, 0\}$ presented in section 3.2.1, a normalized evaluation of the directionality index, or some other. Then the posterior probability of the measure can be evaluated as:

$$p_m \equiv p_{\mathcal{X}}(m = 1) = \int m(c)\, \mathcal{N}_{\mathcal{X}}(c|\bar{c}, \Sigma)\, \mathrm{d}c\,. \tag{3.23}$$

This integral may not have an analytic solution, and in order to keep the generality and practicality of the approach, one can try to solve it by numerical evaluation.

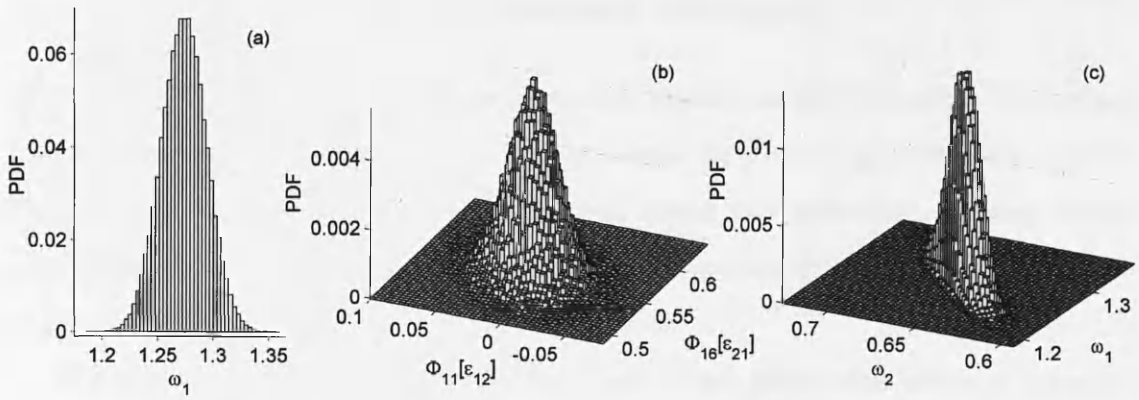

Fig. 3.7: Probability sampling for the inferred parameters of model (3.22). (a) Gaussian-like distribution of frequency ω_1. Bi-variate distribution of two inferred (b) coupling parameters and (c) frequency parameters. Note the high (blade-like) correlation on (c). There was no time-variability, and the parameters were $\omega_1 = 1.27$, $\omega_2 = 0.67$, $\varepsilon_{21} = 0.05$, $\varepsilon_{12} = 0.25$ and the rest same as on Fig. 3.4.

Proceeding in a Monte Carlo manner, using the parameter space, one can sample many realizations m_k, where k labels each testing parameter vector. Fig. 3.7 shows several examples of sampling distributions from the inference of model (3.22). Fig. 3.7 (a) shows the Gaussian-like distribution of single frequency parameter after the sampling of $\mathcal{N}_\chi(c|\bar{c}, \Sigma)$, while Fig. 3.7 (b) and (c) demonstrate the distribution correlation of two inferred parameters. The two latter bivariate distributions only tackle the complexity of the full multivariate normal distribution $\mathcal{N}_\chi(c|\bar{c}, \Sigma)$, which can have many more multivariate dimensions.

To find p_m arbitrarily precisely it is enough to generate a number K of parameters c_k, with $k = 1, \ldots, K$ sampled from $\mathcal{N}_\chi(c|\bar{c}, \Sigma)$, since $p_m = \lim_{K\to\infty} \frac{1}{K} \sum_k^K m(c_k)$. However, this high dimensional integration quickly becomes inefficient with an increasing number of Fourier components. On the other hand, if the posterior probability p_χ is sharply peaked around the mean value $\bar{c}$, then p_m will be indistinguishable from $m(\bar{c})$, and evaluation of $m(\bar{c})$ only, would suffice.

3.5 Application examples

After laying down the theoretical and technical aspects of the inferential framework, here we proceed with application of the technique on several characteristic models. This section demonstrates all the aspects, and shows how optimally, one can exploit and benefit from the method. It also reveals the novelties brought by this approach in respect of application of earlier known methods.

The only requirements (inputs) for the method are phase time-series of interacting oscillators. As long as they are properly defined and detected, the phases are not model-dependent and they can come from any general form of oscillator. This contributes to the generality of the method and its wide applicability. In the following, different types of models are used to demonstrate particular features of the method.

3.5.1 Phase oscillators model

In order to be systematic, and before going to more complicated realistic models, the technique is applied on a simple phase oscillators model. This will give a sufficient base model for synchronization description, which is analytically traceable at the same time. Moreover, the base functions embedded in the inferential framework are a perfect match for the inference of the interacting phase model.

The main objective in this section is to demonstrate how the synchronization detection works, and to investigate the implications when applied to noisy time-series. In this sense, the detection of synchronization means if the examination of the constructed map $M(\psi)$ (followed after Bayesian inference) can distinguish synchronized ($s(c) = 1$) from unsynchronized dynamics ($s(c) = 0$), i.e. whether the root $M(\psi_e) = \psi_e$ exists or not. It is important to notice that a non-zero noise can induce phase slips in a system that would be synchronized in the noiseless limit. Therefore, a genuine inference should not only detect the presence of a phase-slips, but also needs to describe the nature of the phase-slip itself: whether it is noise-induced or dynamic-related. The latter means to describe the dynamics in parameter space in relation to the inferred parameters, without the contribution of the noise. The parameter space for

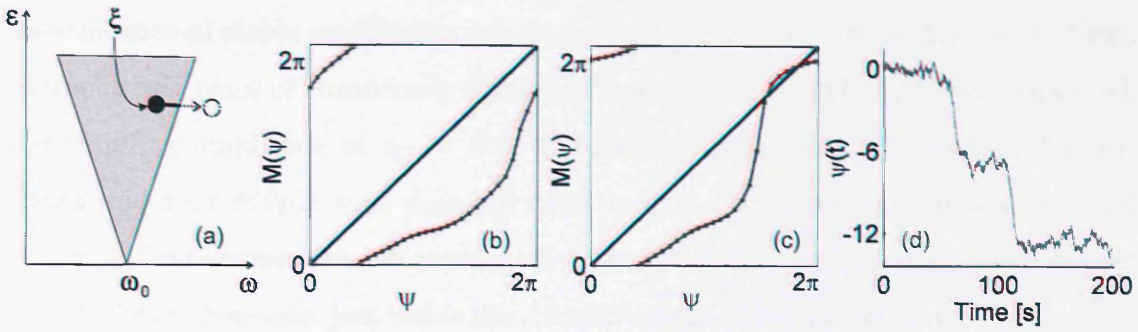

Fig. 3.8: Synchronization discrimination for the coupled phase oscillators (3.24). (a) Schematic Arnold tongue to illustrate synchronization [9]. (b) Map of $M(\psi)$ for $\epsilon_{12} = 0.25$ demonstrating that the oscillators are not synchronized. (c) Map of $M(\psi)$ for (d) demonstrating that a root of $M(\psi) = \psi$ exists, i.e. that the state is, in fact, synchronized. (d) Phase difference, exhibiting two phase slips.

synchronization phenomenon can effectively be described by Arnold tongues [9]. Fig. 3.8 (a) illustrates schematically a particular situation: in a noiseless case the systems are synchronized (black circle inside the Arnold tongue) and only because of the effect from the noise phase-slips occur (white circle outside the Arnold tongue). Thus the main goal is to detect whether the systems are intrinsically synchronized, and if the existence of phase slips is due to effect of the noise.

The model for generating a numerical phase signal for analysis is given by two coupled phase oscillators subject to white noise:

$$\begin{aligned} \dot{\phi}_1 &= \omega_1 + \epsilon_{21} \sin(\phi_2 - \phi_1) + \xi_1(t) \\ \dot{\phi}_2 &= \omega_2 + \epsilon_{12} \sin(\phi_1 - \phi_2) + \xi_2(t). \end{aligned} \tag{3.24}$$

The parameters were $\epsilon_{21} = 0.1$, $\omega_1 = 1.2$, $\omega_2 = 0.8$ and $E_1 = E_2 = 2$. Note that there is no time-variability i.e. all of the parameters are constant in time. Thus the discussion shall be focus more on the effect of the noise, and the inference will be applied to a single block of data.

The dynamics of the phase difference will be described as: $\dot{\psi} = \Delta\omega - \epsilon \sin(\psi) + \xi_1(t) + \xi_2(t)$, where $\Delta\omega = \omega_2 - \omega_1$ is the frequency mismatch and $\epsilon = \epsilon_{21} + \epsilon_{12}$ is the resultant coupling. In the noiseless case, the analytic condition for synchronization i.e.

the existence of stable equilibrium solution $\dot{\psi} < 0$ can be reduced to $\Delta\omega/\epsilon < 1$. Next, characteristic cases of numerically simulated signals from model (3.24) were analyzed. For coupling amplitude of $\epsilon_{12} = 0.25$ the reconstructed map $M(\psi)$ (Fig. 3.8 (b)) shows that root $M(\psi_e) = \psi_e$ does not exist and the oscillators are not synchronized $s(c) = 0$. To demonstrate the novelty of our method, the parameters were such that the oscillators were only just inside the Arnold tongue. This was achieved by enlarging the coupling amplitude to $\epsilon_{12} = 0.35$ – then the analytic condition for synchronization $\Delta\omega/\epsilon = 0.4/0.45 < 1$ is fulfilled and the systems should be synchronized. However, due to the effect of the moderate noise phase-slips occurred, see Fig. 3.8 (d). The application of earlier methods based on the statistics of the phase difference [20–22] suggests that the oscillators are *not* synchronized. In contrast, the proposed technique shows that the oscillators are *intrinsically* synchronized as shown in Fig. 3.8 (c): the phase slips are attributable purely to noise (the intensity of which is inferred in matrix $E_{i,j}$), and not to deterministic interactions between the oscillators. The ability to identify noise-induced phase slip could be important in a number of contexts, including both noise-induced synchronization [65, 66, 92] and desynchronization [93].

3.5.2 Limit-cycle oscillators model

The proposed inferential framework offers a possibility of doing comprehensive analysis within one sole formalism. The following discussion explores this and investigates how the proposed method can trace time-varying parameters, coupling functions, directionality and synchronization.

The model under consideration consisted of two coupled non-autonomous Poincaré

oscillators subject to white noise:

$$\begin{aligned}
\dot{x}_1 &= -\left(\sqrt{x_1^2+y_1^2}-1\right)x_1 - \omega_1(t)y_1 + \varepsilon_1(t)q_1(x_1,x_2,t) + \xi_1(t) \\
\dot{y}_1 &= -\left(\sqrt{x_1^2+y_1^2}-1\right)y_1 + \omega_1(t)x_1 + \varepsilon_1(t)q_1(y_1,y_2,t) + \xi_1(t) \\
\dot{x}_2 &= -\left(\sqrt{x_2^2+y_2^2}-1\right)x_2 - \omega_2(t)y_2 + \varepsilon_2(t)q_2(x_1,x_2,t) + \xi_2(t) \\
\dot{y}_2 &= -\left(\sqrt{x_2^2+y_2^2}-1\right)y_2 + \omega_2(t)x_2 + \varepsilon_2(t)q_2(y_1,y_2,t) + \xi_2(t).
\end{aligned} \tag{3.25}$$

All of the parameters can be time-varying, and the coupling function can have different forms with or without time variability.

First, we consider unidirectional coupling (1→2), where the natural frequency of the first oscillator, and its coupling strength to the second one, vary periodically at the same time: $\omega_1(t) = \omega_1 + \tilde{A}_1 \sin(\tilde{\omega}_1 t)$ and $\varepsilon_2(t) = \varepsilon_2 + \tilde{A}_2 \sin(\tilde{\omega}_2 t)$. The other parameters were: $\varepsilon_2 = 0.1$, $\omega_1 = 2\pi 1$, $\omega_2 = 2\pi 1.14$, $\tilde{A}_1 = 0.2$, $\tilde{A}_2 = 0.13$, $\tilde{\omega}_1 = 2\pi 0.002$, $\tilde{\omega}_2 = 2\pi 0.0014$ and noise $E_{11} = E_{22} = 0.1$. The coupling function was simple linear difference in the state variables: $q_i(x_i, x_j, t) = x_i - x_j$ and $q_i(y_i, y_j, t) = y_i - y_j$. The phases were estimated as the angle variable $\phi_i = \arctan(y_i/x_i)$. With $\varepsilon_1 = 0.1$ there is no synchronization and the time-varying parameters ($f_1(t)$ and $\varepsilon_2(t)$) are accurately traced: see full lines of Fig. 3.9 (a) and (b). The form and the speed of the inferred parameters demonstrate the precision of the method and the benefits of the time-varying information propagation. For a coupling amplitude of $\varepsilon_1 = 0.3$ the two oscillators will be synchronized for part of the time, resulting in intermittent synchronization. The time-variability of the parameters in the non-synchronized intervals is again determined correctly, while in the synchronized intervals they differ in value the intrinsic parameters, Fig. 3.9 (a) and (b), dashed lines. Within these synchronized intervals, all of the base functions are highly correlated, with values lying within the Arnold tongue. The latter was detected as synchronized ($s(c) = 1$) intervals, Fig. 3.9 (a) and (b), grey shaded regions.

The reconstructed sine-like functions $q_1(\phi_1, \phi_2)$ and $q_2(\phi_1, \phi_2)$ are shown in Figs. 3.9 (c) and (d) for the first and second oscillators, respectively. They describe the

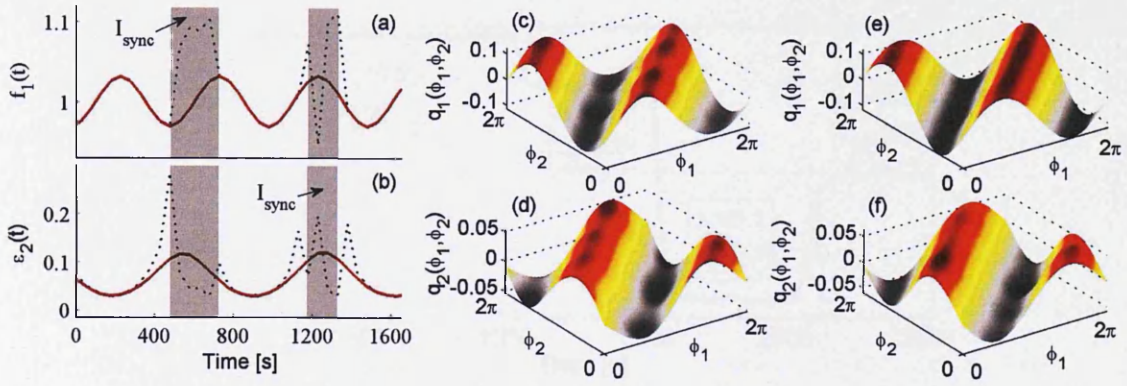

Fig. 3.9: Extraction of time-varying parameters, synchronization and coupling functions from numerical data created by (3.25). The frequency $f_1(t)$ (a) and coupling $\varepsilon_2(t)$ (b) are independently varied. The dotted and full lines plot the parameters when the two oscillators are synchronized for part of the time ($\varepsilon_1 = 0.3$), and not synchronized at all ($\varepsilon_1 = 0.1$), respectively. The regions of synchronization, found by calculation of the synchronization index, are indicated by the gray shaded regions. (c)–(f) show the coupling functions $q_1(\phi_1, \phi_2)$ and $q_2(\phi_1, \phi_2)$ for time windows centered at different times: (c) and (d) at $t = 350s$; (e) and (f) at $t = 1000s$. The window length $t_w = 50s$, and $\varepsilon_{12} = 0.1$ in both cases. Note the similarity in forms of (c) and (e), and of (d) and (f).

functional form of the interactions between the two Poincaré systems (3.25). The application of the proposed approach suggests that the form of the coupling functions does not evolve with time – q_1 and q_2 evaluated for later time segments are presented on Fig. 3.9 (e) and (f) respectively. By comparison of Fig. 3.9 (c) and (e), or of Fig. 3.9 (d) and (f), we see that the coupling functions are time invariant and they did not change qualitatively, even though there were time-varying parameters and weak effects from the noise.

Next, the method was applied to detect the predominant direction of coupling presented through a quantitative measure evaluated as the norm of the inferred coupling base parameters. To illustrate the detection and precision of directionality, the frequencies now were considered to be constant, while both of the coupling strengths to be discretely time-varying. The parameters were $\omega_1 = 2\pi 1.3$, $\omega_2 = 2\pi 1.7$, $E_{11} = E_{22} = 0.2$, and the coupling function were as on the previous example: $q_i(x_i, x_j, t) = x_i - x_j$ and $q_i(y_i, y_j, t) = y_i - y_j$. Synchronization, however, was not reached for these parameters. The couplings alternate (in time intervals as

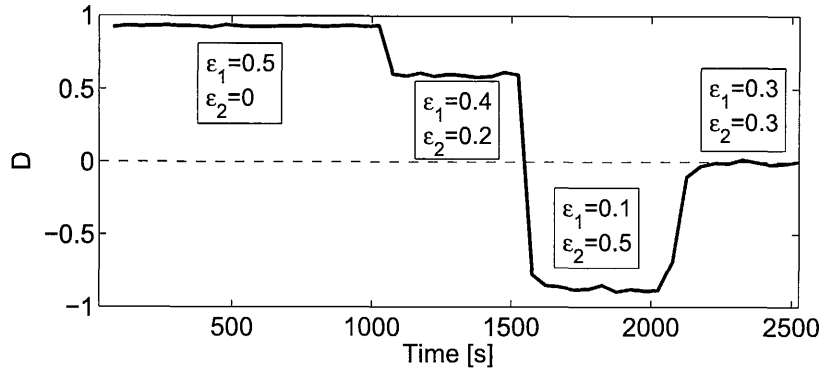

Fig. 3.10: Directionality of coupling for discrete time-varying coupling strengths. Different unidirectionally and bidirectionally cases are reached by different values of the coupling amplitudes ε_1 and ε_2 – as indicated by the square insets.

depicted on Fig. 3.10) from unidirectionally ($1 \rightarrow 2$), to bidirectionally ($1 \rightarrow 2$), then bidirectionally ($2 \rightarrow 1$), so as to finish with zero bidirectional couplings ($1 = 2$). The detected directionality index was consistent with the hypothetical values. Note that the value of unidirectionally coupling has not reached 1, due to the noise disturbance.

The oscillatory models used for studying interactions and synchronization, usually are considered to have time-invariant coupling functions (for example the coupling function on Fig. 3.9 (c)-(f)). However, when the oscillators are open by nature, the functions defining their interactions can also be time-varying processes by themselves. Moreover, as discussed in the previous chapter, the variations of the form of a coupling functions can be the reason alone for which synchronization transitions can occur.

To investigate the issue of time-varying coupling functions and the implications when the inferential technique is applied, the same model (3.25) was used but now the coupling functions were absolute values of the state difference on power of time-varying parameter:

$$q_i(x_i, x_j, t) = |(x_j - x_i)^{\nu(t)}|;\ q_i(y_i, y_j, t) = |(y_j - y_i)^{\nu(t)}|, \tag{3.26}$$

where $i = j = \{1, 2\}$ and $i \neq j$. The exponent parameter varied linearly with time $\nu(t) = \{1 \rightarrow 3\}$, and the rest of the parameters were constant: $\omega_1 = 2\pi 1$, $\omega_2 = 2\pi 2.14$, $\varepsilon_1 = 0.2$, $\varepsilon_2 = 0.3$ and $E_{11} = E_{22} = 0.05$.

Following the Bayesian inference, the phase coupling functions $q_i(\phi_1, \phi_2)$ were calculated from the base parameters for the interacting terms. The results for four consecutive windows are presented on Fig. 3.11. Observing the inferred coupling functions, it can be easily noticed that their complex form now is not constant, but varies with time. Comparing them in neighboring (consecutive) pairs: (a) and (b), then (b) and (c), then (c) and (d), one can actually follow the time-evolution of the functions' form. Even though we can follow the time-variability between them, the two most distant functions Fig. 3.11 (a) and (d) have substantially different forms. It can also be noticed that beside the form, the functions' norm i.e. coupling strength varies too (compare e.g. the scale of maxima on Fig. 3.11 (a) and (d)). This probably happens because the coupling functions were varied in state space, and the way that the oscillators react on this perturbation affects the coupling strength. The latter can be even more significant for inducing synchronization transition.

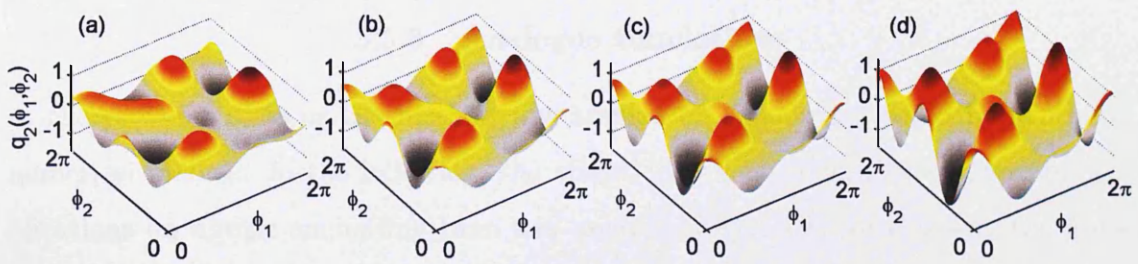

Fig. 3.11: Time-evolution of coupling function from model (3.25) with exponentially varying (3.26). (a)-(d) coupling function $q_2(\phi_1, \phi_2)$ from second oscillator for four consecutive time windows (the window length was $t_w = 50s$). For simplicity and clarity only function $q_2(\phi_1, \phi_2)$ is shown (the behavior of $q_1(\phi_1, \phi_2)$ from the first oscillator was similar).

The proposed method for inference of phase dynamics enables the evolution of the system under study to be tracked continuously. Unlike earlier methods that only detect the occurrence of transitions to/from synchronization, the method reveals details of the phase dynamics, thus describing the inherent nature of the transitions, and at the same time deducing the characteristics of the noise responsible for stimulating them. It can identify the time-varying nature of the functions that characterize interactions between open oscillatory systems. It was shown that not only the parameters,

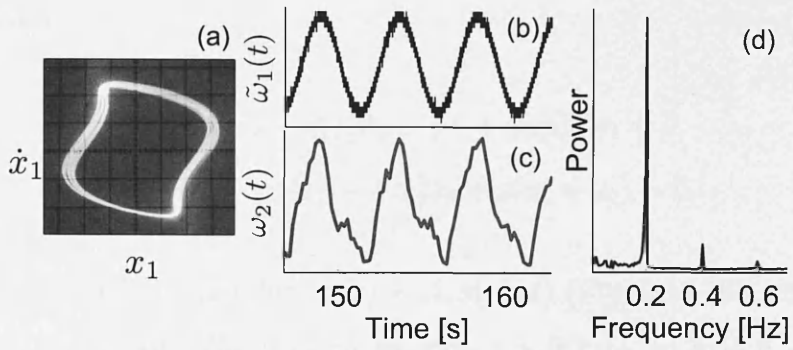

Fig. 3.12: Analysis of signals from analogue simulation of system (5.1). (a) Phase portrait from the oscilloscope; (b) frequency $\tilde{\omega}_1(t)$ from the external signal generator; (c) detected frequency $\omega_2(t)$ of the second driven oscillator; (d) Fast Fourier Transform (FFT) of the detected frequency $\omega_2(t)$.

but also the functional relationships, can be time-varying, and the new technique can effectively follow their evolution.

3.5.3 Analogue simulations

In the previous sections the method was applied on signals generated by synthetic numerical models. In the following, the attention will be concentrated more on applications on signals emanating from real oscillatory systems. In this way the noise embedded in the signals has more realistic meaning, and usually it is attributed to environmental disturbances or imperfections of some properties of the systems. Additionally, during the process of data acquisition and discretization, some amount of measurement noise can be introduced – a noise which has no links with the actual dynamics of the interacting oscillators.

The following example analyzes data from experimental analogue simulation of two coupled van der Pol oscillators. Details about the electronic implementation and further analysis are presented in chapter 5. The noise here is emanating from the imperfections of the electronic elements (determined by their tolerance), from their thermal heating due to inner-dissipation and partly due of measurement noise.

The phase portrait from the first oscillator, whose frequency is time-varying is shown on Fig. 3.12 (a). The first oscillator with time-varying frequency, is driving the

second oscillator:

$$\begin{aligned} \tfrac{1}{c^2}\ddot{x}_1 - \mu_1(1-x_1^2)\tfrac{1}{c}\dot{x}_1 + [\omega_1 + \tilde{\omega}_1(t)]^2 x_1 = 0, \\ \tfrac{1}{c^2}\ddot{x}_2 - \mu_2(1-x_2^2)\tfrac{1}{c}\dot{x}_2 + \omega_2^2 x_2 + \varepsilon(x_1 - x_2) = 0, \end{aligned} \tag{3.27}$$

where the periodic time-variability $\tilde{\omega}_1(t) = \tilde{A}_1 \sin(\tilde{\omega}t)$ (Fig. 3.12 (b)) comes from an external signal generator. The parameters were $\varepsilon = 0.7$, $\omega_1 = 2\pi 15.9$, $\omega_2 = 2\pi 17.5$, $\tilde{A}_1 = 0.03$, $\tilde{\omega} = 2\pi 0.2$ and c is constant resulting from the analogue integration. The phases were estimated as $\phi_i = \arctan(\dot{x}_i/x_i)$.

For the given parameters the oscillators were synchronized. Due to the effect of synchronization, the second driven oscillator changed its frequency from constant into time-varying (as discussed in chapter 2). Applying the inferential technique and investigating the detected synchronization showed that the oscillators were synchronized ($s(c) = 1$) throughout the whole time period. The frequency of the second driven oscillator was inferred as time-varying Fig. 3.12 (c). Performing simple FFT (Fig. 3.12 (d)) showed that $\omega_2(t)$ is periodic with period $0.2Hz$ (exactly as set on the signal generator). Therefore, the technique revealed information regarding the nature and the dynamics of the time-variability of the parameters.

3.5.4 Cardiorespiratory interactions

Another example worth analyzing, given its real-life nature, is the cardiorespiratory interaction. The analysis of physiological signals to detect and quantify cardiorespiratory interactions have already been found to be useful in relation to several diseases and physiological states(see [6] and references therein). Additionally, the transitions in cardiorespiratory synchronization have been studied in relation to anaesthesia [11] and sleep cycles [94].

It is well known that modulations and time-varying sources are present and can affect the synchronization between biological oscillators [6, 95, 96]. For comprehensive and genuine analysis there is a need for technique that can not only identify the time-varying information, but will allow the evaluation of the interacting measures (like

synchronization and directionality) to be based solely on such inferred information.

To demonstrate the method on real biological data, cardiorespiratory measurements from human subject under anaesthesia were analyzed. During the experiment, the breathing rate was paced constantly. In such systems the analytic model is not known (in contrast to analogue and numerical examples), but the oscillatory nature of the signal is easily observed. The instantaneous cardiac phase was estimated by wavelet synchrosqueezed decomposition [97] of the ECG signal. Details about instantaneous phase detection and the respective problems and advantages are discussed in chapter 4. Similarly, the respiratory phase was extracted from the respiration signal. The final phase time-series were reached after protophase-phase transformation [27].

Applying the inferential technique reconstructs the phase parameters that govern the interacting dynamics. Fig. 3.13 (c) shows the time-evolution of the cardiac and respiration frequencies. It is easy to notice that the (approximately) constant pacing of the breathing is well inferred, and that the cardiac frequency i.e. heart rate variability is increasing with time. The set of inferred parameters and how they are correlated can be used to determine whether cardiorespiratory synchronization exists and, if

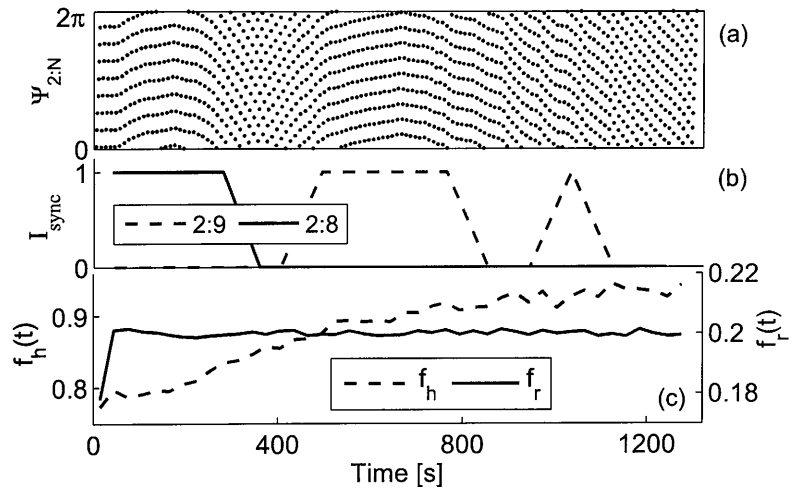

Fig. 3.13: Synchronization and time-varying parameters in the cardiorespiratory interaction. (a) Standard 2:N synchrogram. (b) Synchronization index for ratios 2:8 and 2:9 as indicated. (c) Time-evolution of the cardiac $f_h(t)$ and respiratory $f_r(t)$ frequency. Note the detected constant pacing of the breathing frequency.

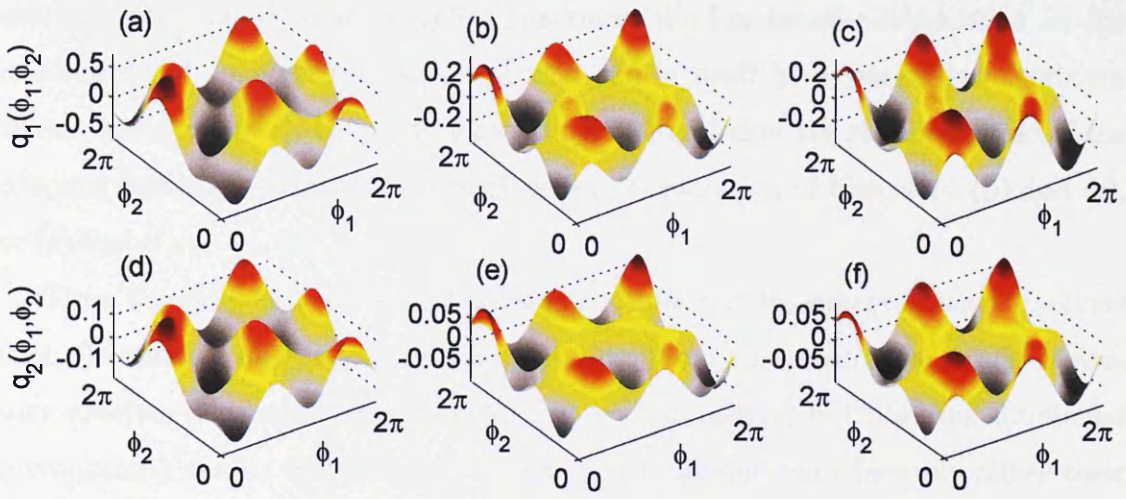

Fig. 3.14: Coupling functions in the cardiorespiratory interaction calculated at different times. (a)-(c) coupling function $q_1(\phi_1, \phi_2)$ from first oscillator, and (d)-(f) $q_2(\phi_1, \phi_2)$ from second oscillator. The window time intervals were calculated at: $t = 725s$ for (a) and (d); $t = 1200s$ for (b) and (e); and at $t = 1250s$ for (c) and (f). The window length was $t_w = 50s$.

so, in what ratio. The synchronization evaluation $I_{sync} = s(c) \in \{0, 1\}$, shown on Fig. 3.13 (b) reveals that several transitions exist between synchronized and non-synchronized states, and transitions between different ratios: from 2:8 (i.e. 1:4) at the beginning to 2:9 synchronization in the later intervals. Because the evaluation of the synchronization state is based on all of the given details about the phase dynamics, the proposed method not only detects the occurrence of transitions, but also describes their inherent nature. The synchronization detection (I_{sync}) was in good agreement with the corresponding synchrogram[2] shown on Fig. 3.13 (a).

The cardiorespiratory coupling functions, evaluated for three different time windows, are presented on Fig. 3.14. The upper figures (a)-(c) show the coupling function $q_1(\phi_1, \phi_2)$ from the first oscillator, and the lower figures (d)-(f) show $q_2(\phi_1, \phi_2)$ from the second oscillator. Note that the interactions are now described by complex functions whose form changes qualitatively over time – compare for example Fig. 3.14 (a) with (b) and (c), or (d) with (e) and (f). This implies that, in contrast to many

[2] Note that the cardiorespiratory example shown on Fig. 3.13 and Fig. 3.14 is the same used for the motivation part in the introductory chapter 1.

systems with time-invariant coupling functions, the functional relationships for the interactions of an open (biological) system can in itself be a *time-varying process.* By analyzing consecutive time windows, we can even follow the time-evolution of the coupling functions – compare the similarities i.e. evolution of Figs. 3.14 (b) and (c), or (e) and (f).

Thus the proposed method identified the time-varying nature of the functions that characterize interactions between open oscillatory systems. The cardiorespiratory analysis demonstrated that not only the parameters, but also the functional relationships, can be time-varying, and the new technique can effectively follow their evolution. This discovery immediately invites many new questions and points out that in future studies and modeling of such open systems, the time-varying coupling functions should be taken into account.

3.6 State space inference

In previous sections of this chapter, an inferential technique for reconstructions of phase dynamics was presented. Starting from the phase time-series and using phase base functions, the method tried to infer and describe the interactions between the oscillators. This section, on the other hand, presents the case of inference in the state space, where the starting point are the state time-series and the base functions are also in state domain. The objective is to describe the interacting oscillatory dynamics by the inference of the state variables.

3.6.1 Main concept

Given the state time-series $x_i(t)$, the estimation of instantaneous phases $\phi_i(t)$ is not often a trivial task. Many procedures for phase extraction are problematic when the state signals come from complex mixed-mode dynamics, or some information from the measurements is not used (or is interpolated). When inferring from the state signals, the technique exploits all of the measurement information. Moreover, if one can effectively use the state variables, then there is no need for the phase extraction

and one step (subprocedure) of the inferential framework can be avoided.

The construction of the Bayesian technique now encloses a set of base functions that describe the state dynamics $\Phi = \{\mathbf{x}_n^i\}$. For example, the base functions can be a finite number of polynomial functions. In general, the choice of the functions is not unique, and usually is model-dependent. The biggest disadvantage comes from not knowing the right number of dimensions, because often the only available input is a one dimensional readout signal. One can choose, for example, a large set of many combinations of base functions, but this will incorporate a lot of noise from the base functions which are not present in the actual dynamics, and the computational expenses and parameter space will be unnecessarily increased.

On the other hand, if the model is known *a priori*, then fewer base functions will be needed, the processing will be faster and more efficient, and the separation of the noise will be more effective. The latter make sense because many of the processes in nature can be described by models – examples include models in biology, chemistry or climate science. Additionally, a lot of situations exist when the model is known and the objective is to determine the dynamical states at any point in time. For example, in interacting technical systems and communications [16], or in chemical Belousov-Zhabotinsky oscillators [81].

The previously proposed Bayesian technique is one of the first to infer phase oscillatory dynamics, while most of the known Bayesian techniques actually infer in state space [30, 31, 84]. Especially relevant is the work by Smelyanskiy et al. [29] where the authors have used Bayesian inference to reconstruct the cardiorespiratory interactions in the state space. However, their analysis was performed on a single stationary (non time-varying) block of data and synchronization was not studied.

The main idea for the following discussion is: starting from the state time-series as inputs and given the model's state base functions, to use the same concepts for the Bayesian framework as discussed in section 3.1.3 to infer the multivariate state dynamics about the interactions of the oscillators. The use of the particular information propagation (section 3.1.4) can allow time-varying dynamics to be followed again. Defined in such a way and assuming that the model is known, the technique

will give explicit inference information about the coupling strength and coupling functions. However, the synchronization in the state domain, also known as generalized synchronization, has not been studied in this manner and in the following section special attention will be given to this issue.

3.6.2 Detection of generalized synchronization

When two oscillators synchronize, their behaviour can be easily explain in terms of phase relationships: synchronization occurs if there exists a bounded phase shift i.e. if the equilibrium solutions of the phase difference are stable [9]. But how is synchronization reflected in the state dynamics of oscillators? Basically, when synchronization is reached, the state trajectories become dependent on each other as a result of the interactions. Thus by investigating the stability of individual oscillators in respect of the interactions, one can effectively determine the synchronization entrainment.

At the beginning of the chaos synchronization era, the concept of identical synchronization was one of the first established forms of state space synchronization. It defines the two oscillators to be synchronized if certain states reach unity i.e. if the Lissajou curves are a diagonal line [46]. Not long afterwards, a more general description was given for the cases of state synchronization, called *generalized synchronization*, where the trajectories do not necessarily reach unity [98]. A more specific definition of generalized synchronization, in terms of asymptotic stability, was also proposed [47].

Directional coupling has been studied in depth and can be viewed as a generalization of periodic or quasiperiodic driving which have been used in physics, mathematics, and engineering for a long time. The unidirectionally coupled systems can be represented with a skew product structure:

$$\begin{aligned} \dot{\mathbf{x}} &= \mathbf{f}(\mathbf{x}) \\ \dot{\mathbf{y}} &= \mathbf{g}(\mathbf{y}, \mathbf{u}) = \mathbf{g}(\mathbf{y}, \mathbf{h}(\mathbf{x})), \end{aligned} \tag{3.28}$$

where $\mathbf{x} \in \mathbf{R^n}$, $\mathbf{y} \in \mathbf{R^m}$, a subset $\mathbf{B} = \mathbf{B_x} \times \mathbf{B_y} \subset \mathbf{R^n} \times \mathbf{R^m}$ is given and the state coupling functions are $\mathbf{u(t)} = (\mathbf{u_1(t)}, \ldots, \mathbf{u_k(t)})$ with $\mathbf{u_j(t)} = \mathbf{h_j(x(t, x_0))}$. The first and second systems in 3.28 are referred to as a drive and driven oscillator, respectively.

The question of under what conditions does generalized synchronization occur for a unidirectionally coupled system 3.28, is addressed in the following theorem (see [47] for proof):

Theorem: Generalized synchronization occurs in system 3.28, if given for all $(\mathbf{x_0}, \mathbf{y_0}) \in \mathbf{B}$ the driven system $\dot{\mathbf{y}} = \mathbf{g}(\mathbf{y}, \mathbf{u}) = \mathbf{g}(\mathbf{y}, \mathbf{h}(\mathbf{x}))$ is asymptotically stable [i.e. $\forall \mathbf{y_{10}}, \mathbf{y_{20}} \in \mathbf{B_y}$: $\lim_{\mathbf{t}\to\infty} ||\mathbf{y}(\mathbf{t}, \mathbf{x_0}, \mathbf{y_{10}}) - \mathbf{y}(\mathbf{t}, \mathbf{x_0}, \mathbf{y_{20}})|| = 0$].

The physical meaning of the theorem indicates that due to interactions the driven oscillator changes its independent stability, for example, from marginally stable to asymptotically stable, because of the entrainment to the drive oscillator. In fact, the vector field $\dot{\mathbf{y}} = \mathbf{g}(\mathbf{y}, \mathbf{h}(\mathbf{x}))$ is non-autonomous in respect of $\dot{\mathbf{x}}(\mathbf{t})$ to which is entrained.

One of the basic techniques for proving asymptotic stability is through numerical evaluation of conditional Lyapunov exponents of the driven oscillator. In this case, generalized synchronization occurs if all of the Lyapunov exponents from the driven oscillator are negative.

Several techniques have been proposed for detection of generalized synchronization from time-series. The most popular are based on mutual false nearest neighbors [98], mutual information [99, 100] or generalized angle [101]. These methods, however, are based on statistics and information flows and they do not take into account the intrinsic dynamics of the systems, nor do they consider the noise embedded in the interacting dynamics.

In the following the discussion is focussed on generalized synchronization detection technique that uses the Bayesian framework to infer the interacting state dynamics and the noise, and determines the existence of synchronization if the driven oscillator is asymptotically stable i.e. if its largest Lyapunov exponent is negative.

Application example

To demonstrate the main concept about the detection of generalized synchronization, a model of two coupled van der Pol oscillators subject to weak noise is considered:

$$\begin{aligned} \ddot{x} - \mu_1(1-x^2)\dot{x} + \omega_1^2 x + \varepsilon_1(t)y + \xi_1(t) = 0 \\ \ddot{y} - \mu_2(1-y^2)\dot{y} + \omega_2^2 y + \varepsilon_2(t)x + \xi_2(t) = 0, \end{aligned} \tag{3.29}$$

where the noise is assumed to be white Gaussian: $\langle \xi_i(t)\xi_j(\tau)\rangle = \delta(t-\tau)E_{ij}$.

In order to apply the inferential technique, first one needs to prescribe appropriate base functions. Each oscillator can be described in two dimensions by a simple variable change: $x_1 = x$, $x_2 = \dot{x}$ and $y_1 = y$, $y_2 = \dot{y}$. Assuming the models are known beforehand, the following base functions were chosen for reconstruction of system (3.29):

$$\Phi = \left\{ \begin{array}{l} x_2 \\ x_1,\ x_2,\ x_1^2 x_2,\ y_1 \\ y_2 \\ y_1,\ y_2,\ y_1^2 y_2,\ x_1 \end{array} \right\}, \tag{3.30}$$

where each row corresponds to the respective dimension of system (3.29).

The coupled system (3.29) was simulated numerically for a specific case – the coupling was considered to be unidirectional ($1 \rightarrow 2$) i.e. $\varepsilon_1(t) = 0$ and the rest of the parameters were set to: $\omega_1 = 1.1$, $\omega_2 = 0.9$, $\mu_1 = 1$, $\mu_2 = 0.7$ and the noise strength $E_1 = E_2 = 0.2$. To demonstrate the properties and precision of the inference in state space, first the coupling was set to a constant value $\varepsilon_2(t) = 0.15$ (for which the oscillators were not synchronized). The Bayesian inferential technique (section 3.1.3) exploiting the state base functions (3.30) was applied on the time-series of the two noisy oscillators. The inferred parameters acting as coefficients of appropriate base functions, are summarized together with the intrinsic parameters in Table 3.6.2. Comparing the last two columns, one observes the validity and precision with which the intrinsic parameters were inferred. The full and the inferred dynamics can be visualized and compared on Fig. 3.15 (a) and (b). Fig. 3.14 (a) shows the phase

Parameter	Base function	Intrinsic values	Inferred mean values
d_x	x_2	1	1.0051
ω_1^2	x_1	-1.21	-1.2099
μ_1	x_2	1	1.0110
μ_1	$x_1^2 x_2$	-1	-0.9925
ε_1	y_1	0	-0.0116
d_y	y_2	1	1.0036
ω_2^2	y_1	-0.81	-0.8144
μ_2	y_2	0.7	0.7104
μ_2	$y_1^2 y_2$	-0.7	-0.6971
ε_2	x_1	-0.15	-0.1563

Tab. 3.1: Results from the inference of numerically simulated system (3.29). The first column describes the physical meaning of the parameters, the second column shows the base functions used within the Bayesian inference, and the last two columns show the values of the intrinsic parameters and the their inferred mean values, respectively.

portrait of the first oscillator from the numerical simulation of (3.29) affected by noise, while Fig. 3.14 (b) shows the phase portrait of the same system simulated with the inferred parameters without the effect of noise.

But how one can use the inferred parameters to determined if the two oscillators are synchronized? Namely, the second driven oscillator $y(t)$, when not synchronized, has limit-cycle dynamics with marginal stability i.e. its largest Lyapunov exponent is zero. According to the theorem for generalized synchronization, when synchronization occurs the driven oscillator becomes asymptotically stable with negative largest Lyapunov exponent. Thus by following the Lyapunov exponents of the inferred driven oscillator one can detect if synchronization exists. Moreover, using the discussed information propagation within the Bayesian framework, one can *follow the generalized synchronization in time.*

To demonstrate the latter, system (3.29) was simulated for unidirectionally interacting case where the coupling was non-autonomous function varying discretely between two predefined values $\varepsilon_2(t) = \varepsilon = \{0, 0.4\}$ for which the two oscillators were intermittently synchronized. The application of the technique and the detection of generalized synchronization are presented on Fig. 3.14 (c). It can be noticed that,

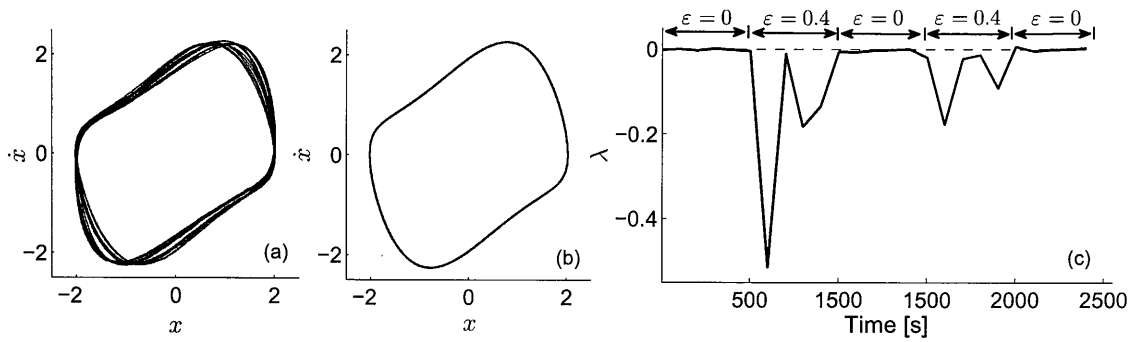

Fig. 3.15: Inferred state dynamics and detection of intermittent generalized synchronization. (a) phase portrait from numerically simulated noisy van der Pol oscillator $x(t)$. (b) phase portrait of van der Pol oscillator numerically simulated with the inferred parameters. (c) Largest Lyapunov exponent λ indication non-synchronized intervals for zero values and synchronized for negative. The coupling amplitude ε was discretely varying on intermittent intervals as indicated on the top of the figure.

when the oscillators are not synchronized, the largest Lyapunov exponent [102] λ is zero, and when synchronization occurs (for $\varepsilon = 0.4$) the driven oscillator becomes asymptotically stable and λ becomes negative. Thus the largest Lyapunov exponent λ can act as synchronization index for detection of generalized synchronization in time.

Many of the concepts discussed broadly for the detection of phase synchronization are valid and can be applied for the detection of state synchronization. The identification of synchronization from the inferred dynamics through Lyapunov exponent λ can be seen as equivalent to the map reconstruction of torus phase dynamics. Using the information propagation procedure, the generalized synchronization and the respective transitions can be traced in time too. As the noise is decomposed separately, if there exist noise-induced phase slips i.e. noise-induced transitions to generalized non-synchronized states, the proposed method will be able to detect it. Having said this, the inferential technique looks to be a useful tool in describing the time-varying nature and transitions of state synchronization in the presence of noise.

3.7 Generalization to networks of oscillators

A network of many complex dynamical systems can describe a large number of processes and system in the nature – examples including chemical reactions, ecological systems, electrical power grid, populations of synchronized crickets, the internet, and many others [103]. Especially important and relevant to this study are networks of complex oscillatory systems. This type of networks often require reconstruction of the coupling links i.e. structure of the network, or detection and study of qualitative phenomena such as synchronization [104].

In the previous presentation, for simplicity and clarity all of applications and demonstration were conducted on systems of two interacting oscillatory processes. It is important to note that in fact, the whole inferential framework is designed for a general number of interacting oscillators. Thus, the proposed inferential framework can be applied in a most strait-forward manner to a network of interacting oscillators. The only requirement is that now there will be an increased number of base function for a greater number of dimensions, and the computational procedures will take more time. This implies that the technique could be applied to networks of biological, ecological and chemical oscillators [7, 80, 81]. The novelty and advantages that this technique might bring is that it can decompose the effect from the noise and it can trace the time-varying dynamics and the transitions associated with it.

4. APPLICATION TO LIFE SCIENCES

Life is when structure acts as a function - is one of the many answers given to the everlasting question "What is life?".
The evolution of such functions of living beings in nature constitutes a vast group of complex dynamical systems. In order to maintain their functioning and activity, many of the processes tend to reach a balance between energy inflow and dissipated energy – forming a periodic i.e. oscillatory process.

But how well is the balance maintained throughout the system's evolution? In general, the biological systems are not isolated and often they are thermodynamically open. This causes a different type of energy exchange, in addition to the dissipated energy needed to maintained the basic functioning of the system. In other words, the system dynamics are no longer autonomic, and other processes contribute to its time-evolution. Within the same environment (for example – the human body) the sources of external influence are often known and closely related processes – which can be regarded as deterministic. The effect of the external dynamics can cause the intrinsic parameters, the interactions, or even functional dependencies to vary with time.

The following chapter focuses on the discussion on effects from external influences on human physiology. The underlying physiological systems are considered to be oscillatory processes and their dynamical characterization is studied. One of the main objectives was to investigate some of the physiological mechanisms with respect to deterministic non-autonomous perturbations. The latter involved physiological measurements while the respiration frequency was varied in time. Another issue discussed is the dynamical characterization of blood flow oscillations and their transient effect when subject to external perturbations. Several methodological issues regarding the

time-varying analysis and estimates are also discussed. By exploiting the measured time-series, the analysis (i.e. the inverse problem approach) employs many of the theoretical and methodological concepts discussed in the previous chapters.

4.1 A short physiological background

This section lays down the necessary human physiological background that any non-biological scientist can find useful for the remaining of the chapter. For a more comprehensive physiological background one can refer to [5, 6, 105, 106].

4.1.1 Cardiovascular system

The cardiovascular system forms a blood distribution network for transport of nutrients, gases and wastes to and from cells. It consists of three principle components: the heart, blood vessels and blood. According to cardiovascular functioning the system can be divided into pulmonary and systemic (peripheral) circulation. The pulmonary circulation connects the lungs where the blood is oxygenated, while the systemic supplies the rest of the body with the oxygenated blood.

The heart is a muscular organ, which forms two separate (right and left) pumps, each composed of atrium and ventricle chambers. The function of the right side is to collect the de-oxygenated blood in the right atrium and to pump it through the right ventricle to the lungs where it is oxygenated. The oxygenated blood is collected in the left atrium and pumped through the left ventricle to the rest of the body. The pumping action of the heart is based on a rhythmic *oscillatory* sequence of relaxation (diastole) and contraction (systole) procedures. The heartbeat coordination is tightly controlled by the sinoatrial node which acts as a pacemaker that determines the hear rate. The cardiac output i.e. the amount of blood pumped for a resting human subject, is about 5 liters in 1 minute.

Depending on the blood flow direction, two types of vessels exist: arteries and veins. The arteries take the blood away from the heart, and veins bring the blood back to the heart. Due to the high pressure, the arteries have strong vascular walls

and blood flows rapidly to the tissues. At the endings of the arterial system are arterioles that act as control valves through which blood is released to the capillaries. The capillaries then allow the actual exchange substances between the blood and the surrounding tissue. The walls of both arteries and capillaries is lined by a thin layer of endothelia cells which cause the smooth muscles to constrict or relax, contributing to the regulation of the vascular tone. The veins transport the blood from the capillaries (through venules) to the heart, and serve as a reservoir of blood. Due to the low pressure, the venous walls are thin.

The blood is a special fluid with the main function of conveying substances within the body, such as gases (oxygen, carbon-dioxide), hormones, vitamins and enzymes. It is composed of a liquid, called blood plasma, and blood cells suspended within the plasma. An average human subject has around 5 liters of blood, which accounts for about 6 – 8% of their body weight.

4.1.2 Respiratory system

The respiratory system introduces respiratory gases to the interior of the body and performs gas exchange. It includes the airways, lungs, and the respiratory muscles. Molecules of oxygen and carbon dioxide are passively exchanged by diffusion between the gaseous external environment and the blood. This exchange process occurs in the alveolar region of the lungs. The respiration process is an oscillatory cycle composed of two sub-processes: inspiration and expiration. Expiration is the movement of air out of the bronchial tubes, through the airways to the external environment during breathing, while inspiration is the movement of air from the external environment through the air ways, and into the alveoli. The way in which the respiratory system works closely in concert with a circulatory system to carry gases to and from the tissues – means it is often considered to be part of the cardiovascular system.

4.1.3 Sympathetic nervous system

The sympathetic nervous system is a part of autonomic nervous system (along with enteric and parasympathetic) which mainly controls involuntary internal processes.

The sympathetic nervous system prepares the body for responses to stressful challenges, allowing sudden strenuous exercise and increased vigilance. Stress is thought to counteract the parasympathetic system, which generally works to promote maintenance of the body at rest.

The sympathetic nervous system is responsible for up- and down-regulating many homeostatic mechanisms in living organisms. Fibers from the sympathetic system innervate tissues in almost every organ system, providing at least some regulatory function to things as diverse as blood flow control, thermoregulation, gut motility, and urinary output. It is perhaps best known for mediating the neuronal and hormonal stress response, commonly known as the fight-or-flight response. This acts primarily on the cardiovascular system and is mediated directly via impulses transmitted through the sympathetic nervous system and indirectly via catecholamines secreted from the adrenal medulla.

Messages travel through the sympathetic nervous system in a bidirectional flow. Efferent messages can trigger changes in different parts of the body simultaneously, such as the acceleration of the heart rate; widening of the bronchial passages; reducing the motility (movement) of the large intestine or the constriction of blood vessels. Afferent messages carry sensations such as heat, cold, or pain.

4.1.4 Oscillatory processes in the cardiovascular system

The functioning of cardiovascular system is characterized by several oscillatory processes [5, 6, 37]. They are responsible for many of the modulations observed (by means of wavelet transform) in the blood flow and the heart rate variability signals. Each of the oscillating processes has a characteristic period and is well defined in a certain frequency interval (summarized in table 4.1.4). Each also has a physiological interpretation, which is described in the following:

I The frequency interval around 1 Hz corresponds to cardiac oscillatory activity. It describes the periodicity for the functioning (pumping) of the heart.

II The oscillatory component around 0.2 Hz describes the respiratory activity and

Interval	Frequency (Hz)	Physiological origin
I	0.6-2	cardiac
II	0.145-0.6	respiratory
III	0.052-0.145	myogenic
IV	0.021-0.052	neurogenic
V	0.0095-0.021	endothelial metabolic
VI	0.005-0.0095	endothelial

Tab. 4.1: The frequency intervals for the distinctive oscillatory processes determined from human blood flow, and their physiological origin.

the periodicity associated with the breathing process that supplies the body with oxygenated blood.

III Around 0.1 Hz, corresponds to myogenic activity. The vessels are able to help control blood flow via a mechanism known as myogenic autoregulation. The vascular smooth muscles contract in response to an increase of intravascular pressure, and relax in response to a decrease of pressure.

IV The periodicity around 0.04 Hz originates from the activity of the autonomic nervous system on the heart, lungs and vessels. The nerves cause the release of substances that affect the activities of smooth muscles, leading in turn to changes in the vessels' radii and resistance, which allows vasoconstriction to take place.

V The oscillations around 0.01 Hz, correspond to nitric oxide (NO)-related endothelial activity. The layer of endothelial cells serves as a barrier between the blood and the tissues of vessels, allowing metabolic regulation and the control of contraction and relaxation of smooth muscle through the release of various substances.

VI The oscillations around 0.01 Hz, apparently corresponds to NO-independent (probably prostaglandin-dependent) endothelial activity.

The differentiation of the oscillatory processes (as described above) will be exploited greatly in the following discussion. For visual representation of the intervals, one can

refer to the analysis of blood flow signal presented on Fig. 4.14 and Fig. 4.12 (a).

4.2 The effect of time-varying respiration on cardiovascular system and sympathetic nerve activity

4.2.1 Introduction

Time-variability and modulations are inherent part of the physiological oscillatory dynamics. One of the most pronounced and early discovered modulation is the respiration sinus arrhythmia, which describes how the breathing patterns modulate the heart rate [107, 108]. Modulations and time-variabilities investigated in different contexts [35, 36, 95], have also shown that their study can be useful in understanding of many physiological processes, their functioning and their existing relationships.

The objective of this study is to analyze the effect of a deterministically varied respiration frequency on human oscillatory processes. The analysis will attempt to uncover how these processes are coordinated and how they influence each other. The time-variability of the respiration frequency is introduced externally, in a predefined procedure known to the investigator – thus in this way *deterministic non-autonomous influences are introduced* to the oscillatory dynamics. The controlled variability of the respiration is performed in order to study specifically how the varying respiration affects other processes, but also to use the perturbation for identifying existing relations and physiological mechanisms.

With its main function to provide oxygen, the respiration is one of the central processes in the human body. As such, it has attracted a lot of attention from physiologic science [34]. The relationship of respiration to heart rate variability has been identified as respiration sinus arrythmia [107]. Several studies have investigated how the sympathetic nerve activity is affected by different modes of breathing [36, 109, 110]. Of special interest is the study of low frequency components and sympathetic nerve activity [111], which also has been analyzed previously in conjunction with blood flow measurements [112]. Saul et al. have studied sympathetic nerve activity and haemodynamic signals under randomly varied breathing processes [113]. However,

their analysis has not taken into account the time-variability, the low frequency components are also not well localized, and the sympathetic nerve activity is not acquired by direct measurements of the nerve activity.

The following reports wavelet phase coherence analysis and information-theoretic approach for the detection of coupling between muscle sympathetic nerve activity and haemodynamic signals under deterministic time-varying perturbation of the respiration frequency. Wavelet phase coherence allows high resolution characterization of coherence i.e. coordination of the oscillatory dynamics at both high and low frequencies. The information-theoretic method quantifies the inter-oscillatory influences and reveals existence of causal relationships. All of the proposed techniques were able to trace (and to quantify statistically) the dynamical behavior and the time-variability, and to assess the time-domain information in accordance with the time-varying ramp perturbation. The main task was to investigate how the deterministic time-varying respiration regulates the neural and haemodynamic processes, and how this is affecting the causal inter-oscillatory relationships.

4.2.2 Measurements, subjects and signals

The total number of subjects analyzed was thirteen, and none of which smoked, had evidence of heart disease or took medication. The length of the recordings had mean of 72.3 minutes and standard deviation of 11.5 minutes. The minimum length was 53.4 minutes. There were two types of ramped paced breathing - first with gradually decreasing frequency (fast-to-slow) and second with gradually increasing frequency (slow-to-fast). Each recording contained several segments, with spontaneous breathing and then followed by several ramp breathing segments – the order and duration of all ramps is presented in Appendix D. The segments between the ramps were not analyzed because of the transient effect of the previous perturbation [39]. The mean length of spontaneous breathing segments was 7.9 minutes, with standard deviation of 2.6 minutes and a minimum of 6 minutes (which allowed the wavelet analysis to trace low frequencies down to 0.021 Hz). The ramps had lengths of approximately 9 minutes, with mean 9.05 and standard deviation of only 0.14 minutes.

The subjects were asked to breath voluntarily in accordance to a sine wave signal with time-varying frequency, which was shown on visual screen in front of them. In this way, the frequency of their respiration was varied with time.

The recordings included: electrocardiogram (ECG), blood pressure (BP) and carbon dioxide (CO_2) concentration signals. From the ECG signal a heart rate variability (HRV) signal was derived through marking of the R-peaks and linear interpolation between the consecutive time differences (for details see e.g. [6]). Similarly, the diastolic and systolic blood pressures were derived from the blood pressure signal. The recording also included the relatively rare and delicate measurement of muscle sympathetic nerve activity (MSNA). A multifiber sympathetic efferent traffic was measured invasively from the peroneal nerve muscle using microelectrodes with uninsulated tip diameters of about 2μm. The sampling frequency of the recordings was 500 Hz.

4.2.3 Methods

This section briefly outlines the methods used for the analysis of the recordings to find the effects of the time-varied respiration. Tools that are needed for the group statistical analysis are presented as well.

Wavelet transform

The nature of the perturbation, where the frequency of the respiration was varied with time, means that the wavelet transform and its ability to trace the time-frequency dynamics was the optimal choice for analysis of the underlying oscillatory processes [37]. The method based on the continuous wavelet transform projects the signal from time- to time-frequency domain with logarithmic frequency resolution [114]. Due to the adjustable length of the mother wavelet, the wavelet transform offers better localization and resolution for low frequency components when compared with the Fourier transform, which was of great importance for this study.

The wavelet transform enables one to derive the frequency content continuously in time by use of wavelets windows with variable length. A wavelet is shifted along the signal and a coefficient is calculated representing the strength of correlation between

the signal and the wavelet. For the following analysis a Morlet mother wavelet was used:

$$\nu(u) = \frac{1}{\sqrt[4]{\pi}} e^{-i2\pi f_0 u} \cdot e^{-u^2/2},$$

where the central frequency was set to be $f_0 = 1\,\mathrm{Hz}$. To create various scales of the wavelet comparable to the original signal, the mother wavelet is stretched and compressed by scaling factor s:

$$\Psi_{s,t}(u) = |s|^{-1/2} \cdot \nu\left(\frac{u-t}{s}\right) \tag{4.1}$$

In order to reach logarithmic resolution for the frequency, the scale factor s is increased exponentially. The transform itself is then a convolution of the wavelet and the original signal:

$$W(s,t) = \int_{-\infty}^{\infty} \bar{\Psi}_{s,t}(u) \cdot g(u) du \tag{4.2}$$

where the $\bar{\Psi}$ represents the complex conjugate of Ψ. Thus any specific scale is avoided and the analysis becomes scale-independent in terms of frequency. The energy density in the time-scale domain is evaluated from the wavelet transform, and the the wavelet power within the f1 : f2 frequency range can be calculated as:

$$\varepsilon(f_1 : f_2) = \int_{1/f_2}^{1/f_1} \frac{1}{s^2} |W(s,t)|^2 ds.$$

For the calculation of the transform the signals were re-sampled to 10Hz, and their spectra below the lowest frequency analyzed (0.021 Hz for the segment and 0.0095 Hz for the whole signals) were removed by moving average technique. Use of longer wavelets for low frequency components, resulted in having higher wavelet amplitudes for the low compared with high frequencies. Due to this effect the low frequency oscillatory components are easily identified and traced. When one needs to detect the actual strength of particular frequency component, the wavelet spectral power can be calculated.

Wavelet phase coherence and windowed wavelet phase coherence

By investigating the phase relationships, the wavelet phase coherence can determine the causality relations between two signals. When inferring the relationships between signals with different or very low powers, a big advantage of the wavelet phase coherence is that it can detect significant coherence. This is particularly meaningful for low-frequency components, which make important, but not necessarily large contributions to total power.

The wavelet transform using Morlet wavelet is described as a complex function. This allows for the instantaneous phases of the signals to be analyzed directly from the transform. The latter was used for calculation of the respective phase difference and thus for evaluation of the phase coherence.It gives normalized measure of coherence ranging between 0 and 1.

Due to the complex nature of the Morlet wavelet, the wavelet transform for each time t_n and scale s_k, consists also of complex values:

$$W(s_k, t_n) = W_{k,n} = a_{k,n} + ib_{k,n}.$$

From here the instantaneous phase can be determined as the angle variable $\phi_{k,n} = arctan(b_{k,n}/a_{k,n})$. To evaluate the wavelet phase coherence, the respective phase difference $\Delta\phi_{k,n} = \phi_{2k,n} - \phi_{1k,n}$ is calculated [38]. To get normalized measure of coherence between 0 and 1, the sine and cosine of the phase difference are averaged in time, yielding the phase coherence function:

$$C_\phi(f_k) = \sqrt{\langle\cos(\Delta\phi_{k,n})\rangle^2 + \langle\sin(\Delta\phi_{k,n})\rangle^2}\,.$$

In order to follow how the phase coherence is varying with time, a windowed wavelet phase coherence can be calculated. A window is slide along the data in time domain and the phase coherence is evaluated and plotted as function of both frequency and time: $C_{W\phi}(f_k, t_k)$ - with window of given size centered on a particular time t_k. The window size is varied for low to high frequencies in the same manner as the wavelet transform was calculated. In this way the same logarithmic scale for the

frequency is preserved. On the end, each windowing is normalized by the particular window size, so that the measure returns normalized phase coherence between 0 and 1. Due to the finite length of the windows on the end of the sliding - there is a cut-off of information, and the corresponding plot has goblet-like shape. Detailed description of the method and its significance for adaptive windows is discussed in [115].

Coupling between interacting oscillators: an information-theoretic approach

An information-theoretic method proposed by Palus & Stefanovska [23] was used for analysis of directionality of couplings and influences between weakly coupled oscillatory processes. The method has been proven useful in number of technical and physiological studies [88, 116, 117].

For inferring causality relationships i.e. directionality between two oscillatory processes, it estimates the 'net' information about certain time units in the future of the first process contained in the second process itself, by using an information-theoretic tool known as conditional mutual information. The two resultant conditional mutual information quantify the significant influence from the first to the second, and from the second to the first oscillatory signal. The influence that has the larger strength determines the predominant direction of coupling.

The information-theoretic method for quantification of couplings is based on conditional mutual information between the first $X_1(t)$ and the second $X_2(t)$ signal. The conditional mutual information is estimated as net information about the τ time units in future of the first signal $X_1(t)$ contained in the second signal $X_2(t)$ itself. First the τ increments are defined:

$$\Delta_\tau X_1 = X_1(t+\tau) - X_1(t).$$

Then the conditional mutual information i.e. the coupling of the first to second signal is defined as:

$$I_{21} = I(X_2, \Delta_\tau X_1 | X_1) = H(X_2|X_1) + H(\Delta_\tau X_1|X_1) - H(X_2, \Delta_\tau X_1|X_1),$$

where $H(x|y)$ and $H(x,y|z)$ are the conditional entropies defined in usual Shannonian sense. Similarly the coupling I_{12} from the first to the second signal is defined. The conditional mutual information I_{12} and I_{21} can be easily calculated by simple box-counting algorithm based on equiquantal marginal bins.

By applying the method one can infer the causality relationships between the signals, quantifying both the total influences and their time-variability by windowing the measure. Thermodynamically open systems and interacting physiological processes often can be mutually (bi-directionally) coupled, therefore it made sense to analyze not only the dominant direction, but also the two separate influences and their time-variations. The number of equiquantal bins used was N=4, time shifts were taken from 5:50 and re-sampled signals to 10 Hz in normalized state space were used.

Statistical analysis

Many data sets were not distributed normally (Kolmogorov-Smirnov test), so only medians, individual values and ranges were analyzed. A non-parametric statistical test was used, together with these quantities, to identify significant coherence, couplings and changes due to the time-varying ramped breathing.

The evaluation of the wavelet transform using different window lengths decomposed the signal into independent observations of particular frequency oscillations. The logarithmic scale for the spontaneous and ramped breathing segments (0.021-2 Hz) was divided into 95 independent segments for statistical analysis. For the statistical investigation of changes in the wavelet power introduced by the ramped breathing, a non-parametric rank sum test on the individual wavelet powers was conducted. The significant segments were denoted as red vertical lines plotted between the two medians. Wherever a contiguous range of frequencies show a significant effect these lines are confluent, forming red areas. Additionally, the fixed frequency ranges for the oscillatory intervals (as described in section 4.1.4) were tested for significance. Their significance was plotted with red asterisks.

When analyzing relationships between oscillatory processes in terms of wavelet phase coherence and coupling directionality, special care is needed. Namely, there can

exist small non-zero values of the measures, even when in reality there are no relations. To overcome this discrepancy and to determine the statistical significance, a surrogate statistical analysis was performed. Amplitude-Adjusted Fourier transform (AAFT) surrogate signals were generated by shuffling the phases of the original time series to create new time series with the same means, variances, autocorrelation functions (and therefore, the same power spectra) as the original sequences, but without their phase relations [90]. The average was calculated for 100 measures (phase coherence or couplings) calculated from 100 surrogate realizations of the signals. The phase coherence and coupling direction were considered to be statistically significant if their values were above the surrogate threshold, which was determined as the mean plus two standard deviations of the surrogate realizations.

When evaluating the wavelet phase coherence, the low-frequencies are represented with fewer periods than the high-frequency components. Consequentially, less variation of phase differences occurs at low-frequencies, and this is reflected in higher coherence values for low than high frequencies. The significant coherence of separate frequency segment was denoted with red area, and the significant ranges with red asterisks. A paired signed rank test was used for comparison of the measures with the surrogate threshold values. For visual inspection of the time-varying couplings only the values above the surrogate threshold were considered as significant. For quantification, the paired signed rank test was performed on the whole segment (spontaneous and ramp breathing) length. In all statistical tests, $P < 0.05$ was considered significant.

4.2.4 Results: wavelet and information-theoretic based analysis

The main results of the individual and group analysis are presented in this section. Three subsections encapsulate the results in conceptual groups.

Oscillatory dynamic analysis

Fig. 4.1 shows recordings made from one subject during spontaneous breathing at the beginning and the following ramp breathing. The carbon dioxide concentration

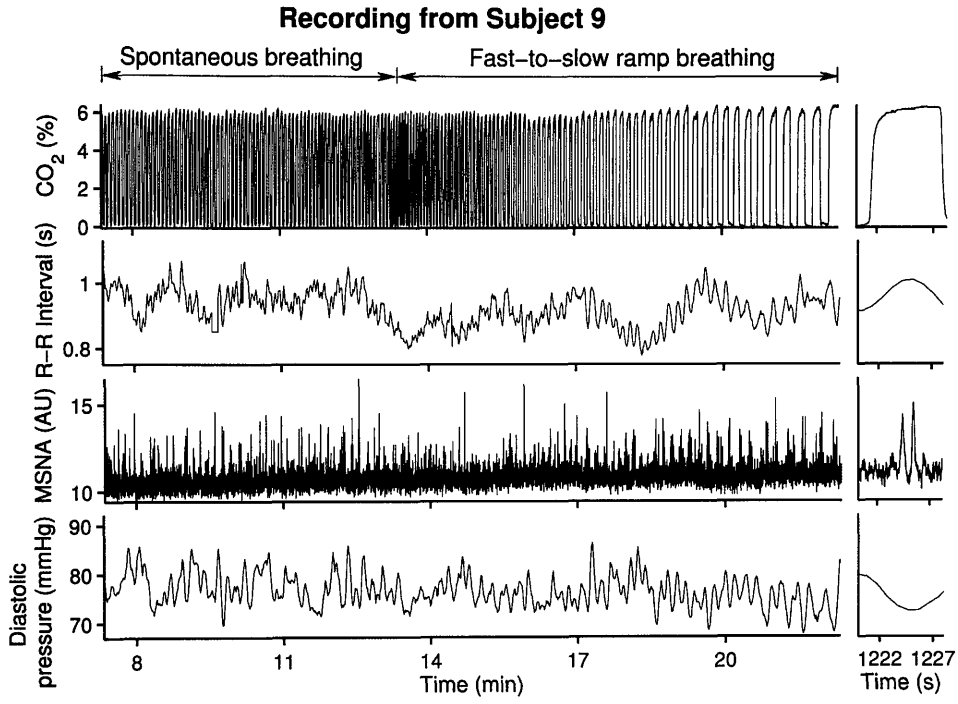

Fig. 4.1: Recording during spontaneous and first ramped breathing from Subject 9. During the first 6 minutes the subject breathed spontaneously, while in the following 9 minutes the breathing was gradually decreasing from fast to slow.

recording reveals the gradual frequency decrease of the breathing oscillatory process. The respiratory imprints are easily noticeable on the R-R interval and the diastolic pressure signal. Low frequency oscillations are also present in these signals (see R-R interval signal during ramp breathing). Muscle sympathetic nerve activity occur as groups of narrow bursts, which seem to appear in coordination with carbon dioxide cycles and are the most conspicuous for the slow breaths within the ramp segment. The enlarged time segments within one cycle of the carbon dioxide are presented on the right of the figure.

Fig. 4.2 shows a wavelet transform of carbon dioxide concentration signal from Subject 4. With the ability to trace the time-frequency domain, the wavelet transform clearly demonstrates the time-varying nature of the ramp perturbation (note that the lines parallel to the ramped breathing are only their higher harmonics). During spontaneous segments the subject breathed freely and the wavelet amplitude

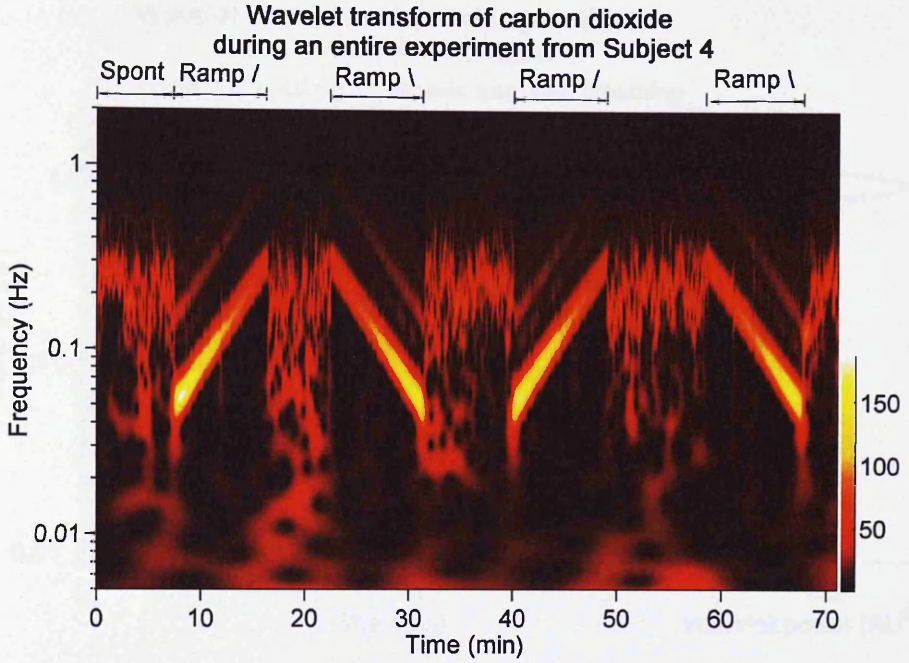

Fig. 4.2: Wavelet transform of carbon dioxide from Subject 4. The contour plot shows the wavelet transform for the whole duration of measurements. It is easy to notice the spontaneous breathing and the four (9 minutes) epochs of ramp breathing, which intermittently change from slow-to-fast to fast-to-slow. The wavelet amplitude during the spontaneous breathing is spread across various frequency bands, while during the ramped breathing the amplitudes are more concentrated around the ramping frequency.

is represented over a wide range of frequencies. The controlled ramp breathing concentrated the wavelet amplitude, making it sharply confined around the time-varying frequency bands introduced deterministically by the perturbation.

The wavelet transform of muscle sympathetic nerve activity and its corresponding wavelet power from one subject are shown on Fig. 4.3. The influence of the respiration on the muscle sympathetic nerve activity is revealed by the presence of the ramp frequency content (compare the frequency components and the time-variability during spontaneous and ramp segments). The wavelet power demonstrates that the predominant periodic oscillations are around 1 Hz, while the lower frequency components that have less power are spread around the ramp breathing frequencies.

Fig. 4.4 compares the median wavelet powers for all subjects and segments during spontaneous (black lines) and ramped (grey lines) breathing. Red shaded areas indi-

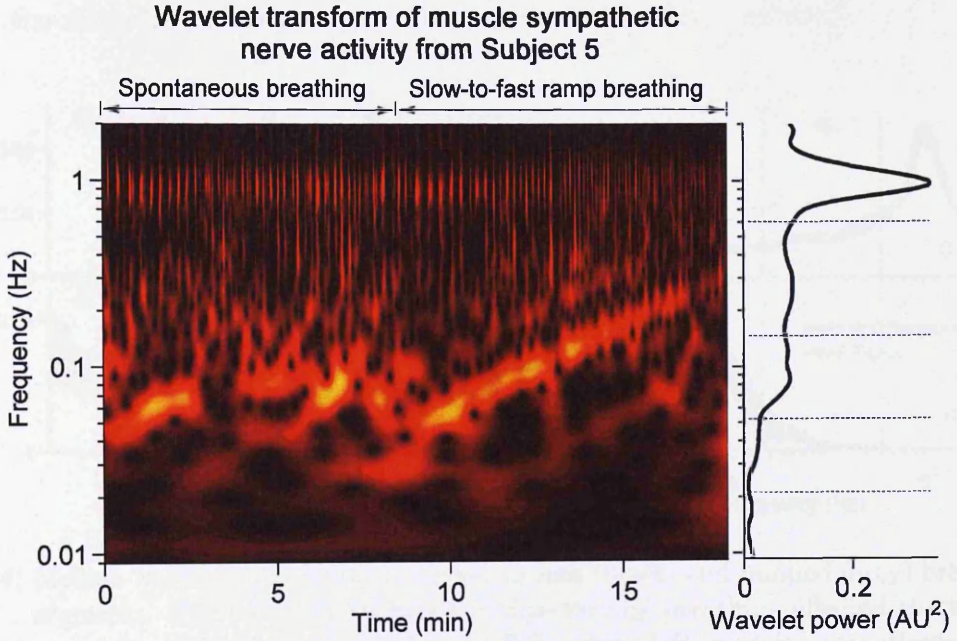

Fig. 4.3: Wavelet transform for muscle sympathetic nerve activity from Subject 5. The left contour plot shows the wavelet transform for the spontaneous breathing (8.5 minutes) and the slow-to-fast ramped breathing (9 minutes). The wavelet amplitudes on lower frequency (around and below 0.1 Hz) during the spontaneous breathing are changed due to the ramped breathing, making them dense around the controlled breathing frequency. The time-averaged wavelet power, plotted on the right, demonstrates that the strength of the higher frequency (around 1Hz) is the highest, while the low frequencies are spread over the ramping bands.

cate specific frequencies at which the effect from the ramped breathing is significant (as indicated, a non-parametric rank sum test was applied to wavelet powers at each of the 95 frequencies). The red asterisks indicate the significance of the ramp effect within frequency ranges. The large significant difference in wavelet powers of spontaneous and ramped carbon dioxide shown on Fig. 4.4 A demonstrates the nature and the effect of the ramp perturbation. The wavelet powers for R-R interval (Fig. 4.4 B) and diastolic pressure (Fig. 4.4 D), show that besides the significant effect on the ramp frequencies (around intervals II and III), there is also a significant difference on the lower frequency bands (interval IV), which are outside the initial frequency range from the ramp perturbation. The ramp breathing had little effect on the wavelet power of muscle sympathetic nerve activity (Fig. 4.4 C), which was significant only

within the ramp frequencies.

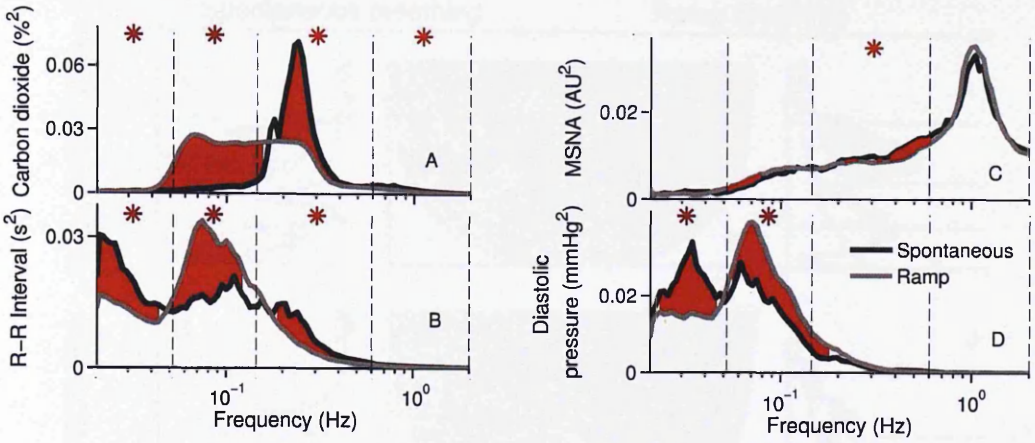

Fig. 4.4: Median wavelet power spectra of spontaneous (black) and ramped (grey) breathing segments. The figure shows how the time-varying breathing affected the wavelet power spectra of carbon dioxide A, R-R interval B, muscle sympathetic nerve activity C and diastolic pressure D. The red areas indicate significant change of individual wavelet powers, while the red asterisks show the significant range change. The perturbation that changed significantly the carbon dioxide, also significantly affected the R-R interval and the diastolic pressure at ramp and lower than ramp frequencies. The muscle sympathetic nerve activity power was not affected greatly.

Coordination and phase coherence

Wavelet phase coherence was used to identify and quantify how the oscillatory signals interact i.e. if they are coordinated on some frequency ranges. Fig. 4.5 A-D shows the coherence for spontaneous breathing while Fig. 4.5 I-L shows ramped breathing coherence. The red shaded area represents statistically significant phase coherence. Due to the time-varying nature of the ramp perturbation, windowed wavelet phase coherence was used to trace the time-variability of the coherence among ramp frequencies - Fig. 4.5 E-H. The phase coherence shown on Fig. 4.5 A, E and I, indicates that carbon dioxide and systolic pressure are highly and significantly coherent on breathing frequencies. The coherence was varying during the ramp breathing, following the frequencies introduced by the deterministic perturbation. Fig. 4.5 B, F and J represent the coherence between carbon dioxide and electrocardiogram (ECG) signal. The ECG signal was analyzed because it contains the 1 Hz oscillatory component of the heart

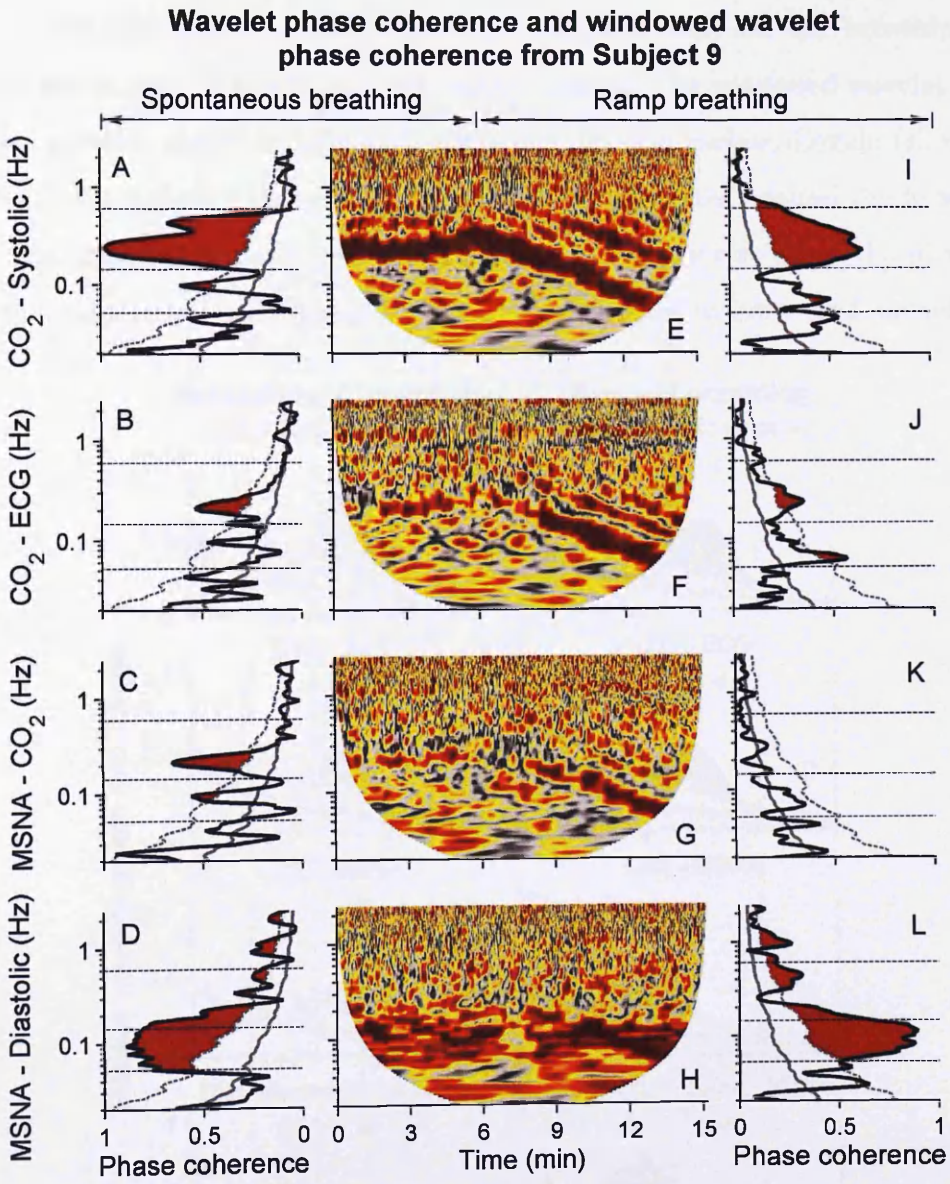

Fig. 4.5: Wavelet phase coherence and windowed wavelet phase coherence from Subject 9. The four contour (goblet-like) plots E-H show the windowed phase coherence for the first 15 (spontaneous 6 + ramp 9) minutes. One can easily notice the time-variability of the coherence from spontaneous to gradually changing during the ramp breathing. The plots A-D are for spontaneous, while I-L are for ramped breathing. The red shaded area represents the significant coherence above the surrogate threshold (mean plus two standard deviations), which is indicated by the gray dashed line. The implications of the coherence between the signals (as given on the left vertical axis-label) are discussed in more detail in the main text.

activity. The relationship showed significant coherence only on the breathing frequencies, which were affected during the ramp segment. The windowed wavelet phase coherence between muscle sympathetic nerve activity and carbon dioxide (shown on Fig. 4.5 G) was not very high, and mostly it was concentrated around the breathing frequencies. During the ramp segment, this phase coherence was affected and spread across the ramp breathing frequencies. The latter resulted in lower and insignificant

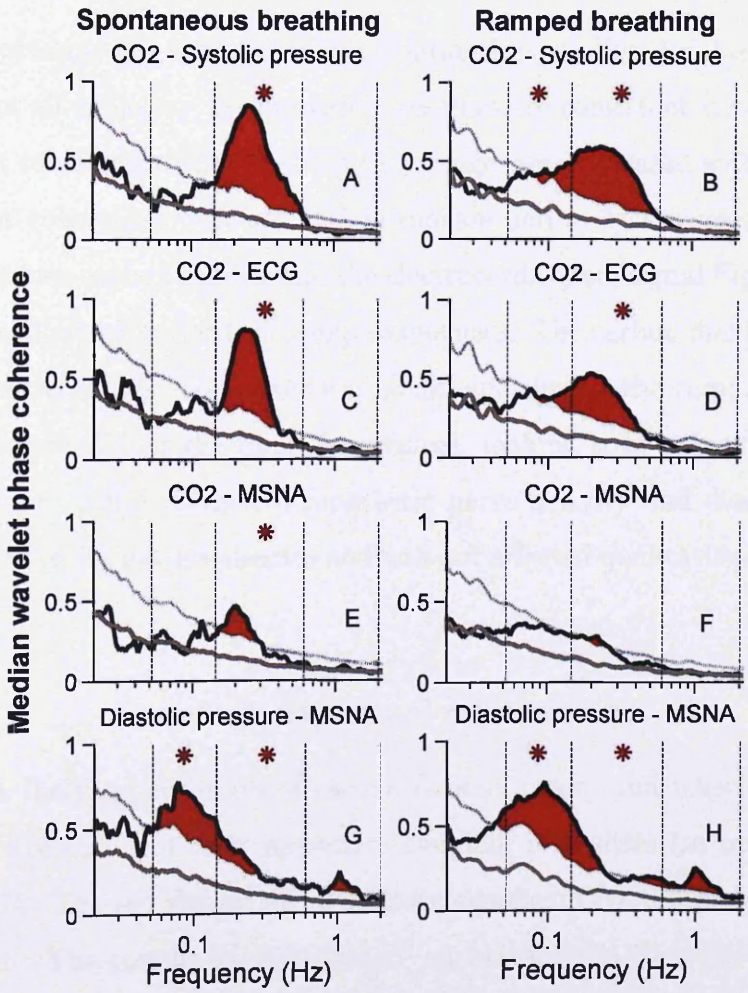

Fig. 4.6: Median phase coherence and the effect from the ramped breathing. The same coherence combinations are shown as on Fig. 4.5, presenting now the medians for all the segments. The left plots (A, C, E and G) show the coherence for spontaneous, and the four plots (B, D, F and H) are for the coherence of the ramp breathing. The red area presents the significant coherence for the separate frequencies, while the red asterisks indicate the statistical significance of the corresponding frequency ranges.

time-averaged coherence (Fig. 4.5 K) - as opposed to the significant coherence during spontaneous breathing shown on Fig. 4.5 C. Unlike the previous three relationships, the phase coherence between muscle sympathetic nerve activity and diastolic pressure was not qualitatively affected by the ramped breathing, and was relatively high at low frequencies. This was evident both from the windowed phase coherence Fig. 4.5 H, and from the comparison of significant phase coherences in Fig. 4.5 D cf. Fig. 4.5 L.

Fig. 4.6 represents the same coherence relationships as Fig. 4.5, but now showing the medians for all subjects - the individual results were consistent with the medians. The significant coherence within the frequency ranges was indicated with red asterisks. The significant coherences between carbon dioxide and systolic pressure Fig. 4.6 A and B, and between carbon dioxide and the electrocardiogram signal Fig. 4.6 C and D, were affected and spread toward the ramp frequencies. The carbon dioxide and muscle sympathetic nerve activity coherence was weak, and during the ramp breathing the coherence was spread over the ramp frequencies, making it not significant overall - Fig. 4.6 E cf. Fig. 4.6 F. Muscle sympathetic nerve activity and diastolic pressure coherence was high for low frequencies and was not affected qualitatively by the ramp breathing.

Couplings and causal relationships

Fig. 4.7 shows the time evolution of carbon dioxide (grey) and muscle sympathetic nerve activity (black), and their respective coupling intensities (in both directions) from Subject 13. The red shaded areas indicate significant coupling above the surrogates threshold. The coupling intensities are an information-theoretic measure that quantifies the inter-oscillatory influences between carbon dioxide and muscle sympathetic nerve activity. The time-evolution of the signals during a ramp breathing shown on Fig. 4.7 A-C demonstrate that muscle sympathetic nerve activity occurs as valleys of bursts appearing mostly during the inspiration cycle. As the ramp breathing progressed, the bursts appeared more frequently and in good coordination with the carbon dioxide cycles. The cause of the latter phenomenon is due to the coupling

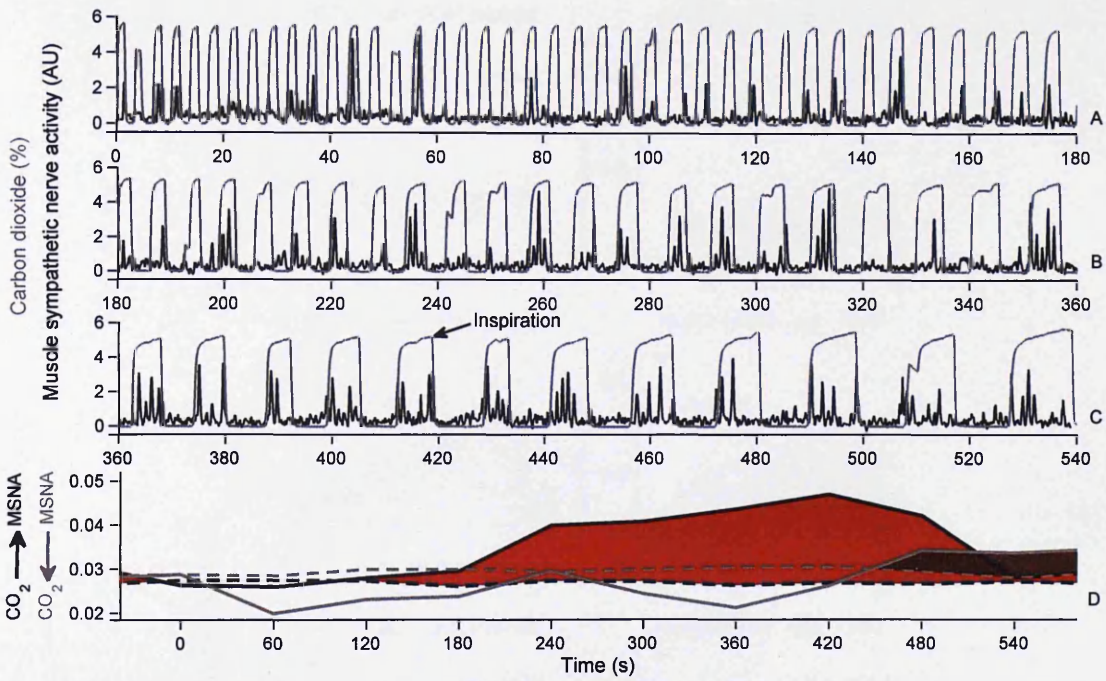

Fig. 4.7: Carbon dioxide and muscle sympathetic nerve activity, and their coupling during one fast-to-slow ramp from Subject 13. The three plots A-C show the time evolution of CO_2 (gray) and MSNA (black) – B continues after A, and C after B. The nerve bursts appear more coordinated with the high value of CO_2 as the ramp progress. D shows the CO_2-to-MSNA coupling (thick black) and MSNA-to-CO_2 coupling (thick gray), and their surrogate thresholds with dashed black and grey lines, respectively. The red shaded areas represent the significant influences of the two directions. One can notice that the CO_2 influenced the MSNA more strongly and this coupling is increased as the ramped breathing progresses.

from carbon dioxide to muscle sympathetic nerve activity - as indicated on Fig. 4.7 D. Namely, the intensities of the inter-oscillatory influences (shown on Fig. 4.7 D) suggest that CO_2 to MSNA is the dominant direction, and its intensity becomes significant and increased as the ramp breathing progresses. The specific time-variability verifies the tight relationship between the influence of CO_2 on MSNA and the deterministic ramp perturbation.

Fig. 4.8 presents the median and individual couplings between carbon dioxide and R-R interval, including the spontaneous (A and B), fast-to-slow (C and D) and slow-to-fast (E and F) ramp breathing segments. On the left plots (A, C and E) are the CO_2 to R-R interval, while on the right (B, D and F) the R-R interval to CO_2

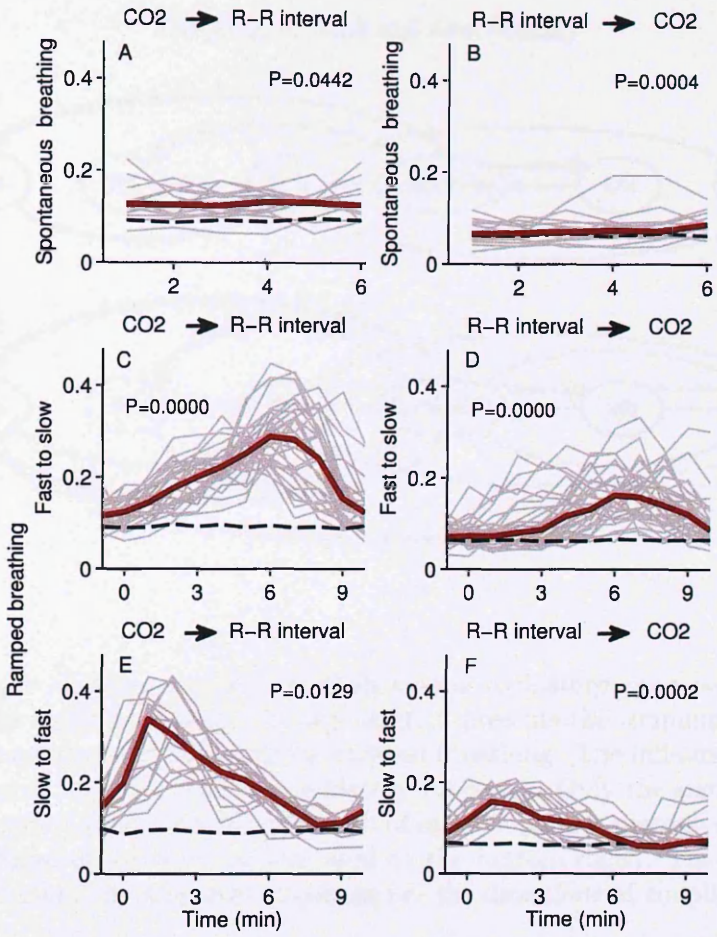

Fig. 4.8: Median (red) and individual (grey) couplings between carbon dioxide and R-R interval. On A, C and E the CO_2 to R-R interval couplings are presented, while B, D and F are showing the R-R interval to CO_2 couplings. The other notations are the same as on Fig. 8. During spontaneous breathing the couplings have almost constant values. The ramped breathing introduced time-variability and increased the influences towards low-frequencies. Overall the CO_2 to R-R interval couplings were more dominant.

couplings. The dashed black lines denote the surrogates' threshold. The P-value on each plot is evaluated within the whole segment between individuals, and indicates if the coupling is significantly higher than the surrogates' threshold. During spontaneous breathing the couplings had almost constant values. The influence from CO_2 to R-R interval was the dominant direction. The ramped breathing enhanced the intensities of the couplings, and this effect was larger for low frequencies. The latter resulted in very clear time-varying imprint of the ramp perturbation (see e.g. Fig. 4.8 C). These

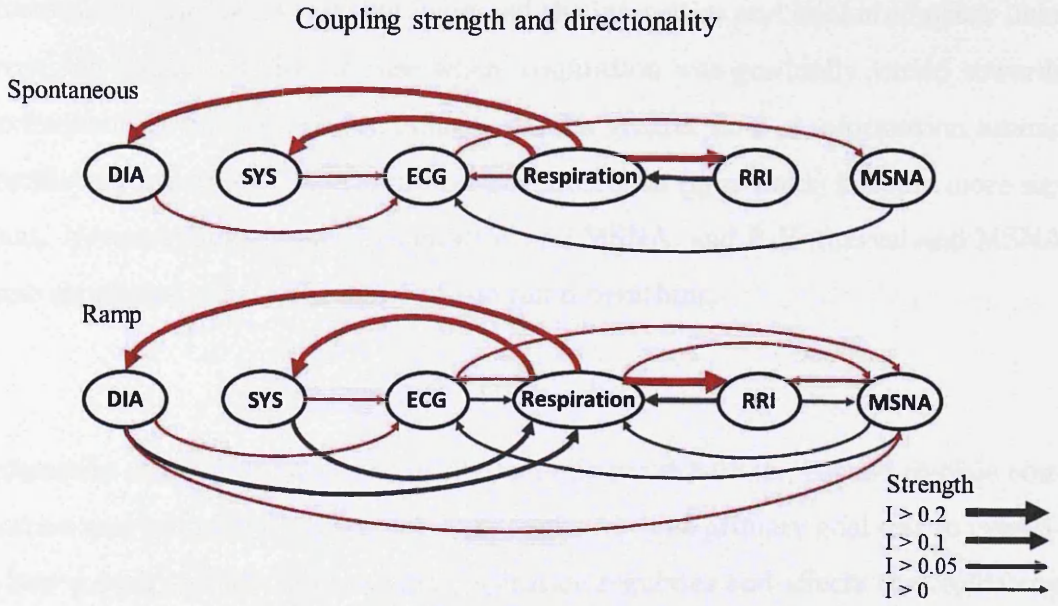

Fig. 4.9: Schematic diagram for the couplings among oscillatory processes and the effect from the ramp breathing. The top diagram presents the couplings during spontaneous and the bottom during the ramped breathing. The influences are presented as directed links between the oscillatory processes. Only the significant ($P<0.05$) couplings are presented. The strength of each coupling is presented with four types of thickness of the links (as indicated on the bottom right). The red links denote the dominant (by strength) couplings i.e. the directions of coupling.

couplings had relatively large intensities, where CO_2 to R-R interval coupling had greater intensity and was the predominant direction.

Fig. 4.9 summarizes the inter-oscillatory influences and how they are affected by the ramp breathing. The directed links on the schematic diagram represent the couplings between the two corresponding oscillatory signals. The different thickness of the links indicates the intensity of the coupling (only the significant couplings are presented). The dominant directions of influence between two signals are presented with red links. During spontaneous breathing the respiration oscillating activity exerts dominant influence on the other (excluding MSNA) oscillatory systems. Diastolic and systolic blood pressure influenced the ECG signal that holds the 1 Hz cardiac activity - which in its own terms coupled dominantly the MSNA. The couplings were weaker and their direction was reversed for MSNA and ECG, and R-R interval and

respiration. The ramped breathing increased the intensities and enhanced other links between the oscillators. In the case where respiration was gradually varied towards lower frequencies there was more influence and a greater flow of information among the oscillatory processes. The weaker reverse directions (grey links) became more significant. New couplings between respiration and MSNA, and R-R interval and MSNA became significant due to the effect of the ramp breathing.

4.2.5 Discussion

Simultaneous recordings from muscle sympathetic nerve activity, carbon dioxide concentration and haemodynamic signals were analyzed. The primary goal was to investigate how a deterministic time-varying respiration regulates and affects the oscillatory processes in cardiovascular and sympathetic neural system. Because their dynamics usually involve influence from several processes with diverse time-scales, which can be also time-varying, the time domain methods (such as time averages) are not appropriate for their analysis. Dynamical characterization (e.g. through wavelet based methods) on the other hand, offered better insight into the dynamics of the oscillators and the existing phenomena.

The advantage of measuring human subjects who can regulate the speed of their breathing voluntarily was used to introduce linearly increasing (decreasing) time-variability in the oscillators' dynamic. The wavelet analysis from CO_2 concentration (Fig. 4.2) showed how the perturbation confined the originally wide frequency range around the ramp frequency, and that the averaged wavelet power was significantly altered on all frequency intervals (Fig. 4.4 A). The time-frequency representation demonstrated that at any frequency and time, the ramp perturbation can be determined consistently with the externally predefined variations.

The strong relationships between the respiration and heart activity, was observed in almost all of the performed analysis. The ramp breathing significantly altered not only the wavelet power at frequencies corresponding to the perturbation, but also at the low frequencies [108] below them (Fig. 4.4 B). The reduced wavelet power indicates that low frequency oscillatory processes (around neurogenic frequency interval)

are dependent on the dynamical variations of the respiration. Fig. 4.5 reveals that CO_2 and ECG are significantly coherent at breathing frequencies, probably due to the respiration sinus arrythmia modulation [107]. This coherence was following the specific time-varying breathing, and it was enhanced for the lower frequencies of the ramping. The high intensities of inter-oscillatory couplings (Fig. 4.8) imply that there is high information flow between CO_2 and RR-interval signals. The results (Fig. 4.8, Fig. 4.9) confirm and support the notion that respiration has a greater influence on the heart [12, 23, 25]. The ramp time-variability of the inter-oscillatory couplings pointed out that these causal relationships are more pronounced on lower breathing frequencies (see e.g. Fig. 4.8 C and E).

The analysis of MSNA oscillatory [118] time-frequency content (Fig. 4.3) showed traces of the specific ramp breathing pattern, which at the same time did not exert a large effect on the averaged wavelet power (Fig. 4.4 C). The phase coherence between MSNA and CO_2 was mostly concentrated around the breathing frequencies and during the ramp intervention it was significantly affected and spread around the ramp breathing frequencies Fig. 4.5. A simple time-domain observation (Fig. 4.7 A-C) also suggests that MSNA appears as volleys of bursts within the CO_2 cycles [34, 36]. The cause of this phenomenon might be due to the coupling from CO_2 to MSNA, which was present throughout the ramp breathing and was significantly increased at low frequencies (in the same way as the bursts Fig. 4.7 D). The influences between MSNA and CO_2 concentration changed from non-significant to significant because of the effect from the time-varying ramp breathing (Fig. 4.9).

The time-varying breathing also affected the diastolic and systolic blood pressure. The low frequency wavelet power of diastolic pressure was reduced outside the ramped frequencies (Fig. 4.4 D). The high phase coherence followed the respiration variations (Fig. 4.5, Fig. 4.6), which could be a consequence of the high inter-oscillatory influences Fig. 4.9. Interestingly, the coherence between the diastolic pressure and muscle sympathetic nerve activity was high before and during the time-varying breathing (Fig. 4.5, Fig. 4.6), with no observable difference seen between the two cases.

In summary, the time-varying breathing process significantly affected the function-

ing and regulation of several mechanisms in cardiovascular and sympathetic neural systems. In general, the gradually slower breathing provoked more 'information' flow, altering the coordination and increasing the influences between the oscillatory processes. Probably the most-important finding was that the manifestations and effects on this multi-coupled oscillatory system had the imprint of the particular form of the externally induced deterministic time-variation. The proposed analysis was able to detect, follow and statistically to quantify these features and phenomena.

4.3 Cardiorespiratory interactions and effects from time-varying respiration

In the previous section the effects from time-varying respiration were analyzed and statistically quantified on the whole group of the measurements. The following discussion, however, investigates more closely how the respiration with deterministic varying frequencies can affect the cardiorespiratory interactions i.e. how the ramped breathing affects the inherent dynamics and transitions between oscillatory processes of the heart and respiration. The Bayesian inferential technique (discussed previously in chapter 3) is employed for the reconstruction of the interacting phase dynamics, and for evaluation of the qualitative states and transitions.

Before presenting the actual analysis, an important technical preprocessing issue is addressed. Namely, in order to infer the phase dynamics, one needs to have good estimate of the phases from the observable time-series. This is even more important when the oscillatory dynamics are time-varying and the analysis requires instantaneous phases. Potential difficulties for the phase estimation occur when the signals emanate from complex and/or mixed-mode oscillatory dynamics. Therefore, attention will first be spent on addressing some of the known methods for phase detection and the problems they hold, and an alternative approach for overcoming these issues will be proposed.

4.3.1 Instantaneous phase detection: methods and problems

The problem faced is to detect the phase at every moment in time from time-series containing oscillatory characteristics [1]. There exist two widely accepted methods for phase detection, which are used differently depending on the form of the signal.

The first method considers the interval between two well-defined events as a cycle, and that the phase increment between the events is exactly 2π. The procedure is similar to having a Poincaré cross section on the phase portrait of the attractor [9]. A cycle is described by only one information point while the intermediate points are linearly interpolated i.e. assigning the values of phase $\phi(t_k) = 2\pi k$ to the times t_k, and for arbitrary instant of time $t_k < \mathrm{t} < t_{k+1}$ the phase is defined as:

$$\phi_m(t) = 2\pi k + 2\pi \frac{t - t_k}{t_{k+1} - t_k}. \tag{4.3}$$

A detection of phase from an ECG signal (which has complex form), was used to present how the methods work. Fig. 4.10 (a) shows the ECG signal and the marked maxima t_k events. From the marked points and using (4.3) the instantaneous phase was estimated Fig. 4.10 (b).

The second method involves construction of the complex analytic signal $\zeta(t)$ [119] from a scalar experimental time series $s(t)$ via the Hilbert transform:

$$\zeta(t) = s(t) + is_H(t) = A(t)e^{i\phi_H(t)}, \quad s_H(t) = \pi^{-1} P.V. \int_{-\infty}^{+\infty} \frac{s(\tau)}{t - \tau} d\tau, \tag{4.4}$$

where $s_H(t)$ is the Hilbert transform of signal $s(t)$. Hence, the angle variable $\phi_H(t)$ from the complex signal $\zeta(t)$ describes the required instantaneous phase. This approach is parameter free, very convenient for implementation, and if the signal is well defined and has narrow band spectra it gives phase information in every point of the time. However, if the two-dimensional embedding possesses loops or intersections this method will fail. In fact, due to its complex form with (P and Q) minor peaks between the maxima R-peak, the ECG signal is one such example. This is illustrated on Fig.

[1] Note that instantaneous or 'every instant of time' in this context is finite and defined by the sampling frequency of the time-series.

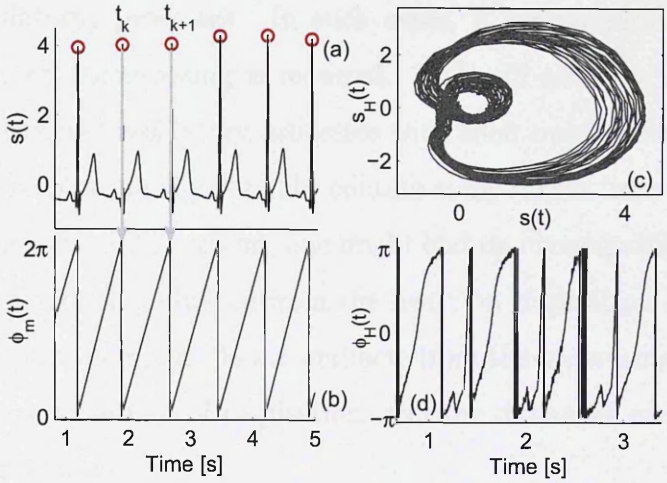

Fig. 4.10: Phase detection with marked-events and Hilbert transform methods. (a) ECG signal and marked maxima R-peaks. The phase estimated as (4.3) using the peaks from (a). (c) The two-dimensional embedding using Hilbert transform (of the same signal as (a)). (d) The spuriously detected phase using Hilbert transform (4.4).

4.10 (c) where the Hilbert transform embedding show clear folding and intersection. Thus the detected instantaneousness phase will be spurious Fig. 4.10 (d).

In studies of cardiorespiratory interactions, the phases from the respiration signal usually are estimated with Hilbert transform, while the ECG phase is detected through the marked events technique [6, 120]. This approach works well enough for observing dynamical behaviour which is longer than several oscillatory cycles, and where having only few phase information is enough (for example phase synchronization with synchrograms). But if one tries to infer the inherent oscillatory dynamics from complex signals, such as the coupling function and intrinsic time-varying parameters, then there is a need for instantaneous phase that contains all of the cycle information. For example, for cardiorespiratory interactions the ECG phase from the marked-events method contains only one genuine piece of information per cycle, while the rest is simple interpolation. Alternatively, the Hilbert phase is not correctly detected either. Hence, there is a need for a phase estimate from complex signals that describes the phase (time-variability) at every instant in time.

Additionally, care must be taken when the signals contain parts and modulations

from other (oscillatory) processes. In such cases, a preprocessing in terms of detrending, filtering or decomposing is required. This will allow for interactions to be studied on self-sustained oscillatory processes with their own fundamental frequency. For example, the respiration signal might contain components from the heart activity, and if they are not taken into account, one might end up investigating synchronization between the heart and the influence from the heart on respiration [121, 122]. This is clearly wrong since the components are artifacts from the measuring procedure rather than the oscillatory dynamics of respiration, and the dynamics are coming from the same (cardiac) oscillator.

4.3.2 Instantaneous phase detection from complex mixed-mode signals

Recent development of techniques for decomposition of mix-mode signals has lead to the synchrosqueezed wavelet transform [97]. This method aims to decompose the signal into intrinsic mode components which can have time-varying spectrum. The transform is a combination of the wavelet transform and a special case of reallocation method which tries to "sharpen" $R(t,\omega)$ by allocating its value to a different point (t',ω') in the time-frequency plane, determined by the local behavior of $R(t,\omega)$ around (t,ω). It is based on wavelet transform $W(s,t)$, as described previously by equation (4.1) and (4.2), which gives a time-scale representation of the frequency content that is spread out in s, but its oscillatory behavior in t are located around the original frequency ω, regardless of the value of s.

The synchrosqueezed transform aims to 'squeeze' the wavelet around the intrinsic frequency in order to provide better frequency localization. For any (s,t) for which $W(s,t) \neq 0$, a candidate instantaneous frequency for the signal g can be calculated as:

$$\omega_g(s,t) = -i\frac{\frac{\partial}{\partial t}W_g(s,t)}{W_g(s,t)}. \tag{4.5}$$

The information from the time-scale plane is transferred to the time-frequency plane, according to a map $(s,t) \rightarrow (\omega_g(s,t),t)$, in an operation called synchrosqueezing. The

synchrosqueezed wavelet transform is then expressed as:

$$T_g(w,t) = \int_{A(t)} W_g(s,t) s^{-3/2} \delta(\omega(s,t) - \omega) \dot{ds}, \tag{4.6}$$

where $A(t) = \{a; W_g(s,t) \neq 0\}$, and $\omega(s,t)$ is as defined in (4.5) above, for (s,t) such that $s \in A(t)$. Defined in this way, the transform is invertible and the signal can be reconstructed after the synchrosqueezing:

$$g(t) = \Re\mathfrak{e}\left[C_\psi^{-1} \int_0^\infty W_g(s,t) s^{-3/2} ds\right], \tag{4.7}$$

where C_ψ^{-1} has a constant value which is calculated from the mother wavelet $C_\psi^{-1} = \frac{1}{2}\int_0^\infty \overline{\Psi(\xi)}\frac{d\xi}{\xi}$. For practical reasons, when dealing with time series the frequency variable ω and the scale variable s can be "binned", i.e. $W_g(s,t)$ can be computed only at discrete values s_k, with $s_k - s_{k-1} = (\Delta s)_k$, and the synchrosqueezed transform $T_g(\omega,t)$ can be likewise determined only at the centers ω_l of the successive bins $[\omega_l - \frac{1}{2}\Delta\omega, \omega_l + \frac{1}{2}\Delta\omega]$, with $\omega_l - \omega_{l-1} = \Delta\omega$. The integral is written in this discrete form as the summation of different contributions, and equation (4.7) becomes:

$$g(t) = \Re\mathfrak{e}\left[C_\psi^{-1} \sum_k W_g(s_k,t) s_k^{-3/2} (\Delta s)_k\right] = \Re\mathfrak{e}\left[C_\psi^{-1} \sum_k T_g(\omega_l,t)(\Delta\omega)\right]. \tag{4.8}$$

Due to the good frequency localizations and invertibility, the synchrosqueezed wavelet transform can be used as an appropriate tool for identification and extraction of intrinsic oscillatory modes in time domain [97]. Moreover, the complex (as with real and imaginary values) nature of the synchrosqueezed transform allows one to extract the phase of non-harmonic signals, or of some of their modes. The instantaneous phase can be calculated as the angle of the synchrosqueezed wavelet transform:

$$\phi_l(t) = \angle\left[\sum_k T_g(\omega_l,t)(\Delta\omega)\right]. \tag{4.9}$$

The transform's great potential lies in its ability to determine instantaneous characteristics from complex signals with non-harmonic waveform [123]. The robust im-

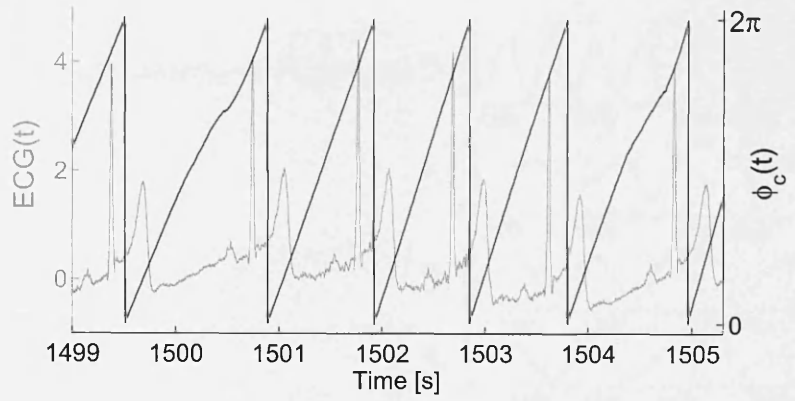

Fig. 4.11: Instantaneous phase detection from ECG signal, using the synchrosqueezed wavelet transform. The ECG signal is shown with grey line, and the phase $\phi_c(t)$ with black.

plementation and the visual time-frequency representation offer a convenient way for identification and analysis of mixed-mode oscillatory dynamics [124].

Fig. 4.11 presents a specific application of the technique as a response to the originally posed question of how to detect reliably the instantaneous phase from ECG signal. One can notice that the phase was detected correctly in respect of the 2π cycles defined by the R-peaks, and that time-variability within the cycle is traced appropriately. Therefore, the ECG phase detected in this way (with instantaneous values) can be used properly by the Bayesian inferential technique.

Exploiting the decomposition property of the transform, the phase can be detected only for certain specific oscillatory modes. For example the cardiac phase can be detected only from the intrinsic mode within the cardiac interval (table 4.1.4), thus at the same time, a preprocessing procedure for removal of undesired modulations will be performed.

However, there exist cases where the modulations and external oscillatory premises can actually be used for further analysis. The latter can be even more important if the oscillatory mode is not directly measurable. For example, the blood flow signal measured with laser Doppler flowmetry (LDF), contains information about the blood propagations which are modulated by several oscillatory components. The activity within these frequency intervals, as elaborated in table 4.1.4, can be decomposed and

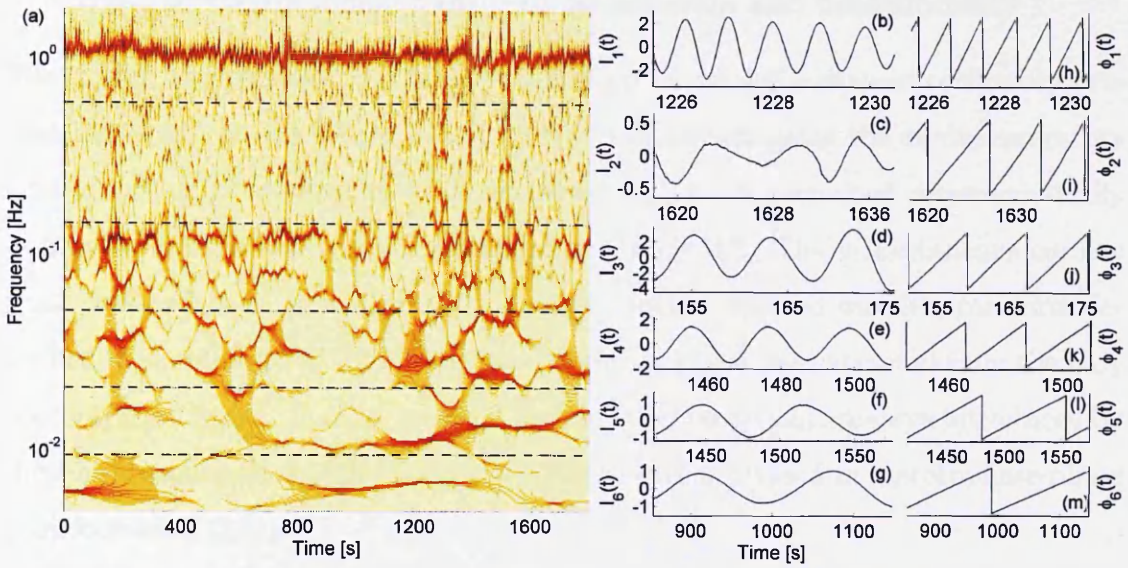

Fig. 4.12: Synchrosqueezed wavelet transform (a) from human blood flow signal. The oscillatory components as explained by table 4.1.4 are separated by black dashed lines. The decomposed time-evolution (b)-(g) and their instantaneous phases (h)-(m), of the respective oscillatory component as shown on the left in (a). For example (d) shows the myogenic signals and (j) its phase.

used for other analysis. Fig. 4.12 (a) shows the synchrosqueezed wavelet transform from human blood flow signal (also given by the wavelet transform and time-averaged wavelet power on Fig. 4.14). It is easy to notice the oscillatory modes in the corresponding frequency intervals (separated by dashed lines). This subject had very low respiratory influence on the blood flow processes. By applying the proposed technique, the oscillating processes were decomposed Fig. 4.12 (b)-(g) and their instantaneous phases were detected directly Fig. 4.12 (h)-(m). Within each interval, the modes were selected as the maximal energy components, preserving their frequency and amplitude time-variations. This novel facility gives the opportunity for further analysis to be performed – including, for example, inter-oscillatory interactions in terms of synchronization and directionality. These results will be even more important because not all of the underlaying oscillatory processes can be measured directly. The inter-oscillatory analysis can give deeper insight into the cardiovascular mechanisms and causal relationships, and are certainly worth pursuing in the future.

4.3.3 Cardiorespiratory synchronization and directionality

The cardiac and respiratory activity can be seen as two self-sustained oscillatory processes that interact with each other. This sections investigates the cardiorespiratory interactions under conditions when the breathing pace is perturbed deterministically in a linear (ramp) manner – as explained in section 4.2. The instantaneous cardiac phase was estimated from the ECG signal by synchrosqueezed wavelet transform described in equation (4.9). Similarly the respiratory phase was extracted from the CO_2 concentration signal. In order to avoid the potential phase disturbances introduced by the synchrosqueezed transform, the two phases were processed in a protophase-phase transformation [27].

The Bayesian framework for inference of phase dynamics (chapter 3) was applied on a segment with fast-to-slow ramp breathing. The results are summarized in Fig. 4.13. The inferred respiratory frequency shown on Fig. 4.13 (c) demonstrates the ramped breathing variability. The secondary purpose for presenting the ramp is for following the changes of other measures with respect to the perturbation applied. By normalizing the inferred coupling parameters, one can determine the net directionality of the interactions. Fig. 4.13 (d) suggests that the degree of directionality is time-varying, but confirms that respiration-to-heart is dominant [6, 24–26]. To determine whether cardiorespiratory synchronization exists in certain ratios, the set of inferred coupling parameters (and how they are correlated) was used to reconstruct the torus map and for investigating whether the root $M(\psi_e) = \psi_e$ exists or not. Fig. 4.13(b) shows the detection of transitions from the non-synchronized to the synchronized state, which in turn change in different ratios: 1:4 to 1:5 to 1:6, as the ramp progressed. The synchronization detection and the respective transitions were consistent with the respective synchrogram Fig. 4.13 (a). The surrogate testing on (b) and (d) was performed in order to refute the hypothesis that the measures happen by chance, and to determine the significance threshold.

The cardiorespiratory coupling function, evaluated for three different time windows indicated by the arrows, is presented on Fig. 4.13 (e)-(g). For simplicity and clarity only q_1 is shown (the behavior of q_2 was similar). The interactions are de-

scribed by complex functions whose form changes qualitatively over time – cf. Fig. 4.13 (e) with (f) and (g). The latter implies that the functional relation for the cardiorespiratory interactions is not a time-invariant function, but is in fact a time-varying process for itself. The time-evolution of the coupling functions is evident by analyzing consecutive time windows– cf. the similarities i.e. evolution of Figs. 4.13 (f) and (g). It is important to note that this variability is not caused by the ramp time-varying respiration frequency (which is decomposed separately), and that the

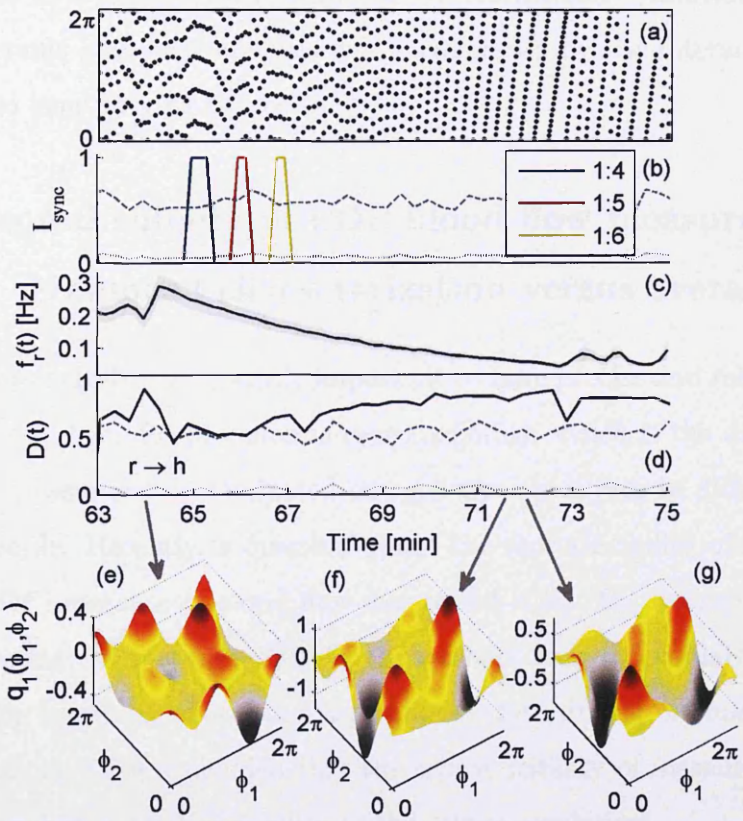

Fig. 4.13: Synchronization, directionality and coupling functions in the cardiorespiratory interaction. (a) Standard 1:N synchrogram. (b) Synchronization index for ratios 1:4, 1:5 and 1:6, as indicated. The dashed line represents the mean (dotted) +2 SD of synchronization indices from 100 surrogate [90] realizations. (c) The time-varying respiration frequency (note the downward ramp due to pacing). The gray areas on (c) represent ±2 SD from the mean value. (d) Directionality index: the dashed lines represent the mean (dotted) +2 SD of directionality indices from 100 surrogate realizations. (e)-(g) coupling functions $q_1(\phi_1, \phi_2)$ calculated at different times, as indicated by the grey arrows.

phenomenon of time-evolving coupling functions was observed also on spontaneously breathing subjects.

The ramped breathing showed that the cardiorespiratory coordination depends and is regulated to a great extent by the respiration dynamics. The analysis indicated that the Bayesian technique detected the occurrence of transitions to/from synchronization and revealed details of the phase dynamics, thus describing the inherent nature of this transitions. It was found that the externally induced varying respiration acts as a cause for these qualitative transitions. Additional complexity for the interactions and their analysis was encountered by the interacting functions which were also time-varying processes.

4.4 Reproducibility of LDF blood flow measurements: dynamical characterization versus averaging

In experimental analysis it is crucially important to have precise and reliable measurements. One of the tests for precision is reproducibility, which is the degree of agreement between measurements conducted on replicate conditions in different locations by different people. Recently, a question about the reproducibility of Laser Doppler Flowmetry (LDF) measure of blood flow was raised [125]. By means of determining cutaneous vascular conductance (CVC), the authors seek to evaluate reproducibility by averaging relatively short time segments of data during or immediately after some perturbation. They concluded that the reproducibility of measurements on the forearm is limited by spatial variability in the microvasculature.

This naturally raised the discussion if the analyzing methods used were appropriate for analysis of LDF blood flow signals, which have a mixed mode oscillatory nature. Another important issue raised was how to assess external (non-autonomous) perturbations, the kind of discrepancy that can occur and how to analyze them properly. These two issues (discussed in [39]) are presented in more detail bellow.

4.4.1 Blood flow analysis

The reproducibility of forearm LDF measurements was investigated in earlier work [126], by means of dynamical characterization of the oscillatory signals. It was established that the issue of spatial variability could be mitigated by careful placement of the sensors: good reproducibility was obtained by avoiding proximity to the larger vessels, hairs, and blemishes. It was found that this is true both for spatial reproducibility, with simultaneous measurements at different positions on the same arm, and for temporal reproducibility, with sequential measurements at the same position.

Time-averages measures are a standard tool for analysis in physiology. But the question raised is whether time-averaging provides a satisfactory method for characterising blood flow, developing LDF criteria, or testing LDF reproducibility. Since

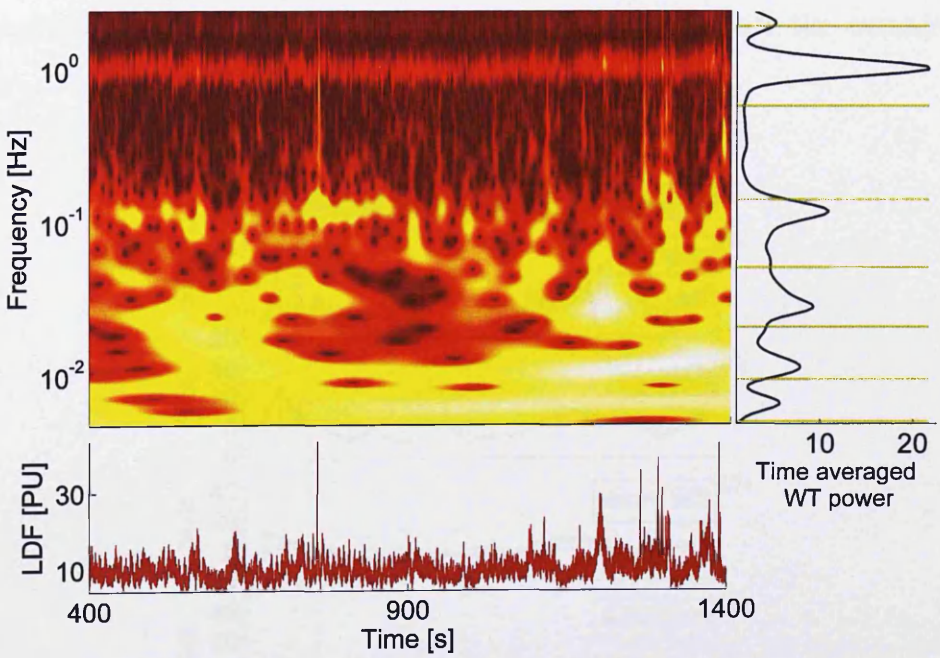

Fig. 4.14: Wavelet transform of LDF variability (top left), plotted above the raw signal in standard perfusion units (bottom) and the averaged wavelet power spectrum (right). The six frequency intervals as presented in table 4.1.4 are indicated by horizontal lines and correspond (from the top) to: cardiac activity; respiration; myogenic oscillations; neurogenic; NO-related endothelial processes; and non-NO-related endothelial processes.

blood flow is inherently oscillatory in nature ([5]), averaging will inevitably produce variable results depending on how the window is positioned relative to the phase of an oscillation unless, of course, the window is very much longer than the oscillation period. In reality, the situation is even more complex because there is not just one oscillatory process in blood flow, but at least six ([127]). Fig. 4.14 shows a wavelet transform of typical LDF blood flow data. The slower of the two endothelial-related oscillations has a period of about 0.007 Hz, so that the averaging window would need to be much longer than 2.4 min in order to avoid irreproducibility from this source. One can in principle always achieve reproducibility of an LDF average by using a long enough averaging interval, or by averaging over a large enough spatial area but, in doing so, one inevitably throws away a lot of potentially useful information.

The dynamical characterization, on the other hand, prescribes that it is better to accept that blood flow is inherently oscillatory, and to frame the criteria for LDF reproducibility on that basis. Thus, rather than asking whether the average blood

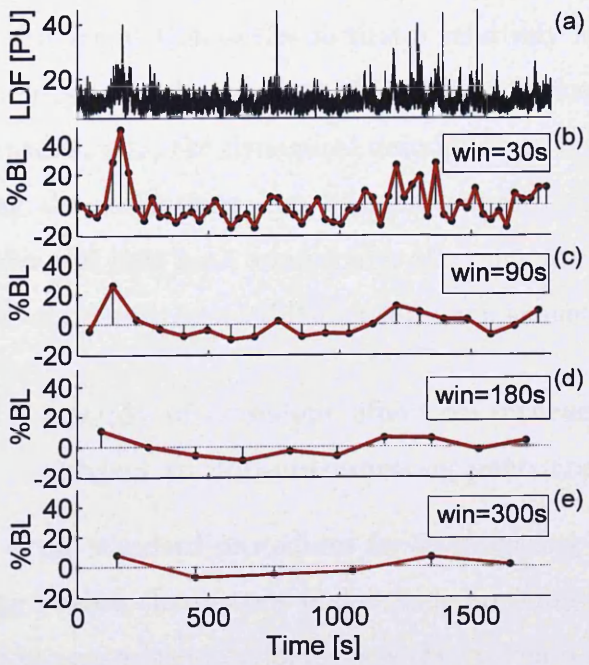

Fig. 4.15: The raw LDF blood flow signal from Fig. 4.14 averaged over successively larger window sizes, as indicated by the numbers in each box.

flow has changed over time or in spatial position, it will be better and more rewarding to ask whether the characteristics of the oscillations have changed, for example: their amplitudes and frequencies, which are already known to be reproducible in time and space; or the extent to which the different oscillations mutually interact and perhaps synchronize with each other. Changes in these quantities have been related successfully to several different pathological conditions e.g. congestive heart failure, hypertension and diabetes as well as to other states of the body like e.g. exercise and anaesthesia [127]. Even if averages could be measured reproducibly, they would do little to characterize or help diagnose these conditions.

To illustrate these points, Fig. 4.15 shows the same LDF segment as Fig. 4.14 and a series of time-averaged flux values made with different window sizes. If a short time is taken to "read" the value, the difference between readings can be as high as 60% of the baseline value. The longer the window is, the less variable the average value becomes. However, as shown in Fig. 4.14 there are distinct patterns in the variability that are missed if only the average is taken into account. Moreover, the patterns are visible on several different time-scales so that a relatively long recording time is needed to capture the dynamical properties of the blood perfusion signal. Thus, for analysis of LDF measurements, the dynamical description in terms of the parameter values characterizing the oscillations, can be more appropriate. In their response [128], the authors also add that both approaches: the time-averaging and dynamical characterizations are of interest, being different but complementary.

4.4.2 Numerical study of transient effect on interacting oscillators subject to non-autonomous perturbations

In physiology, one of the standard procedures for investigating the mechanisms and existing relationships is when the systems under study are subject to external perturbations. In this way the examiners can follow how the system reacts to this influence, and also they can trace if there are some interactions with other systems which are affected by this perturbation. Obvious examples include the ramp breathing discussed in section 4.2, local heating or post-occlusive reactive hyperaemia. Often several per-

turbations are performed consecutively, and in this particular case special care must be taken. When the systems are oscillatory processes, the transient response from the perturbations (if not treated well) can have an effect on the analysis and their reproducibility.

In a complex dynamical system such as the skin microvasculature, any perturbation is likely to involve nonlinear hysteresis effects. Fig. 4.16 shows the results of a numerical simulation of just two coupled oscillatory processes subjected to repeated external perturbation. The model consists of bi-directionally-coupled limit-cycle oscillators (based on Poincaré oscillators), subject to external perturbations and weak noise:

$$\begin{aligned} \dot{x}_1 &= -\alpha_1(r_1 - a_1)x_1 - \omega_1(y_1 - \beta_1 r_1) + \varepsilon_1 x_2 + \xi_1(t) \\ \dot{y}_1 &= -\alpha_1(r_1 - a_1)y_1 + \omega_1(x_1 - \beta_1 r_1) + \varepsilon_1 y_2 + \xi_1(t) - s_1(t) - s_2(t), \end{aligned} \tag{4.10}$$

$$\begin{aligned} \dot{x}_2 &= -\alpha_2(r_2 - a_2)x_2 - \omega_2(y_2 - \beta_2 r_2) + \varepsilon_2 x_1 + \xi_2(t) \\ \dot{y}_2 &= -\alpha_2(r_2 - a_2)y_2 + \omega_2(x_2 - \beta_2 r_2) + \varepsilon_2 y_1 + \xi_2(t) - s_2(t), \\ r_i &= \sqrt{x_i^2 + y_i^2};\ i = \{1, 2\}. \end{aligned} \tag{4.11}$$

The parameters were set to values mimicking the frequency spectra: cycle radii $a1 = a2 = 1$; frequencies $\omega_1 = 2\pi 0.1$, $\omega_2 = 2\pi 0.011$; couplings $\varepsilon_1 = 0.01$, $\varepsilon_1 = 0.001$; parameters for speed of convergence $\alpha_1 = 0.001, \alpha_2 = 0.1$ and parameters for the center of rotation $\beta_1 = 0.4$ and $\beta_2 = 0.01$. The noise is white Gaussian, with zero mean $\langle \xi_i(t) \rangle = 0$ and correlation $\langle \xi_i(t)\xi_i(s) \rangle = D\delta(t-s)$, where D is the noise strength ($D1 = D2 = 0.003$). A long initial transient time (1000 s) was discarded and the stationary state was analyzed. The non-autonomous perturbations $s_1(t), s_2(t)$ are simple step signals, each with length t=200 s and amplitudes $s_{1H} = s_{2H} = 0.2$, as presented on Fig. 4.16 (a).

For the first 200 s the first oscillator is unperturbed and its time-averages are around the baseline (except for small deviations due to weak noise and coupling). During the high value of $s_1(t)$ (t=200–400 s) the first oscillator is perturbed and its time-averages are affected accordingly. It is evident that x_1 is then subject to the

gradually decreasing after- effect of the perturbation. This transient period (t=400–700 s) appears because the oscillator needs a certain time to converge to its limit cycle. The length of the transient depends on the characteristics and the parameters of the oscillator. The associated time-averages are affected and the values are far from the baseline. A second perturbation (t=700–900 s) involves perturbing both of the oscillators by $s_2(t)$. Note that, during this period, the first oscillator is subject to the additional and indirect influence of the second oscillator, resulting in higher time-averages. After the second perturbation $s_2(t)$ finishes, the first oscillator is again left in perturbed state and only gradually returns towards its baseline value.

It is evident that transients in the oscillatory behaviour may persist for much longer than the timescale of the perturbation itself. Due to the coupled nature of the

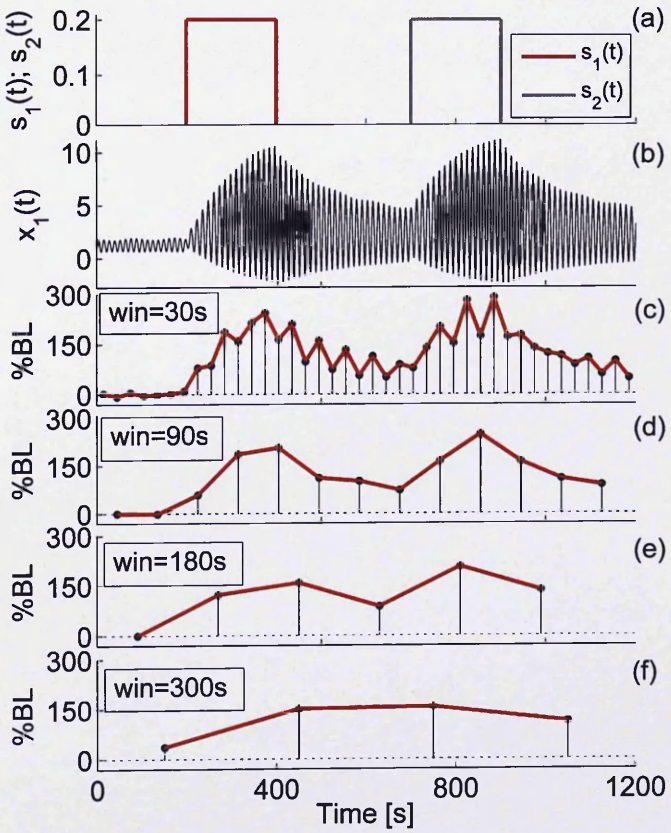

Fig. 4.16: The effect of repeated perturbations on the two-oscillator model described by Eqs. (1) and (2), showing the resultant changes in the mean value and transient effects as they are observed using different window sizes.

oscillatory processes, perturbing either oscillator results in the transient behaviour of both oscillators, leading to changes in the time-averaged values (which obscure the oscillations themselves). Repeated perturbations result in overlapping transient responses. Hence, when subjecting the microvasculature to a perturbation, care should be taken to understand the role of oscillatory processes: short-time average values may capture only a part of the transient physiological response.

5. ANALOGUE SIMULATION AND SYNCHRONIZATION ANALYSIS OF NON-AUTONOMOUS OSCILLATORS

Synchronization is the 'language' used to describe the interactions among oscillatory processes or in some cases (like in networks of oscillators) the reason for the emergence of spontaneous order [8]. It is defined as an adjustment of frequencies due to weak interactions between oscillatory processes [9]. Very often in nature, the oscillatory systems (when not coupled) have basic frequencies that vary with time. Such systems with time-varying frequencies are usually observed in biology, some examples being the cardiorespiratory system [5] and the brain [33]. In general, not only the oscillating frequencies but also other interacting parameters and functional relationships can be time-varying.

Whilst the previous discussion outlined the theoretical background and proposed methods for treatment of synchronization between oscillators that are subject to external influences, this section concentrates on the application and analysis of signals obtained from experimental oscillatory systems. To observe the behaviour of these systems, an analogue simulation of two coupled non-autonomous oscillators was performed.

Analogue experiments have been used widely for studying the dynamics of nonlinear systems [40, 129–132]. They provide a convenient way to study the continuous dynamics and interactions between oscillatory systems and stochastic processes in real time. The electronic implementation and the real experimental environment, allow us to simulate the synchronization phenomenon in a way that is closer to the reality present in the nature. The uncertainty in the system, arising due to the noise embedded in the signals, has more realistic meaning, usually being attributed to environmental disturbances or imperfections of some electronic properties of the systems.

During the process of data acquisition and discretization, some additional amount of measurement noise is introduced, which has no links with the actual dynamics of the oscillators. In analogue simulation the dynamics of the systems are truly continuous, unlike numerical simulation where the continuous dynamics are only approximate due to finite integration step.

The synchronization phenomenon can be studied, among other methods, through phase and generalized synchronization analysis. The former studies the behavior of the phase difference of the oscillatory systems [15]. The generalized synchronization analyzes the stability of the response system with regard to the coupling amplitude in the state space [47]. Both of the definitions are widely used for chaotic systems, but they are equally applicable to the class of limit-cycle oscillators. The comparison and connection between phase and generalized synchronization has been discussed in [133]. The central issue to be addressed here is how to treat the synchronization phenomenon of time-varying oscillators, both from phase and state variables, in experimental conditions. This leads to a common framework within which both types of synchronization can be detected.

5.1 The model

The specific model under investigation includes oscillators whose basic frequencies, as their most essential characteristic, are not constant but time-varying. The motivation for studying this case is the presence of various modulations in biological oscillators, which can qualitatively affect their interactions. The dynamics of such non-autonomous oscillators are explicit functions of time: $dx/dt = f(x(t), t)$, and the synchronization phenomenon is implicitly dependent on the time-varying sources.

Under these constrains, the system to be investigated consists of two coupled van der Pol oscillators, in the following form:

$$\begin{aligned} &\frac{1}{c^2}\ddot{x}_1 - \mu_1(1-x_1^2)\frac{1}{c}\dot{x}_1 + [\omega_1 + \tilde{A}\sin(\tilde{\omega}t)]^2 x_1 = 0, \\ &\frac{1}{c^2}\ddot{x}_2 - \mu_2(1-x_2^2)\frac{1}{c}\dot{x}_2 + \omega_2^2 x_2 + \varepsilon(x_1 - x_2) = 0. \end{aligned} \tag{5.1}$$

where x_i, $i = 1, 2$ are the state variables that describe the dynamics of each subsystem, μ_i are the shape parameters that define the relaxation of each of the oscillator, and ε is the coupling amplitude. When the shape parameters are small ($\mu \to 0$), ω_i are the oscillating frequencies parameters. The constant parameter c appears from each integration procedure and is introduced for electrical stability. The first oscillator has a non-autonomous term (defined with $\tilde{A}$ and $\tilde{\omega}$) in its frequency, that forces it to oscillate with time-varying frequency. The two oscillators are unidirectionally coupled, where the first is driving the second oscillator.

The motivation for using van der Pol oscillators is due to the fact that, when they have curtain relaxation (for $\mu > 0$) the limit cycle is not perfectly circular, as is the case with most of the limit cycle oscillatory processes in nature. In the frequency domain this corresponds to the case when the oscillators have high harmonics. Although the van der Pol oscillator is frequently used and is a popular limit cycle oscillator, it is still not explicitly analytically solvable for the coupled dynamics. Therefore one way of analyzing and studying the two interacting van der Pol oscillators is through numerical and analogue simulation.

5.2 Analogue simulation

By conducting analogue simulation one can investigate the nonlinear dynamical behavior of real experimental systems which can also encounter weak noise, possibly both additive and multiplicative, arising from the imperfection of the electronic components. The conceptual and technical aspects of the implementation followed the discussion in [40].

The block-diagram of the analogue electronic implementation of the system under investigation (5.1), is given in Fig. 5.1. All the operational amplifiers are MC1458N type, while the four-quadrant analogue multipliers are of AD534LD type. The output of each multiplier is divided by a factor of 10, thus after each multiplier there is amplifier with magnification $A_m = 10$ - not shown on the block diagram for compact and clear presentation. From the specific construction on Fig. 5.1 one can determine

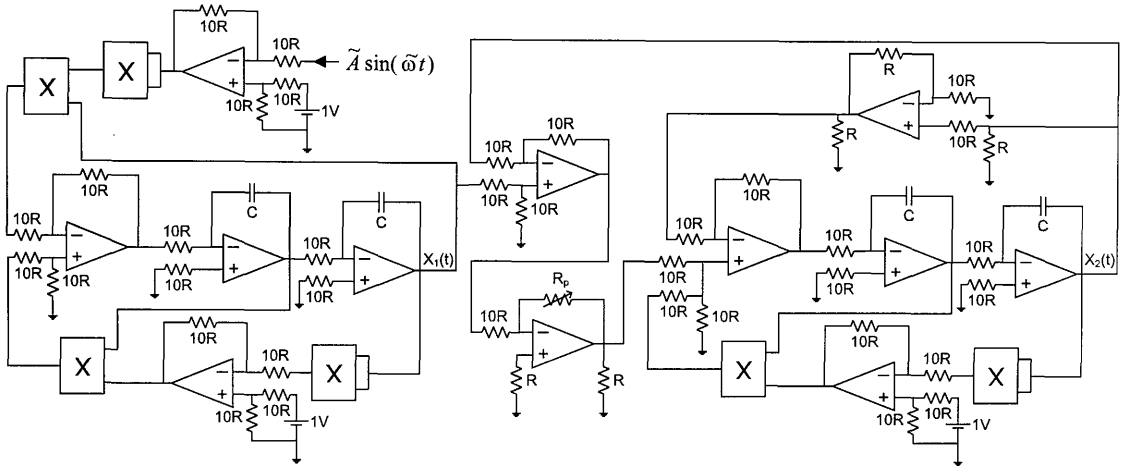

Fig. 5.1: A schematic block diagram of the analogue electronic circuit implementation of two unidirectionally coupled van der Pol non-autonomous oscillators. The standard notations are used: triangles correspond to amplifiers, while the rectangles correspond to the multipliers. For the resistors $R = 1k\Omega$, $C = 1\mu F$ and the resistor potentiometer $R_p = 1 \rightarrow 10k\Omega$.

the values of the parameters of the system (5.1). The shape parameters are both set to unity $\mu_1 = \mu_2 = 1$ and the basic frequencies are $\omega_1 = 1$ and $\omega_2 = 1.1$. The non-autonomoucity is introduced additively in the frequency of the first oscillator through sine wave signal from an analogue signal generator. The control parameters of the non-autonomous term are set to be $\tilde{A} = 0.03$ and $\tilde{\omega} = 0.2$. The constant $c = 100$ is introduced in the circuit integrators for electronic stability. Thus, the true oscillating frequencies are $f_1 = \omega_1 100/2\pi = 15.92Hz$ and $f_2 = \omega_2 100/2\pi = 17.51Hz$. By varying the resistor value on the potentiometer R_p one can change the coupling strength $\varepsilon = 0 \rightarrow 1$ - resulting in a change from not coupled to moderate coupling interaction between the two oscillators. In this way, the investigator is able to observe the dynamics and the synchronization transitions in real time, and to follow the time evolution, which is especially convenient for studying the observed system.

First the oscillator with the non-autonomous term in its frequency was analyzed. Its dynamics are such that it oscillates with constant amplitude (the envelope of $x_1(t)$), while its frequency is varying with time. The phase portrait from the oscilloscope is shown on Fig. 5.2 (a). The constant amplitude and the signal form in the time domain are presented in Fig. 5.2 (b). The time variability of the frequency,

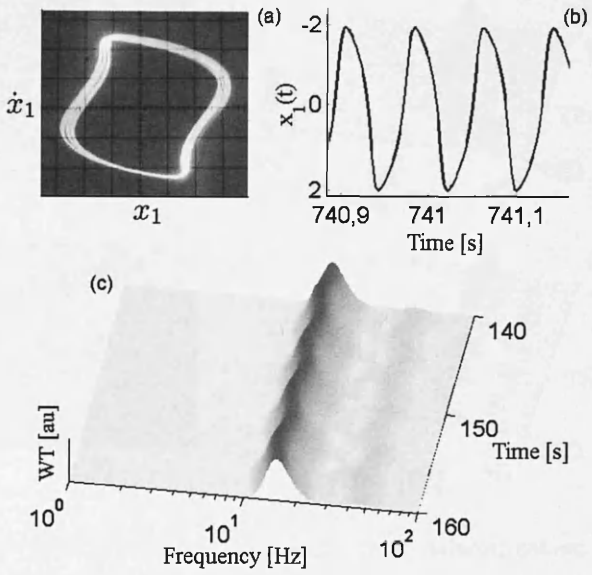

Fig. 5.2: The phase portrait (a), the signal (b), and the time-frequency wavelet analysis (c) from the first ($x_1(t)$) van der Pol oscillator. (b) and (c) are calculated after analogue-to-digital conversion with $1000Hz$ sampling frequency.

as the most significant characteristic of this oscillator, can be studied by the means of wavelet transform analysis. The specific implementation with the use of Morlet mother wavelet is as discussed in chapter 4. From the time-frequency representation of the signal $x_1(t)$ in Fig.5.2(c) one can clearly see that the frequency of the first oscillator is varying over time, and that the form of the variation is as imposed by the non-autonomous sine term.

While the amplitude of the signal $x_1(t)$ is constant over time, the amplitude of the first derivative $\dot{x}_1(t)$ is varying, due to the variations of the oscillating frequency. Therefore, the phase portrait (Fig.5.2(a)) shows that the limit cycle is varying slowly in time, in a bounded region around the mean limit cycle curve. The numerical analysis of the Lyapunov exponents [102] shows that the non-autonomous van der Pol oscillator has negative-close to zero largest Lyapunov exponent, pointing out that the oscillator is still in its quasiperiodic state and that its attractivity did not change qualitatively. If the non-autonomous perturbations, imposed by $\tilde{A}$, are much larger than those used in this study, then the oscillator can turn from quasiperiodic into chaotic with positive largest Lyapunov exponent, its stability can be lost, or its

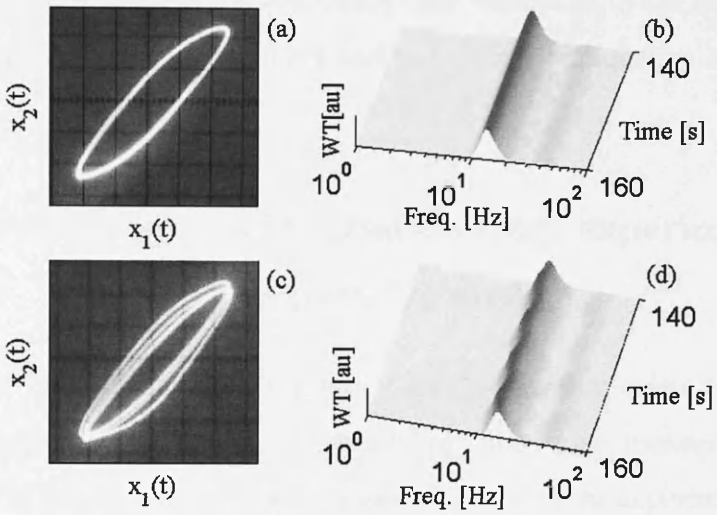

Fig. 5.3: Lissajous curves and wavelet transform of synchronization in autonomous case (a), (b) and in non-autonomous (c), (d) case. Lissajous curves of synchronization for both autonomous oscillators (when $\tilde{A} = 0$) (a). Time-frequency wavelet representation of $x_2(t)$ for autonomous synchronization (b). Lissajous curve for non-autonomous case of synchronization (c) and the corresponding wavelet representation of $x_2(t)$ during this case (d). Compare differences on (a) with (c), and (b) with (d).

oscillations can reduce to zero (oscillation death). These outcomes are not relevant to this study.

The second oscillator is autonomous by itself and its frequency is constant over time, as shown on the time-frequency representation on Fig. 5.3 (b). If the non-autonomous term is very small i.e. ideally zero ($\tilde{A} = 0$), then the frequencies of both the oscillators are constant over time (like the one shown in Fig. 5.3 (b)). For sufficiently large coupling e.g. $\varepsilon = 0.4$ the two oscillators can synchronize. The Lissajous curve of this classical case of synchronization is presented in Fig.5.3 (a). The curve is stable without phase slips and has constant form over time. Next the oscillators are kept synchronized and non-autonomoucity is introduced by increasing the amplitude to $\tilde{A} = 0.03$. The Lissajous curve will again be stable without phase slips, but its form will slowly vary with time Fig. 5.3 (c), in a bounded region around the autonomous Lissajous curve (compare Fig. 5.3 (a) and Fig. 5.3 (c)). Observing the wavelet analysis of the second van der Pol oscillator Fig. 5.3 (d), a variation in frequency can be seen due to synchronization with the first non-autonomous oscillator. The time variability

of the frequency is also followed by amplitude time variations of the second oscillator, in order for it to stay in the entrainment and to follow the frequency variations of the first oscillator.

5.3 Detecting synchronization from experiments– comparative analysis

Detection in this sense means to investigate if synchronization exists between the two oscillators, by analyzing the dynamics described by time-series, measured as electronic voltage signals for the states of the oscillators. As with other experimental measurements, the detections should be able to confirm the underlying synchronization even though the signals can have a harmful amount of noise. Of special interest for this study is the ability to follow the detection in time, because the non-autonomous influences can introduce time-variability and intermittent transitions of the synchronization state.

The time series to be analyzed can represent the state variables ($x_1(t)$ and $x_2(t)$) or the phases extracted from the same signals. In doing so, one will be detecting generalized or phase synchronization, respectively. In the following discussion, the proposed method, based on Bayesian inference, will be employed for the detection of both phase and generalized synchronization (discussed in more detail in chapter 3). Thus, even though the two types of synchronization are defined differently, the methods for detection will have the same inferential base, uniting them together to detect what constitutes the same phenomenon – synchronization. Due to the particular information propagation, the methods will be able to follow the time-variation of the frequencies. The evaluation of the synchronization state will be based on the inferred intrinsic parameters, and the separate inference of the noise, will allow the synchronization state to be determined without the effect from the noise.

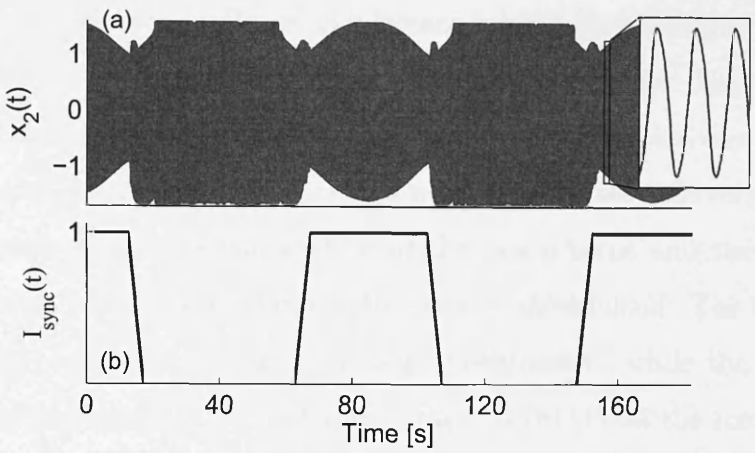

Fig. 5.4: The signal from the second driven oscillator and the phase synchronization detection. The signal from the second response oscillator shows amplitude (see the envelope) variations in periodic intervals as imposed by the external source (a). The inset presents enlarged section of the signal. The synchronization index from the detection (b). Note the detected intermittent synchronization transitions.

5.3.1 Phase synchronization detection

The goal is not only to detect the existence of synchronization state, but also to detect the time-variability and the transitions due to the effect of the external influences. For this reason the parameters for the non-autonomous periodic force were changed i.e. the amplitude was increased to $\tilde{A} = 0.06$, for which synchronization transitions appeared. Due to the periodicity of the external signal, the synchronized and non-synchronized intervals appeared intermittently. On the oscilloscope, it was possible to observe this dynamical behaviour in real time, through Lissajous curves. After digitalizing, the state time-series were obtained. The amplitude of the second driven oscillator was affected due to the synchronization and the non-autonomous influences - Fig. 5.4 (a). During the synchronization intervals the amplitude varies in accordance with the periodic force, while for the non-synchronized interval the envelope returns to its free oscillation modes. The inset shows the specific form of the signal.

Before the synchronization detections, the phases needed to be estimated from the digitalized signals. Because the form of the signals was not complex, the Hilbert transform was appropriate for estimating the phase variables. Details of the Hilbert transform based phase extractions were discussed in chapter 4.

The method based on the Bayesian inference is applied on the phase signals. After the reconstruction of the phase dynamics through the Fourier base functions, the intrinsic parameters and the noise are acquired. Due to the relatively high frequency of the oscillators, small windows $t_w = 0.5s$ were used for the inference. The inferred parameters were used for reconstruction of the phase torus and the corresponding map $M(\psi)$, from which the synchronization can be determined. The intervals where the root $M(\psi) = \psi_e$ existed were judged as synchronized, while the absence of the root indicated non-synchronized dynamics. Fig. 5.4 (b) shows the resultant detected synchronization. It can be seen clearly that the synchronization and the corresponding intermittent transitions were detected successfully. The detection was accurate and in agreement with the amplitude variations imposed by the non-autonomous source.

5.3.2 Generalized synchronization detection

For determination of the generalized synchronization the states of the interacting system are required. In this case, the digitalized voltages of the two oscillators represent the state variables. The two van der Pol oscillators are unidirectionally coupled, where the first has an external source acting on its frequency. The definition of generalized synchronization prescribes that the oscillators are synchronized if the response oscillator is asymptomatically stable. By evaluating the largest Lyapunov exponents, one can determine if the response oscillator is asymptomatically stable and if synchronization exists (detailed discussion can be found in chapter 3).

The signals from the model 5.1 (using direct coupling) are processed through the Bayesian inferential technique. The inference relies on the state base functions for this particular model which were already described in chapter 3. The inference returns the intrinsic parameters about the bi-variate dynamics and the noise. The numerical evaluation of the largest Lyapunov exponents λ can reveal the synchronization state. If λ is zero, there is no synchronization and the response oscillates with its own dynamics. Synchronization occurs if λ has negative values, and the response oscillators are asymptomatically stable.

In order to take advantage of the time-varying propagation process, the analysis

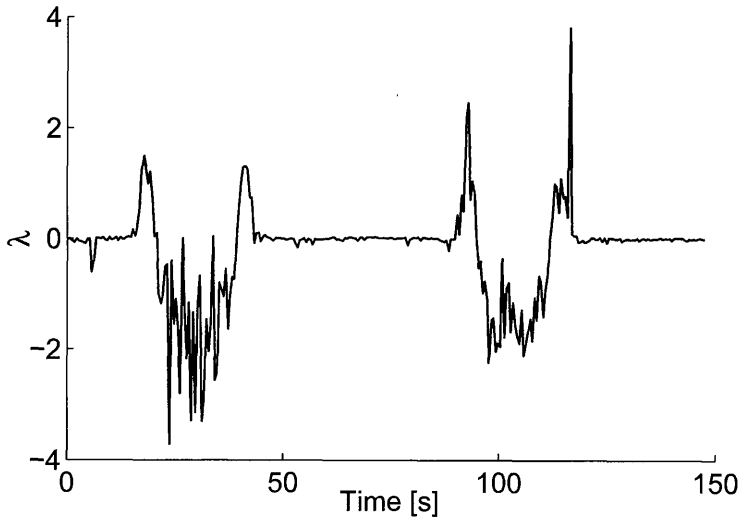

Fig. 5.5: Detected generalized synchronization from system 5.1, expressed through the largest Lyapunov exponent λ. Negative values indicate asymptomatic stability of the response oscillator, and occurrence of synchronization. Note the detected intermittent periodic transitions from in and out of synchronization.

is performed on intermittent case of synchronization. Similarly as in the previous section, the variations introduced in the frequency of the first oscillator are relatively high ($\tilde{A} = 0.06$) and synchronization transitions occur in periodic order. Fig. 5.5 illustrates the evaluated largest Lyapunov exponent λ i.e. the detected generalized synchronization. The proposed method determined the qualitative state of synchronization successfully, which appears as negative Lyapunov exponent λ. Around the transitions the exponent is positive, which indicates that the response oscillator goes through marginally stable into unstable transition, before it reaches the synchronized stable state. Also it can be noticed that the Lyapunov exponent is not very precise and has large variations.

5.4 Discussion

Starting from different variables (phase and states), the two types of phase and generalized synchronization, exploit different characteristics in order to determined the synchronization state. Although defined in different ways, both of the approaches inherently describe phenomenon with same nature. This was demonstrated with the use

of the proposed detection methods, based on the same fundamental concept, which detected the synchronized dynamics emanating from the same system, both through phase and generalized synchronization.

The two methods detected synchronization phenomenon successfully and were able to followed the intermittent transitions. The generalized synchronization approach was more convenient in the respect that it was applied directly on the signals, and did not require the prior phase extractions. But the generalized method relies on inference represented with base functions of specific model. The phase synchronization was more resistant to noise, having less variations, and was able to follow the transition more precisely.

6. CONCLUSION

6.1 Summary

This thesis studies the effect of external dynamical sources on interacting self-sustained oscillators. It outlines the theoretical constraints needed for appropriate understanding of the dynamics and the phenomena that occur as a consequence of non-autonomous influences. An inference technique is proposed for detection of time-evolving dynamics in interacting oscillatory systems in the presence of noise. The method enables synchronization and the respective transitions to be detected and the interactions to be described in terms of time-varying coupling function and directionality. The entire study is motivated by interacting biological oscillators. Of main concern were the oscillatory processes from the cardiovascular system and sympathetic nerve activity, which were analyzed under conditions where the breathing frequency was externally varied in a predefined deterministic way. Several oscillatory models (Poincarè, van der Pol, phase) were used for theoretical, numerical and analogue analysis. However, these models were not intended to model all aspects of fully functioning complex biological systems (e.g. like the heart), but only to capture sufficient dynamical characteristics which effectively describe the interacting oscillatory nature. This indirectly implies that the developed detection techniques need to be equally applicable to time-series obtained from biological systems and from the model oscillators.

As theoretical background, a framework for analysis of interactions between non-autonomous oscillating systems was presented. Multiple-scale analysis was applied on a phase oscillators model with slowly varying frequency. It revealed the analytic form of the synchronization behaviour with respect to slow and fast time-variations.

The investigation of limit-cycle oscillators showed that synchronous transition occurs when the equilibrium solution for the phase difference and amplitudes (ψ_{eq}, r_{1eq}, r_{2eq}) loses its stability through a Hopf bifurcation. Bifurcation diagrams as functions of coupling parameters were constructed for identification of parameter ranges of synchronization, intermittent synchronization and non-synchronization. From the viewpoint of the time series analyst, synchronization between non-autonomous oscillators appears substantially different from the classical autonomous case and several distinct characteristics exist. The phase difference is dynamically varying, the lag synchronization is not possible because of the non-constant time-varying phase shift and the external source can be the cause for synchronization transitions between different synchronization orders. The time-variation of the form of the coupling function, even when the parameters (frequency, coupling amplitude) are constant, can act as a cause for synchronization transitions.

Many practical situations exist where the investigator needs to determine and quantify the interacting dynamics, and if (and how) they are time-varying. For these reasons, a technique was introduced for analysis of the interactions between time-dependent coupled oscillators, based on the signals they generate. At the core of the method lies the Bayesian inference, which relies on either phase or state base functions. Arguably, the representation of the phase dynamics with finite Fourier base functions offers more general applicability than the state dynamics reconstruction, which is model-dependent. The sequential information propagation was customized in order to follow the time-variability of the oscillatory dynamics. Because synchronization was evaluated from the inferred parameters separated from the noise, the method was able to distinguish unsynchronized dynamics from noise-induced phase slips, which could be important in a number of contexts, including both noise-induced synchronization and desynchronization. Several important technical aspects were elaborated on, and the method was applied to reveal and quantify the time-varying nature of numerical, analogue and cardiorespiratory oscillatory systems.

It was demonstrated that the inference enables the evolution of the system under study to be tracked continuously. Unlike earlier methods that only detect the occur-

rence of transitions to/from synchronization, the new method reveals details of the dynamics, thus describing the inherent nature of the transitions, and at the same time deducing the characteristics of the noise responsible for stimulating them. The time-varying nature of the functions that characterize interactions between open oscillatory systems was identified. The cardiorespiratory analysis demonstrated that not only the parameters, but also the functional relationships, can be time-varying, and the new technique can effectively follow their evolution. The variability of the function has an important impact on the nature of the interactions, and can lead to qualitative synchronization transitions. Because the only requirements are the time series, the technique promises wide and general applicability.

The proposed theory and methods were applied for the analysis of biological oscillatory systems affected by external dynamical fields. The analyses were performed on measurements taken under conditions where the respiration was varied linearly in a deterministic way, which introduced non-autonomous time-variability into the oscillating system. The measurements of ECG, CO_2 concentration, blood pressure and muscle sympathetic nerve activity, were analyzed by methods that were able to track their time-variability. Statistical analyses were performed in order to identify significant relationships. It was found that the time-varying breathing process significantly affects the functioning and regulation of several mechanisms in cardiovascular and sympathetic neural systems. In general, the low breathing frequencies provoked more information flow, altering the coordination and increasing the coupling influences between the oscillatory processes. The manifestations and effects on this multi-coupled oscillatory system had the imprint of the particular form of the externally induced deterministic time-variation.

The benefits of using the proposed inferential method were demonstrated on the ramp cardiorespiratory analysis. The technique successfully identified that the cardiorespiratory coordination depends on, and is regulated to a great extent by, the respiration dynamics. The synchronization analysis showed occurrence of consecutive transitions between different orders. It was found that the externally induced varying respiration acts as a cause for these qualitative transitions. The cardiorespiratory coupling

function was found again to be a time-varying process, which introduced additional complexity for the interactions and their analysis.
An alternative method for phase detection, based on wavelet synchrosqueezed transform, showed how the instantaneous phase can be extracted from complex time-varying signals, such as the ECG signal. It was demonstrated that this approach can be very useful in phase extraction from signals with mixed-mode oscillatory components. This opened the door for future in depth analysis of the inter-oscillatory interactions in blood flow signals.
The dynamical characterization for the reproducibility of LDF blood flow was shown to be more appropriate than the time-averaged analysis, and that care must be taken when non-autonomous perturbations are made consecutively.

The analogue simulation presented another model of interacting non-autonomous oscillators which encountered real experimental noise. Two van der Pol oscillators were unidirectionally coupled, where the frequency of the first oscillator was externally and periodically perturbed. The intermittent synchronization was detected both through phase and generalized synchronization, based on common inferential basis.

In summary, this thesis demonstrates how one can study and detect the effect from external fields on interacting oscillators. It lays down the theoretical background and inference tools that can serve as a conceptual basis for appropriate analysis of such oscillatory systems, particularly of those which are biological in nature.

6.2 Future perspectives

During the discovery and development of these methods, theories and their applications, several new perspectives emerged. Some of them could lead to new insights into oscillatory interactions, and deserve to be addressed in the near future. The following outlines some of the aspects that could define the future directions and development of the work proposed in this thesis:

The phase dynamics inferential technique can be applied on oscillatory interactions of different origins. Thus its exploitation for electro-chemical, mechanical and

meteorological oscillatory systems could be potentially useful. The cardiorespiratory application can be further investigated, including more subjects and different states or diseases. In fact, there is an ongoing study about human ageing where the inferential method is already proving to be useful for the characterization of synchronization, directionality and coupling functions with respect to the age of the subjects. This study differs from the ramp breathing case, because in the ageing study, the subjects breathe freely, at rest, with no external perturbations.

The detection of generalized synchronization can be further investigated for its applicability and technical aspects. One direction could be to study the detection of time-varying generalized synchronization between chaotic oscillators. The determination of the asymptotic stability implies that in this case the largest Lyapunov exponents would change from positive to negative due to synchronization. Thus, a better discrimination could be achieved.

The instantaneous phase detection based on wavelet synchrosqueeze transform offers the possibility for the phases to be decomposed from mixed-mode signals. This procedure was demonstrated for one human blood flow signal in this thesis. In future, a more in depth investigation can be conducted, analyzing more subjects in order to infer the inner-interactions between the six oscillatory processes. The application of the inferential method in this way will be generalized for a network of six oscillators, which could analyze the time-evolving synchronization, directionality and coupling functions.

The application of the inferential method identified the time-varying nature of coupling functions. The current literature has not paid much attention to this issue and it requires further exploration. The presence of time-varying coupling functions in open cardiorespiratory systems provides strong evidence that this study is very important. This thesis shows that the time-variability of the form of the functions can cause synchronization transitions. Therefore, a more detailed analytic analysis could reveal additional details and mechanisms of the interactions of open oscillatory systems.

APPENDIX

A. GLOSSARY

Anaesthesia: is a pharmacologically induced and reversible condition of having sensation (including the feeling of pain) blocked or temporarily taken away.

Arnold tongue: in general, is defined as a resonance zone emanating out from rational numbers in a two-dimensional parameter space of variables. For synchronization it defines the entrainment region in coupling and frequency mismatch parameter space.

Blood flow (BF): is the continuous running of blood in the cardiovascular system.

Blood pressure (BP): is the pressure exerted by circulating blood upon the walls of blood vessels.

Cardiovascular system (CVS): consists of the heart and blood vessels, and is responsible for circulation of the blood.

Diastolic blood pressure (DIA): the minimum level of blood pressure measured during the relaxation phase of the cardiac cycle when the heart dilates and its chambers fill with blood.

Dynamical system: a mathematical means of describing how one state develops into another state over the course of time.

Electrocardiogram (ECG): a noninvasive measurement of the electrical activity of the heart using electrodes placed on the body.

Endothelium: the thin layer of cells lining the interior surfaces of all blood vessels. It forms an interface between the circulating blood and the rest of the vessel wall.

Generalized synchronization: occurs in unidirectionally coupled systems, if the driven system is asymptotically stable.

Heart rate variability (HRV): is the continuous variations with time in the heart rate of a healthy human, even in repose.

Lag synchronization: is synchronous regime where the states of two oscillators are nearly identical, but one system lags in time to the other.

Laser Doppler flowmetry (LDF): is a noninvasive method for measuring the continuous circulation of blood flow on a microscopic level.

Lyapunov exponent (LE): of a dynamical system is a quantity that characterizes the rate of separation of infinitesimally close trajectories.

Multiple scale analysis: comprises techniques used to construct uniformly valid approximations to the solutions of perturbation problems, both for small as well as large values of the independent variables.

Muscle sympathetic nervous activity (MSNA): is the activity of SNS (q.v.), often measured invasively from the efferent traffic of the peroneal muscle nerve.

Myogenic: contraction is an inherent property of smooth muscle. It occurs rhyth-

mically with a period of around 10 s, without any external stimulus.

Non-autonomous system: is a system of ordinary differential equations which explicitly depends on the independent variable. From dynamical point of view, non-autonomous system includes an explicit time-dependance.

Non-isochronous oscillator is one which rotation frequency is amplitude dependent. Its definition includes amplitude terms that reflect the non-isochronicity or shear of phase flow around the limit cycle.

Phase oscillator: is an approximative notation of phase dynamics of weakly interacting oscillators.

Phase synchronization: is an adjustment of rhythms of oscillating objects due to their weak interaction.

Respiration: is defined as the transport of oxygen from the outside air to the cells within tissues, and the transport of carbon dioxide in the opposite direction.

Respiratory sinus arrhythmia (RSA): is a natural variation in the heart rate that occurs during breathing. Heart rate increases during inspiration and decreases during expiration.

Self-sustained oscillator: is the oscillator that exhibits stable limit cycles in the absence of external contribution.

Sinus node: is the impulse-generating (pacemaker) tissue located in the right atrium of the heart, and thus the generator of the sinus rhythm.

Sympathetic nervous system (SNS): is a part of autonomic nervous system which

mainly controls involuntary internal processes. It prepares the body for responses to stressful challenges, allowing sudden strenuous exercise and increased vigilance.

Systolic blood pressure (SYS): is the maximum level of blood pressure measured during the contraction phase of the cardiac cycle when blood is driven into the aorta and pulmonary artery.

B. DETAILED ANALYTIC MANIPULATIONS FOR THE COUPLED LIMIT-CYCLE OSCILLATORS MODEL

This appendix shows the relatively straight forward algebraic steps through which the main analytical results were derived.

The Poincarè oscillator can be written as follows in either cylindrical

$$\begin{aligned} \dot{r} &= \alpha r(a-r) \\ \dot{\phi} &= -\omega \end{aligned} \tag{B.1}$$

or Euclidean coordinates

$$\begin{aligned} \dot{x} &= \omega y - x\,\alpha\left(\sqrt{x^2+y^2}-a\right) \\ \dot{y} &= -\omega x - y\,\alpha\left(\sqrt{x^2+y^2}-a\right). \end{aligned} \tag{B.2}$$

Now consider a pair of such coupled oscillators:

$$\begin{aligned} \dot{x}_1 &= -q_1 x_1 - \omega_1(t) y_1 + \epsilon_1(t) g_{11}(x_1, x_2) \\ \dot{y}_1 &= -q_1 y_1 + \omega_1(t) x_1 + \epsilon_1(t) g_{12}(y_1, y_2) \\ \dot{x}_2 &= -q_2 x_2 - \omega_2(t) y_2 + \epsilon_2(t) g_{21}(x_1, x_2) \\ \dot{y}_2 &= -q_2 y_2 + \omega_2(t) x_2 + \epsilon_2(t) g_{22}(y_1, y_2) \end{aligned}$$

$$q_i = \alpha_i\left(\sqrt{x_i^2+y_i^2}-a_i\right).$$

Writing explicitly the velocities of the phases $\dot{\phi}_i = \frac{d}{dt}\arctan\frac{y_i}{x_i}$ and of the amplitudes

$\dot{r}_i = \frac{d}{dt}\sqrt{(x_i^2 + y_i^2)}$ one obtains:

$$\begin{aligned}
\dot{\phi}_1 &= -\tilde{\omega}_1 + \frac{\cos\phi_1}{r_1}\tilde{\epsilon}_1 g_2(x_1, x_2) - \frac{\sin\phi_1}{r_1}\tilde{\epsilon}_1 g_1(x_1, x_2) \\
\dot{\phi}_2 &= -\tilde{\omega}_2 + \frac{\cos\phi_2}{r_2}\tilde{\epsilon}_2 g_4(x_1, x_2) - \frac{\sin\phi_2}{r_2}\tilde{\epsilon}_2 g_3(x_1, x_2) \\
\dot{r}_1 &= \alpha_1 r_1(a_1 - r_1) + \cos\phi_1\tilde{\epsilon}_1 g_1(x_1, x_2) + \sin\phi_1\tilde{\epsilon}_1 g_2(x_1, x_2) \\
\dot{r}_2 &= \alpha_2 r_2(a_2 - r_2) + \cos\phi_2\tilde{\epsilon}_2 g_3(x_1, x_2) + \sin\phi_2\tilde{\epsilon}_2 g_4(x_1, x_2)
\end{aligned}$$

For convenience the time-variability has been denoted with a tilde ($\sim$) overscript: for example $\tilde{w}_1 \equiv w_1(t)$.

The coupling function is general, and an explicit form must be chosen. If

$$\begin{aligned}
g_1(x_1, x_2) &= x_2 - x_1; \quad g_2(y_1, y_2) = y_2 - y_1; \\
g_3(x_1, x_2) &= x_1 - x_2; \quad g_4(y_1, y_2) = y_1 - y_2;
\end{aligned} \tag{B.3}$$

the derivative of the phase difference is expressed as:

$$\begin{aligned}
\dot{\psi} \equiv \dot{\phi}_2 - \dot{\phi}_1 = &-\tilde{\omega}_2 + \tilde{\epsilon}_2\frac{r_1}{r_2}\cos\phi_2\sin\phi_1 + \\
&- \tilde{\epsilon}_2\cos\phi_2\sin\phi_2 - \tilde{\epsilon}_2\frac{r_1}{r_2}\sin\phi_2\cos\phi_1 - \tilde{\epsilon}_2\sin\phi_2\cos\phi_2 + \\
&+ \tilde{\omega}_1 - \tilde{\epsilon}_1\frac{r_2}{r_1}\cos\phi_1\sin\phi_2 + \tilde{\epsilon}_1\cos\phi_1\sin\phi_1 + \\
&+ \tilde{\epsilon}_1\frac{r_2}{r_1}\sin\phi_1\cos\phi_2 - \tilde{\epsilon}_1\sin\phi_1\cos\phi_1
\end{aligned} \tag{B.4}$$

If the dynamics of the variables ψ, r_1 and r_2 is slow relative to the fast variables ϕ_i, one can consider the velocity of the phase difference as being averaged over a period of (let us say) ϕ_1 by integrating over one period. Thus, ϕ_2 was substituted with $\psi + \phi_1$ and next integral was evaluated :

$$\begin{aligned}\frac{1}{2\pi}\int_0^{2\pi}\dot{\psi}\,d\phi_1 \simeq \dot{\psi} = \frac{1}{2\pi}\int_0^{2\pi}\Big[&-\tilde{\omega}_2+\tilde{\omega}_1\\ &+\tilde{\epsilon}_2\frac{r_1}{r_2}(\cos\psi\cos\phi_1-\sin\psi\sin\phi_1)\sin\phi_1+\\ &-\tilde{\epsilon}_2(\cos\psi\cos\phi_1-\sin\psi\sin\phi_1)(\sin\psi\cos\phi_1+\\ &+\cos\psi\sin\phi_1)-\tilde{\epsilon}_2\frac{r_1}{r_2}(\sin\psi\cos\phi_1+\cos\psi\sin\phi_1)\cos\phi_1+\\ &-\tilde{\epsilon}_2(\sin\psi\cos\phi_1+\cos\psi\sin\phi_1)(\cos\psi\cos\phi_1+\\ &-\sin\psi\sin\phi_1)-\tilde{\epsilon}_1\frac{r_2}{r_1}\cos\phi_1(\sin\psi\cos\phi_1+\cos\psi\sin\phi_1)+\\ &+\tilde{\epsilon}_1\frac{r_2}{r_1}\sin\phi_1(\cos\psi\cos\phi_1-\sin\psi\sin\phi_1)\Big]d\phi_1\end{aligned} \tag{B.5}$$

which yields the result:

$$\dot{\psi} = \tilde{\omega}_1-\tilde{\omega}_2-\tilde{\epsilon}_2\frac{r_1}{r_2}\sin\psi-\tilde{\epsilon}_1\frac{r_2}{r_1}\sin\psi.$$

Integrating also $\dot{r}_i$ over ϕ_1 gives:

$$\begin{aligned}\langle\dot{r}_1\rangle &= \frac{1}{2\pi}\int_0^{2\pi}\dot{r}_1\,d\phi_1 = a_1r_1\alpha_1-{r_1}^2\alpha_1-\tilde{\epsilon}_1(r_1-r_2\cos\psi)\\ \langle\dot{r}_2\rangle &= \frac{1}{2\pi}\int_0^{2\pi}\dot{r}_2\,d\phi_1 = a_2r_2\alpha_2-{r_2}^2\alpha_2-\tilde{\epsilon}_2(r_2+r_1\cos\psi).\end{aligned}$$

Then the resulting system is expressed as:

$$\begin{cases}\dot{\psi}=0=\tilde{\omega}_1-\tilde{\omega}_2+(-\frac{r_2\tilde{\epsilon}_1}{r_1}-\frac{r_1\tilde{\epsilon}_2}{r_2})\sin\psi\\ \dot{r}_1=0=a_1r_1\alpha_1-{r_1}^2\alpha_1-r_1\tilde{\epsilon}_1+r_2\tilde{\epsilon}_1\cos\psi\\ \dot{r}_2=0=a_2r_2\alpha_2-{r_2}^2\alpha_2-r_2\tilde{\epsilon}_2+r_1\tilde{\epsilon}_2\cos\psi\end{cases} \tag{B.6}$$

Eq.(B.6) might or might not admit a solution, depending on the numerical values of the parameters.

C. SYNCHROGRAM

Synchrograms can be used to obtain visual and qualitative measures of synchronization at different frequency ratios [9]. They are constructed by plotting the normalized relative phase of one oscillator within m cycles of the other oscillator, according to

$$\Psi_m(t_k) = \frac{1}{2\pi}\phi(t_k) \bmod 2\pi m$$

where t_k is the time of the k-th marked event of the first oscillator, $\phi(t_k)$ is the instantaneous phase of the second oscillator at time t_k, and *mod* is the modulo operation function. In the case of autonomous oscillators, perfect synchronization corresponds to horizontal stripes on the synchrogram. When studying synchronization of non-autonomous oscillators, synchrograms enable one to follow qualitatively the time variations of the relative phase difference.

D. ORDER, TYPE AND DURATION OF THE RAMP BREATHING SEGMENTS FOR EACH SUBJECT

Each of the subjects was measured having paced respiration intervals with linear "ramp" variations. In respect of the change of the breathing frequency, there were two types of ramps: fast-to-slow and slow-to-fast. The order of the ramps was not strictly defined, and in some subjects there was only one type of ramp breathing, while in other the two types were changing intermittently. However, the length of the ramps and the frequency band within which the respiration was varied, were (approximately: mean 9.05 and standard deviation of 0.14 minutes) constant for all of the subjects and segments. The following table (D.1) summarizes the order and the duration of the ramp breathing segments and the respective spontaneous segments in between, for each subject. For example, subject 4 had four ramp segments, two fast-to-slow and two slow to fast, which changed intermittently. Compared this notation and the respective wavelet transform illustration on Fig. 4.2 for the same subject 4.

Subject nr.	Segment 1		Segment 2		Segment 3		Segment 4		Segment 5		Segment 6		Segment 7		Segment 8		Segment 9		Segment 10	
1	-	9.5	\	9.1	-	5.8	\	9.1	-	5.4	\	9.1	-	5.2						
2	-	15.2	\	9.2	-	5.7	/	9.1	-	5.9	/	9	-	7.4	\	9.2	-	4.5		
3	-	6.7	/	9.2	-	4.7	\	9.1	-	9.6	\	9.2	-	6.9	\	9.2	-	6.3	/	9.2
4	-	7.4	/	9.2	-	5.9	\	9.1	-	8.4	/	9.1	-	9.5	\	9.1	-	6.5		
5	-	7	/	9.5	-	5.6	\	9.1	-	8.3	\	9.1	-	9.5	/	8.9	-	8.9		
6	-	8.2	\	9.1	-	10.2	\	9.3	-	7	\	9	-			-				
7	-	6	\	9.1	-	7.2	\	9	-	9.5	\	9	-	6.6		-				
8	-	6	\	9.1	-	5.9	\	9.1	-	6.4	\	9.1	-	5.4		-				
9	-	10.8	\	9	-	6.1	/	9	-	8.7	/	9.1	-	9.5	\	9.2	-	6.1		
10	-	6.2	\	9.3	-	5.5	/	8.9	-	7.7		-				-				
11	-	6.7	\	9	-	6.3	/	9.3	-	15.2	\	9.5	-	9.1	/	9.5	-	6.2		
12	-	7	/	9.1	-	6.6	\	8.9	-	8	/	9.3	-	8.8	\	9.2	-	3.7		
13	-	6.1	\	-		/		-		\		-		/		-				

Fig. D.1: Order and duration of segments for each subject. The segments can be: spontaneous breathing denoted as "-", and two types of ramps fast-to-slow denoted as "\", and slow-to-fast ramp denoted with "/". The numerical values represent the duration of each segment in minutes.

E. LIST OF PUBLICATIONS

The following publications were produced:

T Stankovski, A Duggento, A Stefanovska and P V E McClintock, "Inference of time-evolving coupled dynamical systems in the presence of noise" *Physical Review Letters*, in submission.

A Stefanovska, L W Sheppard, T Stankovski and P V E McClintock, "Reproducibility of LDF blood flow measurements: Dynamical characterization versus averaging", *Microvascular Research* 82(3), 274-6 (2011).

T Stankovski, W H Cooke, L Rudas, A Stefanovska, D L Eckberg, "Voluntary ramped-frequency breathing: a powerful experimental tool to modulate and explore human autonomic mechanisms", *Journal of Physiology*, in preparation for submission.

T Stankovski, "Phase detection from the respiration signal", Section 4.5 of *Nonlinear Dynamics of Anæsthesia: from Theory to Clinical Application*, editors A Stefanovska, P V E McClintock, J Ræder and A F Smith, to be published by Springer.

The following presentations were made:

"Synchronization and stability analysis of interacting non-autonomous self-sustained oscillators", in *Non-autonomous and Random Dynamical Systems in the Life Sciences*, Inzell, Germany, 1-5 August 2011 (oral presentation).

"Detection of synchronization, directionality and time-varying dynamics of coupled oscillatory processes", in *Fluctuations and Coherence: from Superfluids to Living Systems*, Lancaster, UK, 13-16 July 2011 (oral presentation).

"Synchronization of interacting oscillators subject to external non-autonomous influences", 8th International Summer School and Conference *Let's Face Chaos Through Nonlinear Dynamics*, Maribor, Slovenia, 26 June - 10 July 2011 (poster presentation).

"Phase detection from the respiration signal", ESGCO 2010: *6th Conference of the European Study Group on Cardiovascular Oscillations*, Berlin, Germany, 12-14 April 2010 (poster presentation).

BIBLIOGRAPHY

[1] G. D. Birkhoff. *Dynamical Systems, vol. 9 of Colloquium Publications.* American Mathematical Society, New York, 1927.

[2] P. E. Kloeden and M. Rasmussen. *Nonautonomous Dynamical Systems.* AMS Mathematical Surveys and Monographs, New York, 2011.

[3] H. Haken. Cooperative phenomena in systems far from thermal equilibrium and in nonphysical systems. *Rev. Mod. Phys.*, 47:67–121, 1975.

[4] A. A. Andronov, A. A. Vitt, and S. H. Khaikin. *The Theory of Oscillators.* Dover Publications Inc., New York, 2009.

[5] A. Stefanovska and M. Bračič. Physics of the human cardiovascular system. *Contemp. Phys.*, 40:31–55, 1999.

[6] Y. Shiogai, A. Stefanovska, and P. V. E. McClintock. Nonlinear dynamics of cardiovascular ageing. *Physics Reports*, 488:51 – 110, 2010.

[7] A. T. Winfree. Biological rhythms and the behavior of populations of coupled oscillators. *J. Theor. Biol.*, 16:15, 1967.

[8] S. H. Strogatz. *SYNC: The Emerging Science of Spontaneous Order.* Hyperion, New York, 2003.

[9] A. Pikovsky, M. Rosenblum, and J. Kurths. *Synchronization – A Universal Concept in Nonlinear Sciences.* Cambridge University Press, Cambridge, 2001.

[10] Y. Kuramoto. *Chemical Oscillations, Waves, and Turbulence.* Springer-Verlag, Berlin, 1984.

[11] A. Stefanovska, H. Haken, P. V. E. McClintock, M. Hožič, F. Bajrović, and S. Ribarič. Reversible transitions between synchronization states of the cardiorespiratory system. *Phys. Rev. Lett.*, 85:4831–4834, 2000.

[12] C. Schäfer, M. G. Rosenblum, J. Kurths, and H. H. Abel. Heartbeat synchronised with ventilation. *Nature*, 392(6673):239–240, 1998.

[13] M. Rasmussen. *Attractivity and Bifurcation for Nonautonomous Dynamical Systems.* Springer, Berlin, 2007.

[14] A. Pikovsky, M. Rosenblum, and J. Kurths. Phase synchronisation in regular and chaotic systems. *Int. J. of Bif. and Chaos*, 10(10):2291–2305, 2000.

[15] M. G. Rosenblum, A. S. Pikovsky, and J. Kurths. Phase synchronization of chaotic oscillators. *Phys. Rev. Lett.*, 76(11):1804–1807, 1996.

[16] L. Kocarev and U. Parlitz. General approach for chaotic synchronization with applications to communication. *Phys. Rev. Lett.*, 74(25):5028–5031, 1995.

[17] R. Brown and L. Kocarev. A unifying definition of synchronization for dynamical systems. *Chaos: An Interdisciplinary Journal of Nonlinear Science*, 10(2):344–349, 2000.

[18] P. E. Kloeden. Synchronization of nonautonomous dynamical systems. *Elect. J. Diff. Eqns.*, 1:1–10, 2003.

[19] P. E. Kloeden and R. Pavani. Dissipative synchronization of nonautonomous and random systems. *GAMM-Mitt.*, 32(1):80–92, 2009.

[20] P. Tass, M. G. Rosenblum, J. Weule, J. Kurths, A. Pikovsky, J. Volkmann, A. Schnitzler, and H.-J. Freund. Detection of $n : m$ phase locking from noisy data: Application to magnetoencephalography. *Phys. Rev. Lett.*, 81:3291–3294, Oct 1998.

[21] F. Mormann, K. Lehnertz, P. David, and C. E. Elger. Mean phase coherence as a measure for phase synchronization and its application to the eeg of epilepsy patients. *Physica D*, 144:358–369, 2000.

[22] B. Schelter, M. Winterhalder, R. Dahlhaus, J. Kurths, and J. Timmer. Partial phase synchronization for multivariate synchronizing systems. *Phys. Rev. Lett.*, 96:208103, May 2006.

[23] M. Paluš and A. Stefanovska. Direction of coupling from phases of interacting oscillators: An information-theoretic approach. *Phys. Rev. E*, 67:055201, 2003.

[24] M. G. Rosenblum and A. S. Pikovsky. Detecting direction of coupling in interacting oscillators. *Phys. Rev. E.*, 64:045202, 2001.

[25] A. Bahraminasab, F. Ghasemi, A. Stefanovska, P. V. E. McClintock, and H. Kantz. Direction of coupling from phases of interacting oscillators: A permutation information approach. *Physical Review Letters*, 100:084101, 2008.

[26] J. Jamšek, M. Paluš, and A. Stefanovska. Detecting couplings between interacting oscillators with time-varying basic frequencies: Instantaneous wavelet bispectrum and information theoretic approach. *Phys. Rev. E*, 81:036207, 2010.

[27] B. Kralemann, L. Cimponeriu, M. Rosenblum, A. Pikovsky, and R. Mrowka. Uncovering interaction of coupled oscillators from data. *Phys. Rev. E*, 76:055201, Nov 2007.

[28] B. Kralemann, L. Cimponeriu, M. Rosenblum, A. Pikovsky, and R. Mrowka. Phase dynamics of coupled oscillators reconstructed from data. *Phys. Rev. E*, 77:066205, Jun 2008.

[29] V. N. Smelyanskiy, D. G. Luchinsky, A. Stefanovska, and P. V. E. McClintock. Inference of a nonlinear stochastic model of the cardiorespiratory interaction. *Physical Review Letters*, 94:098101, 2005.

[30] D. G. Luchinsky, V. N. Smelyanskiy, A. Duggento, and P. V. E. McClintock. Inferential framework for nonstationary dynamics. i. theory. *Phys. Rev. E*, 77:061105, 2008.

[31] A. Duggento, D. G. Luchinsky, V. N. Smelyanskiy, I. Khovanov, and P. V. E. McClintock. Inferential framework for nonstationary dynamics. ii. application to a model of physiological signaling. *Phys. Rev. E*, 77:061106, 2008.

[32] A. Duggento, D. G. Luchinsky, V. N. Smelyanskiy, and P. V. E. McClintock. Inferential framework for non-stationary dynamics: theory and applications. *Journal of Statistical Mechanics: Theory and Experiment*, 2009:P01025 (14pp), 2009.

[33] D. Rudrauf, A. Douiri, C. Kovach, J. P. Lachaux, D. Cosmelli, M. Chavez, C. Adam, B. Renault, J. Martinerie, and M. L. Van Quyen. Frequency flows and the time-frequency dynamics of multivariate phase synchronization in brain signals. *Neuroimage*, 31(1):209–227, 2006.

[34] D. L. Eckberg. The human respiratory gate. *The Journal of Physiology*, 548(2):339–352, 2003.

[35] L. J. Badra, W. H. Cooke, J. B. Hoag, A. A. Crossman, T. A. Kuusela, K. U. O. Tahvanainen, and D. L. Eckberg. Respiratory modulation of human autonomic rhythms. *American Journal of Physiology - Heart and Circulatory Physiology*, 280(6):H2674–H2688, 2001.

[36] V. G. Macefield and B. G. Wallin. Modulation of muscle sympathetic activity during spontaneous and artificial ventilation and apnoea in humans. *Journal of the Autonomic Nervous System*, 53(23):137 – 147, 1995.

[37] A. Stefanovska, M. Bračič, and H. D. Kvernmo. Wavelet analysis of oscillations in the peripheral blood circulation measured by laser Doppler technique. *IEEE Trans. Bio. Med. Eng.*, 46(10):1230–1239, 1999.

[38] A. Bandrivskyy, A. Bernjak, P. McClintock, and A. Stefanovska. Wavelet phase coherence analysis: Application to skin temperature and blood flow. *Cardiovascular Engineering*, 4(1):89–93, 2004.

[39] A. Stefanovska, L. W. Sheppard, T. Stankovski, and P. V. E. McClintock. Reproducibility of ldf blood flow measurements: Dynamical characterization versus averaging. *Microvascular Research*, 82(3):274 – 276, 2011.

[40] D. G. Luchinsky, P. V. E. McClintock, and M. I. Dykman. Analogue studies of nonlinear systems. *Reports on progress in physics*, 61(8):889–997, AUG 1998.

[41] W. Horsthemke and R. Lefever. *Noise Induced Transitions.* Springer, Berlin, 1984.

[42] S. H. Strogatz, D. M. Abrams, A. McRobie, B. Eckhardt, and E. Ott. Crowd synchrony on the millennium bridge. *Nature*, 438(7064):43–44, 2005.

[43] G. B. Ermentrout and J. Rinzel. Beyond a pacemaker's entrainment limit – phase walk-through. *Am. J. Physiol.*, 246(1):R102–R106, 1984.

[44] B. Blasius, A. Huppert, and L. Stone. Complex dynamics and phase synchronization in spatially extended ecological systems. *Nature*, 399(6734):354–359, 1999.

[45] A. A. Castrejón-Pita and P. L. Read. Synchronization in a pair of thermally coupled rotating baroclinic annuli: understanding atmospheric teleconnections in the laboratory. *Phys. Rev. Lett.*, 104:204501, 2010.

[46] L. M. Pecora and T. L. Carroll. Synchronization in chaotic systems. *Phys. Rev. Lett.*, 64(8):821–824, Feb 1990.

[47] L. Kocarev and U. Parlitz. Generalized synchronization, predictability, and equivalence of unidirectionally coupled dynamical systems. *Phys. Rev. Lett.*, 76(11):1816–1819, Mar 1996.

[48] R. L. Stratonovich. *Topics in the Theory of Random Noise: General theory of random processes, nonlinear transformations of signals and noise.* Mathematics and its applications. Gordon and Breach, 1963.

[49] P. E. Kloeden. Nonautonomous attractors of switching systems. *Dynamical Systems*, 21(2):209–230, 2006.

[50] V. Anishchenko, T. Vadivasova, and G. Strelkova. Stochastic self-sustained oscillations of non-autonomous systems. *Eur. Phys. J. Special Topics*, 187:109–125, 2010.

[51] M. Desroches, J. Guckenheimer, B. Krauskopf, C. Kuehn, H. M. Osinga, and M. Wechselberger. Canards, clusters, and synchronization in a weakly coupled interneuron model. *to be published - SIAM Journal on Applied Dynamical Systems*, 2011.

[52] B. Ermentrout and M. Wechselberger. Canards, clusters, and synchronization in a weakly coupled interneuron model. *SIAM Journal on Applied Dynamical Systems*, 8:253–278, 2009.

[53] M. Galassi, J. Davies, J. Theiler, B. Gough, G. Jungman, P. Alken, M. Booth, and F. Rossi. *GNU Scientific Library Reference Manual* Version 1.14, Chapter 35: Multidimensional Root-Finding. Network Theory, UK, 2010.

[54] G. A. Johnson, D. J. Mar, T. L. Carroll, and L. M. Pecora. Synchronization and imposed bifurcations in the presence of large parameter mismatch. *Phys. Rev. Lett.*, 80:3956–3959, May 1998.

[55] J. N. Blakely, D. J. Gauthier, G. Johnson, T. L. Carroll, and L. M. Pecora. Experimental investigation of high-quality synchronization of coupled oscillators. *Chaos*, 10:738–744, September 2000.

[56] N. J. Corron. Loss of synchronization in coupled oscillators with ubiquitous local stability. *Phys. Rev. E*, 63:055203, Apr 2001.

[57] D. G. Aronson, G. B. Ermentrout, and N. Kopell. Amplitude response of coupled oscillators. *Physica D*, 41(3):403–449, 1990.

[58] S. H. Strogatz. *Nonlinear Dynamics And Chaos.* Westview Press, Boulder, 2001.

[59] U. Parlitz and W. Lauterborn. Period-doubling cascades and devil's staircases of the driven Van der Pol oscillator. *Phys. Rev. A*, 36(3):1428–1434, 1987.

[60] R. Mettin, U. Parlitz, and W. Lauterborn. Bifurcation structure of the driven van der Pol oscillator. *Int. J. Bifurcation & Chaos*, 3(6):1529–1555, 1993.

[61] U. E. Vincent and A. Kenfack. Synchronization and bifurcation structures in coupled periodically forced non-identical duffing oscillators. *Physica Scripta*, 77(4):045005, 2008.

[62] M. G. Rosenblum, A. S. Pikovsky, and J. Kurths. From phase to lag synchronization in coupled chaotic oscillators. *Phys. Rev. Lett.*, 78(22):4193–4196, Jun 1997.

[63] S. Boccaletti, J. Kurths, G. Osipov, D. L. Valladares, and C. S. Zhou. The synchronization of chaotic systems. *Phys. Rep.*, 366(1-2):1–101, 2002.

[64] B. Lindner, J. Garcia-Ojalvo, A. Neiman, and L. Schimansky-Geier. Effects of noise in excitable systems. *Phys. Rep.*, 392(6):321–424, 2004.

[65] D. Garcia-Alvarez, A. Bahraminasab, A. Stefanovska, and P. V. E. McClintock. Competition between noise and coupling in the induction of synchronisation. *EPL*, 88(3):30005, 2009.

[66] A. Neiman, L. Schimansky-Geier, A. Cornell-Bell, and F. Moss. Noise-enhanced phase synchronization in excitable media. *Phys. Rev. Lett.*, 83(23):4896–4899, 1999.

[67] J. Teramae and D. Tanaka. Robustness of the noise-induced phase synchronization in a general class of limit cycle oscillators. *Phys. Rev. Lett.*, 93(20):204103, 2004.

[68] J. N. Teramae, H. Nakao, and G. B. Ermentrout. Stochastic phase reduction for a general class of noisy limit cycle oscillators. *Phys. Rev. Lett.*, 102(19):194102, 2009.

[69] D. S. Goldobin, J. N. Teramae, H. Nakao, and G. B. Ermentrout. Dynamics of limit-cycle oscillators subject to general noise. *Phys. Rev. Lett.*, 105(15):154101, 2010.

[70] T. L. Carroll and L. M. Pecora. Synchronizing nonautonomous chaotic circuits. *IEEE Trans. on Circuits and Systems–II*, 40(10):646–650, 1993.

[71] I. Bove, S. Boccaletti, J. Bragard, J. Kurths, and H. Mancini. Frequency entrainment of nonautonomous chaotic oscillators. *Phys. Rev. E*, 69(1):016208, 2004.

[72] E. N. Lorenz. Deterministic non-periodic flow. *J. Atmos. Sci.*, 20(2):130–141, 1963.

[73] J. J. Suárez-Vargas, J. A. González, A. Stefanovska, and P. V. E. McClintock. Diverse routes to oscillation death in a coupled-oscillator system. *EPL*, 85(3):38008, 2009.

[74] B. Blasius, E. Montbrio, and J. Kurths. Anomalous phase synchronization in populations of nonidentical oscillators. *Phys. Rev. E*, 67(3):035204, 2003.

[75] E. Montbrio and B. Blasius. Using nonisochronicity to control synchronization in ensembles of nonidentical oscillators. *Chaos*, 13(1):291–308, 2003.

[76] H. Daido. Onset of cooperative entrainment in limit-cycle oscillators with uniform all-to-all interactions: bifurcation of the order function. *Physica D: Nonlinear Phenomena*, 91:24 – 66, 1996.

[77] H. Daido. Multibranch entrainment and scaling in large populations of coupled oscillators. *Phys. Rev. Lett.*, 77:1406–1409, Aug 1996.

[78] J. D. Crawford. Scaling and singularities in the entrainment of globally coupled oscillators. *Phys. Rev. Lett.*, 74:4341–4344, May 1995.

[79] R. F. Galán, G. B. Ermentrout, and N. N. Urban. Efficient estimation of phase-resetting curves in real neurons and its significance for neural-network modeling. *Phys. Rev. Lett.*, 94:158101, Apr 2005.

[80] I. Z. Kiss, Y. Zhai, and J. L. Hudson. Predicting mutual entrainment of oscillators with experiment-based phase models. *Phys. Rev. Lett.*, 94:248301, Jun 2005.

[81] J. Miyazaki and S. Kinoshita. Determination of a coupling function in multicoupled oscillators. *Phys. Rev. Lett.*, 96:194101, May 2006.

[82] I. T. Tokuda, S. Jain, I. Z. Kiss, and J. L. Hudson. Inferring phase equations from multivariate time series. *Phys. Rev. Lett.*, 99:064101, Aug 2007.

[83] Z. Levnajić and A. Pikovsky. Network reconstruction from random phase resetting. *Phys. Rev. Lett.*, 107:034101, Jul 2011.

[84] V. N. Smelyanskiy, D. G. Luchinsky, D. A. Timucin, and A. Bandrivskyy. Reconstruction of stochastic nonlinear dynamical models from trajectory measurements. *Phys. Rev. E*, 72(2):026202, 2005.

[85] T. Bayes. *Essay towards solving a problem in the doctrine of chances.* Philosophical Transactions of the Royal Society of London, 1973.

[86] K. J. Friston. Bayesian estimation of dynamical systems: An application to fMRI. *NeuroImage*, 16(2):513–530, 2002.

[87] E. B. Sudderth, A. T. Ihler, M. Isard, W. T. Freeman, and A. S. Willsky. Nonparametric belief propagation. *Commun. ACM*, 53:95–103, 2010.

[88] B. Musizza, A. Stefanovska, P. V. E. McClintock, and et al. Interactions between cardiac, respiratory and eeg- oscillations in rats during anaesthesia. *The Journal of Physiology*, 580(1):315–326, 2007.

[89] S. Hempel, A. Koseska, J. Kurths, and Z. Nikoloski. Inner composition alignment for inferring directed networks from short time series. *Phys. Rev. Lett.*, 107:054101, Jul 2011.

[90] T. Schreiber and A. Schmitz. Improved surrogate data for nonlinearity tests. *Phys. Rev. Lett.*, 77(4):635–638, 1996.

[91] M. Paluš. Bootstrapping multifractals: Surrogate data from random cascades on wavelet dyadic trees. *Phys. Rev. Lett.*, 101(13):134101, 2008.

[92] C. Zhou and J. Kurths. Noise-induced phase synchronization and synchronization transitions in chaotic oscillators. *Phys. Rev. Lett.*, 88:230602, May 2002.

[93] O. V. Popovych, C. Hauptmannn, and P. A. Tass. Effective desynchronization by nonlinear delayed feedback. *Phys. Rev. Lett.*, 94:164102, Apr 2005.

[94] R. Bartsch, J. W. Kantelhardt, T. Penzel, and S. Havlin. Experimental evidence for phase synchronization transitions in the human cardiorespiratory system. *Phys. Rev. Lett.*, 98:054102, Feb 2007.

[95] M. B. Lotrič and A. Stefanovska. Synchronization and modulation in the human cardiorespiratory system. *Physica A*, 283(3-4):451–461, 2000.

[96] C. D. Lewis, G. L. Gebber, S. Zhong, P. D. Larsen, and S. M. Barman. Modes of baroreceptor-sympathetic coordination. *Journal of Neurophysiology*, 84(3):1157–1167, 2000.

[97] I. Daubechies, J. Lu, and H.-T. Wu. Synchrosqueezed wavelet transforms: An empirical mode decomposition-like tool. *Appl. and Comput. Harmon. Anal.*, 30(2):243–261, 2011.

[98] N. F. Rulkov, M. M. Sushchik, L. S. Tsimring, and H. D. I. Abarbanel. Generalized synchronization of chaos in directionally coupled chaotic systems. *Phys. Rev. E*, 51:980–994, Feb 1995.

[99] M. Paluš and *at al.* Synchronization as adjustment of information rates: Detection from bivariate time series. *Phys. Rev. E*, 63:046211, Mar 2001.

[100] C. J. Stam and B. W. van Dijk. Synchronization likelihood: an unbiased measure of generalized synchronization in multivariate data sets. *Physica D: Nonlinear Phenomena*, 163(34):236 – 251, 2002.

[101] Z. Liu, J. Zhou, and T. Munakata. Detecting generalized synchronization by the generalized angle. *EPL (Europhysics Letters)*, 87(5):50002, 2009.

[102] J. P. Eckmann and D. Ruelle. Fundamental limitations for estimating dimensions and lyapunov exponents in dynamic systems. *Physica D*, 56:185–187, 1992.

[103] M. E. J. Newman. The structure and function of complex networks. *SIAM Review*, 45(2):pp. 167–256, 2003.

[104] A. Arenas, A. Daz-Guilera, J. Kurths, Y. Moreno, and C. Zhou. Synchronization in complex networks. *Physics Reports*, 469(3):93 – 153, 2008.

[105] E. N. Marieb. *Human Anatomy and Physiology.* Benjamin Cummings VII edition, 2007.

[106] B. Charlie. *Nervous system.* Edinburgh: Mosby, 2003.

[107] J. A. Hirsch and B. Bishop. Respiratory sinus arrhythmia in humans: how breathing pattern modulates heart rate. *American Journal of Physiology - Heart and Circulatory Physiology*, 241(4):H620–H629, 1981.

[108] T. E. Brown, L. A. Beightol, J. Koh, and D. L. Eckberg. Important influence of respiration on human r-r interval power spectra is largely ignored. *Journal of Applied Physiology*, 75(5):2310–2317, 1993.

[109] D. R. Seals, N. O. Suwarno, and J. A. Dempsey. Influence of lung volume on sympathetic nerve discharge in normal humans. *Circulation Research*, 67(1):130–141, 1990.

[110] P. Van De Borne, N. Montano, K. Narkiewicz, J. P. Degaute, A. Malliani, M. Pagani, and V. K. Somers. Importance of ventilation in modulating interaction between sympathetic drive and cardiovascular variability. *American Journal of Physiology - Heart and Circulatory Physiology*, 280(2):H722–H729, 2001.

[111] A. Bernjak, J. Cui, S. Iwase, T. Mano, A. Stefanovska, and D. L. Eckberg. Human sympathetic outflows to skin and muscle target organs fluctuate concordantly over a wide range of time-varying frequencies. *The Journal of Physiology*, 2011.

[112] T. Soderstrom, A. Stefanovska, M. Veber, and H. Svensson. Involvement of sympathetic nerve activity in skin blood flow oscillations in humans. *American Journal of Physiology - Heart and Circulatory Physiology*, 284(5):H1638–H1646, 2003.

[113] J. P. Saul, R. D. Berger, P. Albrecht, S. P. Stein, M. H. Chen, and R. J. Cohen. Transfer function analysis of the circulation: unique insights into cardiovascular regulation. *American Journal of Physiology - Heart and Circulatory Physiology*, 261(4):H1231–H1245, 1991.

[114] G. Kaiser. *A Friendly Guide to Wavelets*. Birkhäuser, Boston, 1994.

[115] L. W. Sheppard, A. Stefanovska, and P. V. E. McClintock. Testing for time-localized coherence in bivariate data. *Phys. Rev. E*, Accepted Mar 08, 2012.

[116] A. Porta, A. M. Catai, A. C. M. Takahashi, V. Magagnin, T. Bassani, E. Tobaldini, P. van de Borne, and N. Montano. Causal relationships between heart period and systolic arterial pressure during graded head-up tilt. *American journal of physiology-regulatory integrative and comparative physiology*, 300(2):R378–R386, Feb 2011.

[117] K. Lehnertz. Assessing directed interactions from neurophysiological signals-an overview. *Physiological measurement*, 32(11):1715–1724, Nov 2011.

[118] S. M. Barman. Sympathetic nerve activity has more character than you may think. *The Journal of Physiology*, 587(20):4767–4768, 2009.

[119] D. Gabor. Theory of communication. *J. IEEE*, 93:429–457, 1946.

[120] M. G. Rosenblum, A. S. Pikovsky, and J. Kurths. Synchronization approach to analysis ofbiological systems. *Fluctuation and Noise Letters*, 4(1):53, 2004.

[121] T. Stankovski, B. Musizza, P. V. E. McClintock, and A. Stefanovska. Phase detection from the respiration signal. *Proceedings of the 6th ESGCO, Berlin, Germany*, 2010.

[122] T. Stankovski, editors:, A. Stefanovska, P. V. E. McClintock, Ræder J, and A. F. Smith. *Nonlinear Dynamics of Anæsthesia: from Theory to Clinical Application.* Springer - to be published.

[123] H. Wu. Instantaneous frequency and wave shape functions. *arXiv:1104.2365v1*, 2011.

[124] E. Brevdo, N. S. Fuckar, G. Thakur, and H. Wu. The synchrosqueezing algorithm: a robust analysis tool for signals with time-varying spectrum. *arXiv:1105.0010v1*, 2011.

[125] M. Roustit, S. Blaise, C. Millet, and J. L. Cracowski. Reproducibility and methodological issues of skin post-occlusive and thermal hyperemia assessed by single-point laser Doppler flowmetry. *Microvasc. Res.*, 79(2):102–108, 2010.

[126] M. Bračič and A. Stefanovska. Wavelet based analysis of human blood flow dynamics. *Bull. Math. Biol.*, 60(5):919–935, 1998.

[127] A. Stefanovska. Coupled oscillators: Complex but not complicated cardiovascular and brain interactions. *IEEE Eng. Med. Bio. Magazine*, 26(6):25–29, 2007.

[128] J. Cracowski and M. Roustit. Reproducibility of ldf blood flow measurements: Dynamical characterization versus averaging. a response to the letter from stefanovska. *Microvascular Research*, (0):–, 2012.

[129] D. G. Luchinsky and P. V. E. McClintock. Irreversibility of classical fluctuations studied in analogue electrical circuits. *Nature*, 389:463–466, 1997.

[130] F. Peterka. Bifurcations and transition phenomena in an impact oscillator. *Chaos, Solitons & Fractals*, 7:1635–1647, 1996.

[131] A. G. Balanov, N. B. Janson, D. E. Postnov, and P. V. E. McClintock. Coherence resonance versus synchronization in a periodically forced self-sustained system. *Phys. Rev. E*, 65:041105–041109, 2002.

[132] A. A. Temirbayev, Z. Zh. Zhanabaev, S. B. Tarasov, V. I. Ponomarenko, and M. Rosenblum. Experiments on oscillator ensembles with global nonlinear coupling. *Phys. Rev. E*, 85:015204, Jan 2012.

[133] U. Parlitz, W. Lauterborn L. Junge, and L. Kocarev. Experimental observation of phase synchronization. *Phys. Rev. E*, 54:21152117, 1996.